Intermolecular Potentials, Internal Motions, and Spectra of van der Waals and Hydrogen-Bonded Complexes

Paul E. S. Wormer and Ad van der Avoird*

Institute of Theoretical Chemistry, NSR Center, University of Nijmegen, Toernooiveld 1, 6525 ED Nijmegen, The Netherlands

Received January 26, 2000

Contents

1. Introduction 4109
2. Calculation of Spectra of van der Waals Molecules 4110
   2.1. Coordinates; Kinetic and Potential Energy 4110
   2.2. Calculation of the Vibration–Rotation–Tunneling States 4112
   2.3. Symmetry Aspects 4112
   2.4. Computation of the Spectrum 4113
3. Rovibrational Spectrum of Argon–Methane 4113
   3.1. The Schrödinger Equation and Its Solution 4114
   3.2. The Spectrum and Its Assignment 4117
4. Water Pair Potential and Dimer Spectrum 4118
   4.1. Tunneling Processes in the Water Dimer 4119
   4.2. Dynamics Calculations 4120
   4.3. Pair Potential and Dimer VRT Levels 4121
5. Three-Body Interactions; Water Trimer Spectrum 4123
   5.1. Torsion and Bifurcation Tunneling 4124
   5.2. Torsional Model Hamiltonian 4126
   5.3. Effective Rotational and Tunneling Hamiltonian 4127
   5.4. Experimental Results and Analysis 4128
   5.5. Three-Body Interactions; Trimer VRT Levels 4130
6. Other Recent Developments 4131
   6.1. Complexes of Nonpolar Molecules 4131
      6.1.1. Atom–Linear Molecule Dimers 4131
      6.1.2. Ar–Benzene 4132
      6.1.3. Trimers and Larger Clusters 4133
   6.2. Hydrogen-Bonded Complexes 4134
      6.2.1. HF and HCl Dimers 4134
      6.2.2. Water Clusters 4136
      6.2.3. Benzene–Water, π-Electron Hydrogen Bonding 4137
   6.3. Conclusion 4138
7. Acknowledgment 4139
8. Appendix A 4139
9. Appendix B 4139
10. References 4140

1. Introduction

This review deals with the relation between intermolecular potentials and the spectra of van der Waals molecules. Intermolecular potentials cannot be measured directly, but the intermolecular—or van der Waals—modes of a van der Waals molecule depend directly and sensitively on the potential that holds such a complex together. As the intermolecular forces are rather weak, these van der Waals modes have large amplitudes and are very soft: frequencies are a few tens of reciprocal centimeters for complexes with nonpolar monomers to a few hundreds for hydrogen-bonded complexes. Experimentally the modes are observed directly in laser-based far-infrared spectroscopy,[1−5] as sidebands in the mid-IR,[6,7] and in the UV.[8] Often van der Waals molecules are observed in cold supersonic molecular beams, but also infrared spectroscopy of cold gases[9] can give useful information.

In high-resolution laser spectra, the line positions are usually determined in as many as six or more decimal digits. When using such data to probe the intermolecular potential, one does not wish to sacrifice too much of this precision, which implies that one must solve nearly exactly the Schrödinger equation to obtain the bound quantum levels of the complex from a given potential surface. Standard methods of rovibrational analysis based on the harmonic oscillator−rigid rotor model are not applicable because of the large-amplitude motions and, in most cases, tunneling between multiple minima on the potential surface. Hence, the usual assignment and fitting of the spectra in terms of (fundamental) vibrational frequencies (band origins) and rotational, distortion, and Coriolis coupling constants is often not possible.

We will start with an overview of the computational methods leading to ab initio spectra that may be compared directly with experimental spectra. This overview is rather brief; for mathematical details, we refer to two recent reviews.[10,11] Then we will discuss some examples of the synergy between theory and experiment. The first example, Ar−CH_4, illustrates that for complexes with moderately hindered internal rotations, the spectrum shows a complicated, irregular structure. The standard procedure to assign and fit the rotational structure in the high-resolution spectrum with the aid of a semirigid rotor Hamiltonian fails completely in this case. Only after an ab initio spectrum became available, it was possible to interpret the infrared spectrum measured a few years earlier. At the same time, this confirmed the accuracy of the ab initio Ar−CH_4 potential. The second example, the water dimer, is a convincing case of the use of experimental data to probe intermolecular potentials. The measured dimer spectrum has been employed, via the theory, to discriminate between

10.1021/cr990046e CCC: $35.00
Published on Web 10/05/2000

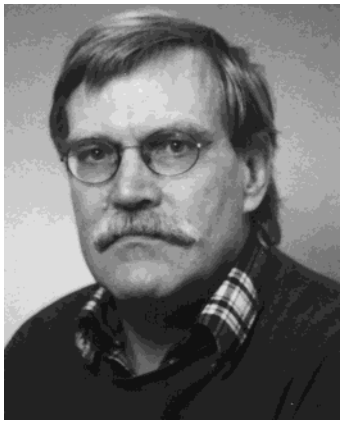

Paul E. S. Wormer was born in Amsterdam, The Netherlands, in 1942. He did his undergraduate work in chemistry at the Technical University Delft, where he received his degree (with honors) in 1969. After graduation he spent a year as a research assistant at Duke University with D, B, Chestnut. After returning to The Netherlands, he received his doctorate degree in Theoretical Chemistry from the University of Nijmegen in 1975 (with honors); A. van der Avoird was his promoter. Since then he has held a permanent position in Nijmegen. He spent a sabbatical year and a few summers with J. Paldus in the Department of Applied Maths of the University of Waterloo, Canada, and was a Visiting Fellow of the Royal Society in 1986 as a guest of J. Gerratt, University of Bristol, U.K. His main research interests are the topics covered in the present review, the electronic correlation problem, and the group theory of many-particle systems.

Ad van der Avoird studied chemical engineering at the Technical University in Eindhoven, The Netherlands, from 1959 to 1964. From 1964 to 1971 he worked at the Battelle Institute in Geneva, Switzerland, and at the Unilever Research Laboratory in Vlaardingen, where in 1968 he became Head of the Molecular Physics section. In 1968 he obtained his Ph.D. degree at the Technical University in Eindhoven, and in the same year he became a part-time professor at the University of Nijmegen. In 1971 he became Full Professor of Theoretical Chemistry in Nijmegen. Since 1979 he has been a member of the Netherlands Royal Academy of Arts and Sciences (KNAW) and since 1997 a member of the International Academy of Quantum Molecular Science. In 1992 he worked in the spectroscopy group of Richard Saykally at the University of California at Berkeley as a Visiting Miller Research Professor. He is presently a member of the Editorial Board of the *Journal of Chemical Physics*.

high- and low-quality empirical and ab initio water potentials. Furthermore, a semiempirical potential has been obtained from a fit of the spectral data, and the same data were used for improving the best available ab initio water pair potential. Our third example, the water trimer, shows that also for a more structured hydrogen-bonded complex it may be necessary to abandon the standard rigid rotor Hamiltonian for a fit of the rotational and tunneling structure in the experimental spectrum. Instead, a new effective Hamiltonian has been derived which explicitly takes into account the occurrence of the soft and coupled internal rotations and tunneling flips of the monomers in the trimer. We also describe the use of the trimer spectrum in further tests of the water pair potential and of the nonadditive three-body interactions. Meanwhile, the combination of theory and experiment provides useful insights into the hydrogen-bond network rearrangement processes which occur in these water clusters but also in liquid water.

Finally, we present an overview of the recent literature—since the last *Chemical Reviews* issue on van der Waals molecules in 1994. As the number of new van der Waals and hydrogen-bonded complexes identified experimentally or studied via ab initio calculations is very rapidly expanding, we focus on some prototype systems which have received the most attention and for which the development of theory and experiment have gone hand in hand.

2. Calculation of Spectra of van der Waals Molecules

The softness of van der Waals modes is in contrast to the vibrational modes in chemically bound molecules, which usually lie in the mid-infrared. Another difference between chemically bound and van der Waals bound molecules is that in the former the different equivalent minima on the potential-energy surface are usually well separated by large energy barriers. van der Waals molecules, on the other hand, show quite often considerable tunneling from one equivalent minimum to the other, indicating that the barriers between the minima are not large. These physical observations have important consequences for the theoretical study of the spectroscopy of van der Waals molecules. Let us first recall that the theoretical description of the rovibrational spectra of 'classical' molecules usually departs from a single well-defined equilibrium geometry. By means of the Eckart conditions[12] and the knowledge of the equilibrium coordinates, a body-fixed frame[13] can be introduced. The use of such an Eckart frame decouples as much as possible the rotations from the vibrations. In this frame one describes the displacements of the nuclei away from their equilibrium positions; the linearization of these motions leads to the well-known GF method.[14] The Eckart−GF approach breaks down completely for van der Waals molecules because of the two facts just mentioned: (i) these molecules do not have well-separated equilibria and (ii) the rovibrational motions are not small enough for a linearization of the coordinates to be meaningful.

2.1. Coordinates; Kinetic and Potential Energy

As in the case of 'normal' molecules, one starts the quantum mechanical study of van der Waals molecules by assuming the Born−Oppenheimer separation between the nuclear and electronic motions. In solving the nuclear motion problem, one first separates off the center of mass motion of the total complex (the van der Waals molecule). This yields

three linear conditions, and assuming that the system consists of N nuclei, one thus decomposes the $3N$-dimensional configuration space into a direct sum of a 3- and a $(3N - 3)$-dimensional linear subspace. The former linear space is associated with the translational motion of the complex as a whole and the latter with the rovibrational motions of the complex. In chemically bound molecules, the rotational motion is then decoupled from the vibrations by means of the Eckart equations (ref 15, p 208), which leads to $3N - 6$ internal coordinates. For lack of a single well-defined minimum, the Eckart conditions are usually not applicable in van der Waals molecules. However, transformation to a body-fixed frame[10,16,17] unveils the term in the kinetic-energy operator that describes the Coriolis coupling between the overall rotation and the internal motions of the complex. In first instance one may neglect this coupling, thus separating the external from the internal motions of the complex. In a second step the Coriolis coupling may be reintroduced, e.g., in perturbation theory. Even with neglect of the Coriolis interaction, the remaining number of degrees of freedom is still considerable in most van der Waals molecules, so that an exact solution of the Schrödinger equation for the rovibrational motion is still out of the question. Other approximations must be introduced.

The approximation most widely applied is the assumption that the monomers constituting the complex are rigid. This approximation is in fact equivalent to introducing a set of nonlinear constraints and thus gives rise to a nonlinear subspace M of the configuration space. The Schrödinger equation must be solved on M. Therefore, one is faced with the following problems: (i) finding a suitable set of coordinates $\boldsymbol{q} = (q_1, q_2,...)$ for M, (ii) expressing the kinetic energy in these coordinates, and (iii) finding the potential-energy function on all of M. The last problem arises due to the fact that linearization of the coordinates is physically unacceptable: a Taylor expansion of the potential around a certain point of M will not do. First and higher derivatives of the potential at a single point of M are of no use.

The second of these problems, i.e., finding the kinetic energy in the generalized coordinates $\boldsymbol{q}$, is a standard textbook problem. One defines the metric tensor G by

$$G_{ij} = \sum_{\nu=1}^{N} m_\nu \sum_{\alpha=1}^{3} \frac{\partial r_{\nu\alpha}}{\partial q_i} \frac{\partial r_{\nu\alpha}}{\partial q_j}$$

where m_ν is the mass of nucleus ν and $r_{\nu\alpha}$ is its αth Cartesian component with respect to an arbitrary space-fixed frame. The classical kinetic energy can concisely be written as

$$T = \frac{1}{2}\dot{\boldsymbol{q}}^T \mathrm{G} \dot{\boldsymbol{q}} \text{ with } \dot{\boldsymbol{q}} \equiv \frac{d\boldsymbol{q}}{dt}$$

Defining as usual the linear momentum p_i conjugate to q_i by $p_i \equiv \partial T/\partial \dot{q}_i$, so that $\boldsymbol{p} = \mathrm{G}\dot{\boldsymbol{q}}$, we find that the classical kinetic energy can also be written as

$$T = \frac{1}{2}\boldsymbol{p}^T \mathrm{G}^{-1} \boldsymbol{p} \tag{1}$$

The Laplace operator in generalized coordinates is (see for instance ref 18, p 174)

$$\nabla^2 = g^{-1/2} \sum_{ij} \frac{\partial}{\partial q_i} g^{1/2} G^{ij} \frac{\partial}{\partial q_j} \tag{2}$$

where g is det(G) and G^{ij} is the (i, j) element of G^{-1}. Podolsky[19] pointed out long ago that the proper quantum mechanical kinetic-energy operator is

$$\hat{T} = -\frac{1}{2}\hbar^2 \nabla^2$$

with the Laplacian (2). Let us define $p_j = -i\hbar\partial/\partial q_j$, and since, as is shown in Appendix A,

$$p_i^\dagger = g^{-1/2} p_i g^{1/2} \tag{3}$$

we may write

$$\hat{T} = \frac{1}{2}\boldsymbol{p}^\dagger \mathrm{G}^{-1} \boldsymbol{p} \tag{4}$$

where $\boldsymbol{p}^\dagger$ stands for the row vector $(p_1^\dagger, p_2^\dagger,...)$. Note that this quantum mechanical expression for $\hat{T}$ has a strong resemblance to the classical Hamiltonian of eq 1. We also show in Appendix A that $(p_j^\dagger)^\dagger = p_j$. This latter relation is very convenient in matrix-element-based solution methods of the Schrödinger equation, because application of the turnover rule shows that matrix elements of $\hat{T}$ are easy to calculate: in bra and ket we must simply apply $p_j = -i\hbar\partial/\partial q_j$. This was pointed out earlier by Chapuisat et al.[20] and used extensively in refs 21 and 22.

A *general* solution to the first problem, the choice of suitable coordinates for M, is probably impossible, because it depends very much on the nature of the van der Waals molecule under study; one must decide for each case separately what the most convenient coordinates are. The most natural choice—the Cartesian components of the mass centers and the Euler angles (see Appendix B) of all the monomers with respect to the *same* space-fixed frame—is not very convenient because it is generally difficult to express the interaction potential in these coordinates.

In the case of two rigid molecules with similar masses, A and B, a suitable coordinate system is obtained by embedding a frame with its origin at the mass center of the dimer such that the z-axis coincides with $\vec{R}$. This vector points from the center of mass (c.m.) of A to the c.m. of B. Since only the two spherical polar angles of $\vec{R}$ with respect to a space-fixed frame enter its definition, it is a two-angle embedded frame. The polar angles of $\vec{R}$, together with the Euler angles of A and B with respect to the two-angle embedded frame, form a set of angular coordinates. The kinetic energy was first obtained by explicit transformation of the Cartesian ∇^2 to this system of coordinates.[23] Later[10] the metric tensor G

was derived and inserted into the Podolsky formula; the two derivations give identical final results. Note that embedded frames can also be useful when the rigidity of the monomers is relaxed. For example, Qiu et al.,[24] in a recent calculation on the HCl dimer, use the two-angle embedded frame and introduce the two intramonomer H−Cl distances among the degrees of freedom.

In strongly asymmetric dimers, as for instance the benzene−argon complex,[25,26] it can be convenient to fix a frame to one monomer, for example to the benzene. The Euler angles of the monomer frame and the coordinates of the position vector of argon with respect to the monomer frame are the coordinates to be considered. The kinetic energy was derived directly in refs 25 and 26 and via the metric tensor in 10. See also refs 16, 17, and 27−29 for recent discussions of kinetic-energy operators.

The third problem, obtaining the potential on all of M, can be solved by ab initio electronic structure calculations on a finite grid of points of M followed by a fit or interpolation. One may use perturbation methods, see for instance Jeziorski et al.,[30] or supermolecule methods.[31] Using the latter method, one must not forget to correct for basis set superposition errors.[32] Alternatively, one may try to invert spectroscopic data and work backward to the potential. In practice, this is extremely difficult without any help from electronic structure calculations. Usually one employs a hybrid method, with some input from calculations and some free parameters that are fit to the experimental spectrum. Recent examples of potentials obtained by this approach are for He−CO,[33] the water dimer,[34] and Ne−HF.[35]

2.2. Calculation of the Vibration–Rotation–Tunneling States

Once we have defined the coordinates and set up the Hamiltonian, we are ready to solve the Schrödinger equation. Its solutions are the rovibrational states which usually exhibit tunneling from one minimum to the other. Methods for the computation of these so-called vibration−rotation−tunneling (VRT) states[36] in van der Waals molecules can be classified as variational and nonvariational. In the linear variational methods, one chooses an expansion basis of square-integrable functions, the functional dependence of which depends obviously on the choice of the coordinates. Usually one employs product functions: (products of) Wigner D-matrices[37] for the Euler angles multiplied by functions for the radial coordinate(s). Note that D-matrices are a generalization of spherical harmonic functions. In the case of closed-shell linear molecules, one Euler angle is zero and the D-matrix 'shrinks' to a spherical harmonic function.[37]

For the radial basis, one may use analytic functions, such as associated Laguerre functions,[38,39] or distributed Gaussians,[40,41] or numerical functions defined on a grid of R points.[42]

The traditional nonvariational method to obtain the VRT states of dimers is the close-coupling method, as implemented for scattering calculations.[43,44] The angular basis functions used in such calculations are also D-matrices or spherical harmonic functions. The radial functions are not expanded in a basis, however, but they are written as the R-dependent 'coefficients' in the expansion of the exact wave function in the complete set of angular (channel) functions. When this expansion is substituted into the Schrödinger equation, one obtains a set of coupled differential equations for the radial functions of the different channels.[45]

Nonvariational approaches which are based on discrete representations of the wave function are the discrete variable representation (DVR)[46−49] and the collocation method.[50−54] A major advantage of the latter methods is that they are easy to program. This also holds for the pseudospectral method,[55,56] which uses—just as DVR—two basis sets: one in spectral (function) space and one in 'grid space'. A larger number of grid points x_p than functions u_n is used. The collocation matrix $R_{pn} \equiv u_n(x_p)$ allows switching from the spectral to the grid representation. The inverse transformation is carried out by means of a generalized inverse, which provides the best transformation in the least-squares sense. The use of a grid is particularly efficient for evaluating the action of a Hamiltonian on a wave function in spectral space. The timing of most iterative diagonalization methods is dominated by the latter matrix−vector multiply.

Finally, we mention the diffusion Monte Carlo (DMC) method, originally designed for calculating energies and wave functions of atomic and molecular systems.[57] The technique is computationally simple and roughly scales linearly with size but has the disadvantage that only ground states can be computed straightforwardly. The rigid-body version of DMC[58] rigorously factors out the high-frequency intramolecular vibrations of the monomers, so that in this approach, too, only the rovibrational motions of the whole monomers are considered. It has been demonstrated that rigid-body DMC is able to calculate accurate energies with longer time steps than conventional DMC.[59,60]

2.3. Symmetry Aspects

The multiple minima in the potential surface and the large-amplitude vibrations make the concept of a point group—which describes the symmetry of a rigid body—useless for van der Waals molecules. However, the following symmetry operations do still apply: (i) permutations of identical nuclei, (ii) space-inversion, and (iii) products of i and ii. It is legitimate to consider all such possible permutation−inversions (PIs), but since only a minority of them is physically meaningful, this would lead to a group which is much larger than necessary. Only a subset of the full PI group gives rise to observable splittings: these are the so-called 'feasible' PIs.[61,62] We distinguish two kinds of these: the first kind is equivalent to a rotation of the molecule in isotropic space. In this case, no energy barrier is surmounted. The second kind of feasible PIs requires the tunneling through some barrier, deforming the molecule to another equivalent structure that is distinguished from the earlier structure by the change in one or more

internal coordinates. It is very hard to predict a priori if an operation of the second kind is feasible. Detailed experiments or elaborate calculations are required to do so. Furthermore, whether an operation is considered to be feasible depends on the resolution of the measuring device. In most cases tunneling through the barriers of van der Waals surfaces (including hydrogen-bonding surfaces) gives rise to observable splittings so that the corresponding permutations are feasible. For instance, a cyclic permutation of the three protons of a single ammonia molecule is of the first kind but becomes of the second kind in the ammonia dimer. This is because the original and permuted structure are separated by a barrier in the van der Waals potential. However, this barrier is so low that the cyclic permutation remains feasible in the dimer.

The PI group can be used for several purposes. First, in the calculation of the VRT states, the adaptation of the basis to the irreducible representations (irreps) of the PI group leads to a separation of the Hamiltonian matrix into smaller blocks. In some examples, such as $(NH_3)_2$,[63,64] this simplification was essential to make the calculations possible. Second, since the VRT states are symmetry adapted and since the dipole operator is invariant under all permutations of identical nuclei and antisymmetric under space inversion E^*, we obtain exact selection rules. Finally, we note that also the nuclear spin functions must be adapted to the permutations of (all) identical nuclei. The spin functions are invariant under space inversion. Since the nuclei are bosons (for integer spin quantum number I) or fermions (for half-integer I), it follows from the Pauli principle that the spatial wave functions of the VRT states are explicitly related, through their permutation symmetry, to the occurrence of specific nuclear spin quantum numbers. It is this relation that determines the nuclear spin statistical weight[15] of each VRT level.

2.4. Computation of the Spectrum

Once we have computed the VRT states, we can compute the spectrum. In accordance with Fermi's golden rule and the multipole expansion of the laser field, we must compute the square of transition dipole matrix elements. In principle, the full dipole surface of the van der Waals molecule arises here as the operator. If one or more of the monomers have a fairly large permanent electronic dipole, the dipole surface may be approximated by applying a rotation to the permanent moment. Consider, for instance, the dipole surface of a rigid molecule with a monomer-fixed frame that has Euler angles α, β, and γ with respect to a reference frame (e.g., the frame of the laser or a frame embedded in the complex). The dipole surface may be approximated by

$$\boldsymbol{\mu}(\alpha, \beta, \gamma) = \mathrm{R}(\alpha, \beta, \gamma)\boldsymbol{\mu}_{\mathrm{elec}}$$

where $\boldsymbol{\mu}_{\mathrm{elec}}$ is the electronic dipole moment in the monomer-fixed frame and $\mathrm{R}(\alpha, \beta, \gamma)$ is the 3×3 rotation matrix describing the rotation of the latter frame (see Appendix B). When the reference frame is not the frame of the laser field, a further rotation of $\boldsymbol{\mu}(\alpha, \beta, \gamma)$ is needed.

This approximation can be refined by introducing induced dipole moments.[65] When none of the monomers has a permanent multipole, the dipole surface is due to penetration, exchange, and dispersion effects and may be computed by ab initio methods.[66]

Since the VRT levels are usually closely spaced, it is common to include in the calculated far-infrared spectrum simultaneously the effects of absorption and stimulated emission and to assume that all states are populated according to a Boltzmann distribution. The intensity is then given by eq 29 of ref 10.

3. Rovibrational Spectrum of Argon–Methane

A series of argon$-XH_n$ complexes has been studied to date. The amplitude of the intermolecular vibrational motion is particularly large in these complexes due to the fact that the internal rotation involves essentially only the motion of hydrogens. In the case of Ar$-$HF,[67,68] the hydrogen undergoes wide amplitude bending excursions and the vibrationally averaged structure changes wildly upon intermolecular vibrational excitation. In Ar$-H_2O$,[69,70] the water molecule undergoes hindered rotation within the complex, as is also the case for Ar$-NH_3$.[71] Although the moments of inertia become progressively larger as we move down the series (more hydrogen atoms are moving), the larger systems tend to be even more delocalized, as the number of equivalent configurations increases. The complex that completes the above series, namely Ar$-CH_4$, has been the subject of numerous experimental and theoretical studies.

Traditional bulk methods used to determine potentials for Ar$-CH_4$ include the measurement and fitting of diffusion coefficients,[72−74] viscosities,[75−77] second virial coefficients,[78−81] and thermal diffusion factors.[82,83] This bulk data does not provide enough detail for the determination of all of the features of the associated multidimensional potential. The more recent scattering experiments for Ar$-CH_4$[84−87] provide more information on the potential anisotropy, as do the results of rotational relaxation experiments.[88,89] Recent experimental work on this system is by Chapman et al.,[90] who have measured the state-to-state integral cross sections for rotational excitation of methane upon collision with argon. (Parenthetically it may be remarked that they performed[91] the same kind of measurements for Ar$-H_2O$.) The comparison between this Ar$-CH_4$ data and the calculated results based upon the empirical potential developed previously by Buck et al. from total differential scattering[85] and energy-loss measurements[86] is quite reasonable, although there are still significant differences for several of the cross sections.

Recently argon$-$methane was studied spectroscopically with rotational resolution.[9,92,93] McKellar[9] presented a mid-infrared spectrum at the 1994 Faraday Discussion. This spectrum, measured in the bulk, lies around the ν_3 mode (3019.5 cm^{-1}) of the free methane molecule. Miller,[92] in his comment on the McKellar presentation, showed a similar spectrum taken in the molecular beam. Just as is the case for Ar$-$HF, Ar$-H_2O$, and Ar$-NH_3$, the methane undergoes nearly free rotation within the complex so that a rigid

molecule description is inappropriate for describing the rotational states of the complex.

A number of ab initio studies of Ar−CH_4 have also been performed. The long-range dispersion coefficients were reported by Fowler et al.,[94] while more recently Szczęśniak et al.[95] calculated a few slices through the potential using MP2 methods with a relatively small basis. The most complete study to date is that of Heijmen et al.,[96] who made use of symmetry-adapted perturbation theory (SAPT) and computed enough points on the surface to enable a fit of the surface to an analytical potential. This potential has been shown to reproduce much of the experimental data that is currently available. In particular, for the total differential scattering cross sections of argon from methane, the results[97] obtained from this potential are in excellent agreement with experiment. Also, the rotationally inelastic integral cross sections[96] are generally in good agreement with the experimental values of Chapman et al.[90]

In refs 98 and 99 the spectrum for the binary Ar−CH_4 complex was reported and assigned. The assignment of the spectrum was made possible by carrying out exact quantum calculations on the system on the basis of the ab initio potential surface reported previously.[96] The effects of vibrational angular momentum in the v_3 excited state were included in the calculations. In the following we will briefly review this work.

3.1. The Schrödinger Equation and Its Solution

We begin by introducing the six coordinates that enter the nuclear motion problem. The CH_4 molecule is assumed to be rigid and of tetrahedral symmetry, i.e., it has the point group T_d. Vector R, which points from the carbon atom to the argon, has spherical polar angles β and α with respect to a space-fixed frame $\vec{\boldsymbol{e}} \equiv (\vec{e}_x, \vec{e}_y, \vec{e}_z)$. We define a frame $\vec{\boldsymbol{f}} = (\vec{f}_x, \vec{f}_y, \vec{f}_z)$, which has its z-axis along $\vec{R}$

$$\vec{\boldsymbol{f}} = \vec{\boldsymbol{e}}\mathrm{R}_z(\alpha)\mathrm{R}_y(\beta) \tag{5}$$

See Appendix B for the definition of the matrices. A frame $\vec{\boldsymbol{g}}$ fixed to methane is shown in Figure 1. Explicitly,

$$\vec{g}_x = (\overrightarrow{CH_2} - \overrightarrow{CH_1})/\sqrt{2}$$

$$\vec{g}_y = (\overrightarrow{CH_4} - \overrightarrow{CH_3})/\sqrt{2}$$

$$\vec{g}_z = (\overrightarrow{CH_1} + \overrightarrow{CH_2} - \overrightarrow{CH_3} - \overrightarrow{CH_4})/2 \tag{6}$$

This frame is right-handed and orthonormal (with the appropriate unit of length) and has Euler angles $\boldsymbol{\omega} = (\omega_1, \omega_2, \omega_3)$ with respect to $\vec{\boldsymbol{f}}$, i.e.,

$$\vec{\boldsymbol{g}} = \vec{\boldsymbol{f}}\mathrm{R}(\boldsymbol{\omega}) \equiv \vec{\boldsymbol{f}}\mathrm{R}_z(\omega_1)\mathrm{R}_y(\omega_2)\mathrm{R}(\omega_3) \tag{7}$$

The ab initio potential[96] $V(R, \Theta, \Phi)$ contains the spherical polar angles of $\vec{R}$ with respect to the frame $\vec{\boldsymbol{g}}$. It is easy to show from eqs 5 and 7 that $\vec{R} = \vec{R}(-\vec{g}_x$ cos ω_3 sin $\omega_2 + \vec{g}_y$ sin ω_3 sin $\omega_2 + \vec{g}_z$ cos ω_2), so that the spherical polar angles of $\vec{R}$ with respect to $\vec{\boldsymbol{g}}$ are $\Phi = \pi - \omega_3$ and $\Theta = \omega_2$. Note that the map of the polar angle $\Phi \rightarrow -\Phi$ is a symmetry operation due to the choice of positioning two protons in the xz-plane. This symmetry simplifies the computations discussed below. The body-fixed Hamiltonian[10] describing the complex can be written as

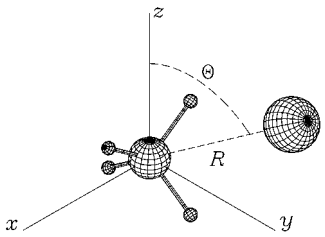

Figure 1. Molecule fixed frame for the Ar−CH_4 complex. Protons 1 and 2 are in the xz-plane above the xy-plane and have negative and positive x-components, respectively. Protons 3 and 4 are in the zy-plane below the xy-plane and have negative and positive y-components, respectively. The carbon atom is positioned at the origin.

$$H = T + \frac{1}{2\mu_{AB}R^2}\left[-\hbar^2\frac{\partial}{\partial R}R^2\frac{\partial}{\partial R} + (J^{\mathrm{tot}})^2 + j^2 - 2\boldsymbol{j}\cdot\boldsymbol{J}\right] + V(R, \omega_2, \omega_3) \tag{8}$$

where T is the kinetic energy of CH_4, $\boldsymbol{J}^{\mathrm{tot}}$ is the total angular momentum of the complex, $\boldsymbol{J} \equiv [\mathrm{R}_z(\alpha)\mathrm{R}_y(\beta)]^{\mathrm{T}}\boldsymbol{J}^{\mathrm{tot}}$, $\boldsymbol{j}$ is the angular momentum operator of methane (which has the usual space-fixed rigid rotor form), and $j^2 \equiv \boldsymbol{j}\cdot\boldsymbol{j}$. Finally, μ_{AB} is the reduced mass of the Ar−CH_4 complex. Note that $\boldsymbol{J}^{\mathrm{tot}}$ and its projection J_z on $\vec{e}_z$ are exact constants of the motion with conserved quantum numbers J and M, respectively.

In the ground vibrational state of CH_4, we simply have the spherical top Hamiltonian for the free methane, namely, $T = B_0\, j^2$. In the vibrationally excited v_3 mode, there is first-order Coriolis coupling between the vibrational angular momentum $\boldsymbol{l}^{\mathrm{vib}}$ and the body-fixed angular momentum $\boldsymbol{j}^{\mathrm{BF}}$ of methane.[12] That is, when the molecule is in the v_3 mode, the kinetic energy T takes the form

$$T = B_3 j^2 - 2\zeta_3 B_3 \boldsymbol{l}^{\mathrm{vib}}\cdot\boldsymbol{j}^{\mathrm{BF}} \tag{9}$$

Experimental values were used for the constants entering the kinetic energy. They are $B_0 = 5.2410356$ and $B_3 = 5.19970$ cm^{-1} for the ground state[100] and the v_3 excited[101] state, respectively. The Coriolis parameter ζ_3 was fixed[101] at 0.05533, and the following masses[102] were used: ^{40}Ar, 39.9627 amu; ^{1}H, 1.007825 amu; and ^{12}C, 12 amu.

As stated above, the potential $V(R, \Theta, \Phi) = V(R, \omega_2, \omega_3)$ was obtained in ref 96 by means of the SAPT method.[103] Five intermolecular distances, ranging from $R = 5$ to 10 bohr, were considered and for each distance six sets of polar angles. The T_d symmetry was used to section each sphere of constant R into 24 irreducible segments. The six sets of polar angles covered such a segment. Long-range dispersion and induction coefficients were computed separately and held fixed in the analytic fit of the surface. The

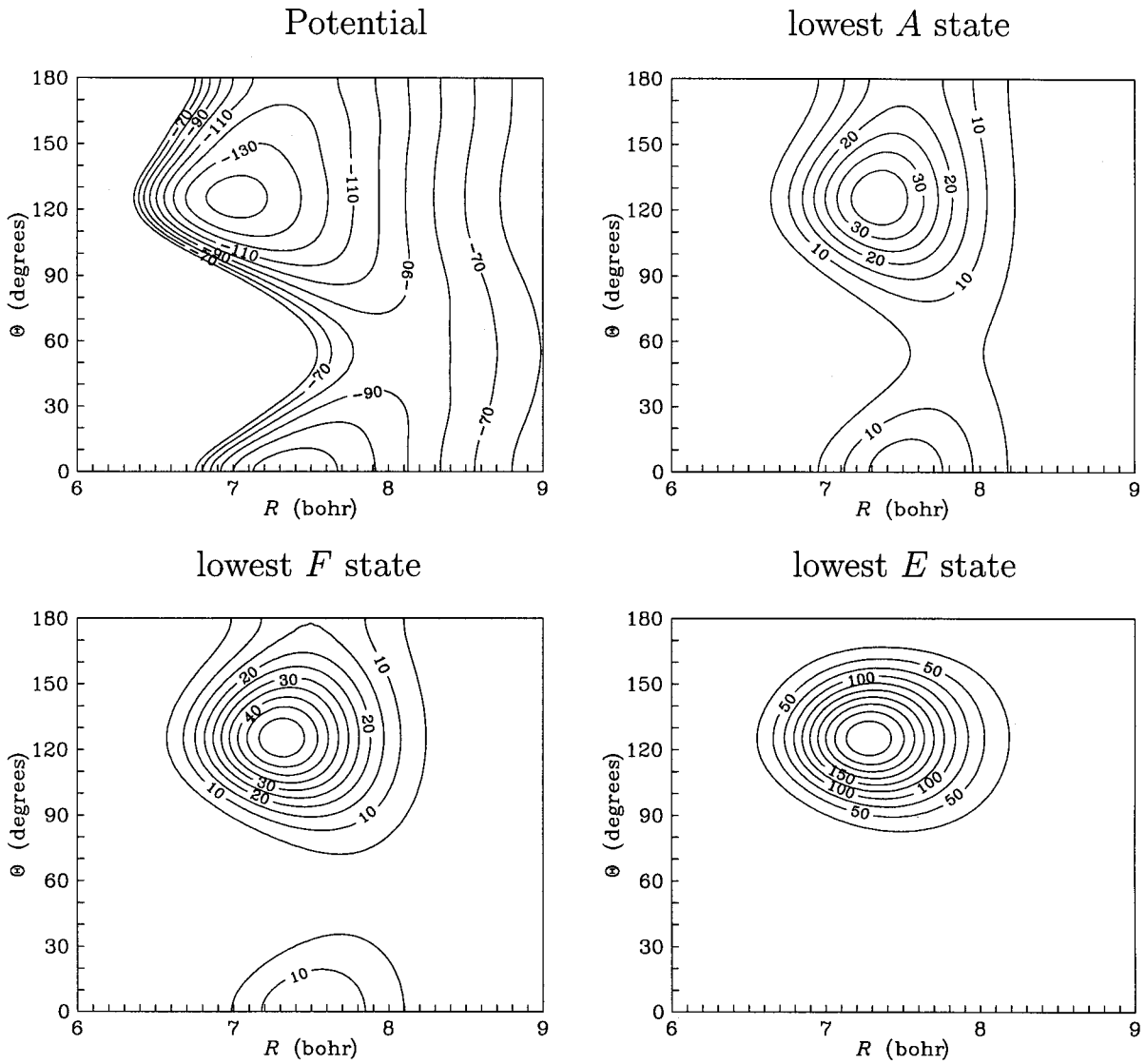

Figure 2. Cuts through the ab initio Ar−CH_4 potential-energy surface (in cm^{-1}) and the lowest *A*, *F*, and *E* state rovibrational wave functions of Ar−CH_4 at $\Phi = 0°$. The wave functions squared are shown (in 10^{-6} $bohr^{-3}$); the degenerate states have been averaged over their components. The *A* and *F* state wave functions have quantum numbers $J = K = 0$, while the *E* state wave function has $J = 1$ and $K = -1$ or 1. The azimuthal angle $\Phi = 0°$. Note that $\Theta = 54.74°$ corresponds to a vertex position of argon (a linear C−H···Ar configuration), $\Theta = 125.26°$ to a facial position (between three C−H bonds), and $\Theta = 0°$ and 180° to edge positions (Ar, C, and two H atoms in one plane).

angular part of both the long- and the short-range interaction was expanded in a set of A_1 tetrahedral harmonics, i.e., linear combinations of spherical harmonics transforming as A_1 under T_d. See Figure 2 for a cut through the surface for $\Phi = 0°$.

After having defined the Hamiltonian for the nuclear motion of the Ar−CH_4 complex, we turn to the computation of its bound states. These were obtained variationally and to that end a body-fixed basis was used, namely

$$|n, j, k, K\rangle = \left[\frac{(2j+1)(2J+1)}{32\pi^3}\right]^{1/2} \chi_n(R) D^{(j)}_{Kk}(\boldsymbol{\omega})^* D^{(J)}_{MK}(\alpha, \beta, 0)^* \quad (10)$$

where we suppress J and M in the short-hand notation on the left-hand side, since these quantum numbers are constant throughout the calculations. The functions $D^{(l)}_{mm'}$ are elements of Wigner *D*-matrices (symmetric top functions).[37] Bound-state levels were calculated for total angular momentum J up to and including $J_{max} = 7$. Angular basis functions for the CH_4 monomer were included up to and including $j_{max} = 12$. The radial functions, $\chi_n(R)$, are Morse-type oscillator functions;[38] they were included through $n_{max} = 10$. In the case of methane in its ground vibrational state, the basis of eq 10 is used as its stands, while for the vibrationally excited states it is multiplied by $|v_3, m_l\rangle$, thus tripling the dimension of the Hamilton matrix. These v_3 functions are eigenfunctions of the operator $(l^{vib})^2$ with eigenvalue $l(l+1)$ with $l = 1$ and of l_z^{vib} with eigenvalues $m_l = 1$, 0, and −1, respectively. These eigenfunctions behave in the usual manner under the step-up and step-down operators $l_\pm^{vib}$. It was assumed that the intermolecular potential is the same for CH_4 in the ground vibrational state and in the v_3 excited state.

Table 1. Lowest Energy Levels of Ar−CH_4 Calculated from the Ab Initio SAPT Potential[a]

j	$\|K\|$	n	Γ[b]	$J=0$	$J=1$	$J=2$
0	0	0	$A_{1,2}$	−90.473	−90.289	−89.922
1	0	0	$F_{2,1}$	−81.738	−81.593	−81.295
1	1	0	$F_{1,2}$		−80.645	−80.276
1	1	0	$F_{2,1}$		−80.606	−80.169
2	1	0	E		−68.702	−68.345
2	2	0	E			−63.830
0	0	1	$A_{1,2}$	−61.267	−61.097	−60.757
2	2	0	$F_{2,1}$			−60.065
2	2	0	$F_{1,2}$			−60.064
2	0	0	$F_{2,1}$	−58.571	−58.499	−58.280
2	1	0	$F_{1,2}$		−57.952	−57.561
2	0	0	E	−58.065	−57.882	−57.517
2	1	0	$F_{2,1}$		−57.857	−57.350
2	2	0	E			−52.316
1	1	1	$F_{1,2}$		−49.653	−49.309
1	1	1	$F_{2,1}$		−49.647	−49.293
2	1	0	E		−45.904	−45.550
1	0	1	$F_{2,1}$	−45.885	−45.708	−45.355

[a] Energies are in cm^{-1}, relative to the dissociation limit. The CH_4 monomer is in the vibrational ground state. [b] For the A and F irreps, the first subscript on the symbol refers to states with even J and the second to states with odd J.

Since $|K|$ is a reasonably good quantum number, it is advantageous to use a basis that contains K explicitly because it allows the calculation of the VRT states to be performed in two steps. First, the off-diagonal Coriolis interactions terms in $\boldsymbol{j}\cdot\boldsymbol{J}$ were neglected, which implies that K is an exact quantum number and that levels with $\pm K$ are degenerate. The Hamiltonian was diagonalized in the basis of eq 10 for constant J and K, with K ranging from −min (J, K_{max}) through +min (J, K_{max}). The maximum absolute value of K was fixed at $K_{max} = 3$. In the second step the off-diagonal Coriolis interaction terms in the Hamiltonian are included, which mix functions with different K. This Hamiltonian was diagonalized in the basis formed by a truncated set of eigenfunctions generated in the first step. In these dynamical calculations the symmetry was not used explicitly, but the resulting states are symmetry adapted, of course.

Since we assume that, apart from weak Coriolis coupling, the internal v_3 vibrational mode of the CH_4 monomer is decoupled from the intermolecular modes i and i', the frequency of the transition ($v = 0$, i, $J \rightarrow v_3 = 1$, i', J') is given by

$$\nu(v=0,\, J,\, i \rightarrow v_3=1,\, J',\, i') = E^{J'}_{v_3=1,i'} - E^{J}_{v=0,i} + \bar{\nu}_3 \tag{11}$$

where $E^J_{v,i}$ denotes the energy of the state labeled by (v, i, J) with respect to the dissociation limit and $\bar{\nu}_3$ is the monomer v_3 transition frequency, which was fixed[101] at 3019.4883 cm^{-1}.

In Table 1 we report the bound levels of the Ar−CH_4 complex for $J = 0$, 1, and 2. The states in this table are labeled by their symmetry, which was assigned by inspection, and by the j, K, and n quantum numbers of the dominant contributions, where n refers to the intermolecular stretch. The A, F, and E symmetries are associated with different nuclear spin species. Figure 2 shows contour plots of the lowest A, F, and E wave functions and—for comparison—the potential. We see that the A-state is highly delocalized with a maximum amplitude not quite in the global minimum of the potential but at a slightly larger R-value. The potential well is rather narrow, so that localization of the wave function in this minimum would give a considerable increase of kinetic energy, which explains the outward shift of the position of maximum amplitude. The same observations can be made for the F-state, although the density in the intermediate region, connecting the global minima via the saddle point at $\Theta = 0°$, is somewhat lower than that of the A-state. The E-state, on the other hand, is completely localized near the minimum. This is due to the fact that the first and dominant anisotropic term in the potential (V_3) interacts in first order with this state; see ref 98 for the group theoretical explanation why E-states interact in first order while A and F states do not.

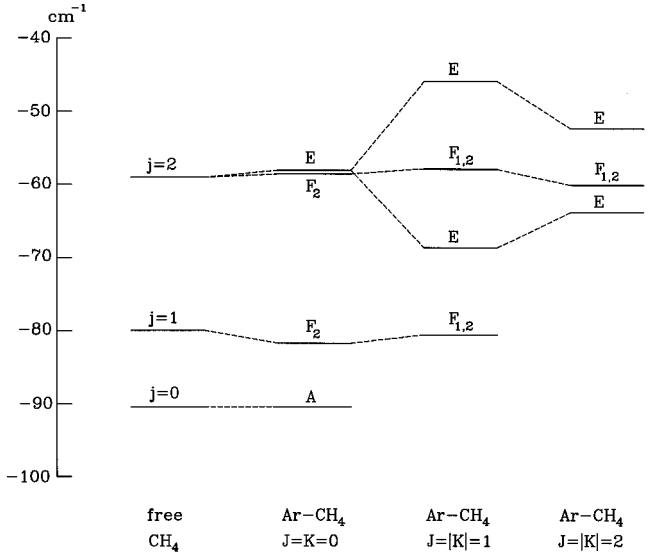

Figure 3. Selection of energy levels of Ar−methane corresponding to the lowest three rotational levels of free CH_4. The energy of the lowest $J = 0$ level of the complex (−90.473 cm^{-1}) was added to the monomer levels. Note that for $|K| > 0$, the F_1 and F_2 levels are nearly degenerate.

Figure 3 shows the energies of the lowest bound states of each symmetry. It is clear from this energy-level diagram that the $K = 0$ states essentially follow the free rotor energy pattern, namely, $E_j = Bj(j + 1)$, and that j is a good approximate quantum number for these states. This shows that the CH_4 monomer behaves like a slightly hindered rotor within the complex. The E and F levels associated with $j = 2$ and $K = 0$ are split by 0.51 cm^{-1} under the influence of the potential.

The levels of F symmetry with $|K| > 0$ are only slightly split by the potential, the splitting being approximately 0.1 cm^{-1}. On the other hand, the E levels with $|K| > 0$ are split by as much as 10−20 cm^{-1}. Furthermore, the splitting for the E levels with $|K| = 1$ is nearly twice as large as that for $|K| = 2$, in agreement with the group theoretical analysis of ref 98. For $J = 2$, for instance, this ratio is equal to 1.98. From these results, we can conclude that $|K|$ is a good approximate quantum number. Although the A and F states with different $|K|$ are nearly degenerate, there are clearly large differences for the E states

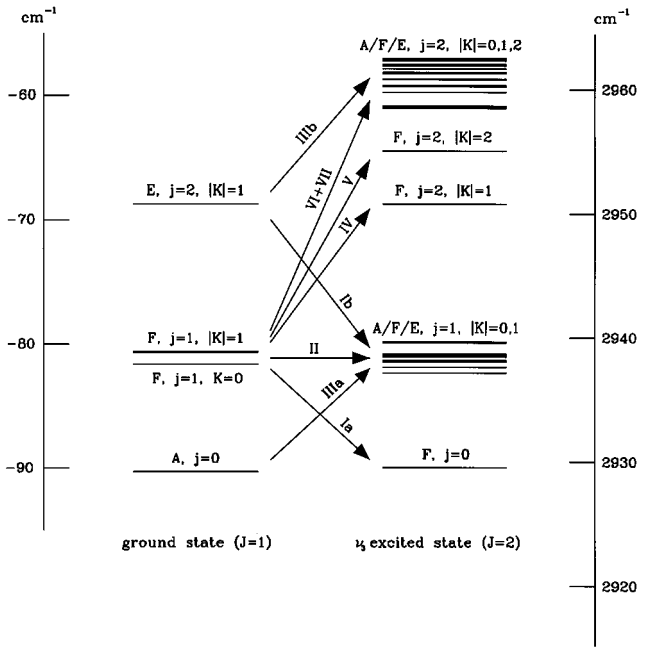

Figure 4. Transitions between ground- and excited-state levels of Ar−methane, leading to bands I−VII shown in Figure 5. For clarity, we depicted only the ground-state levels with $J = 1$ (energy scale on the left-hand side) and the ν_3 excited-state levels with $J = 2$ (energy scale on the right-hand side).

owing to this first-order splitting. Therefore, the conclusion that Ar−CH_4 is an almost free internal rotor, as suggested by the levels with $K = 0$, has to be qualified. The levels with $|K| \neq 0$ show that the choice of a body-fixed embedding for the basis functions is legitimate. Since the rotational constant of methane and the splittings of the levels with different K are of the same order of magnitude, we have here one of the few cases where a van der Waals complex is really intermediate between a rigid rotor and a free internal rotor.

In a previous study[104] Hutson and Thornley obtained the bound levels of the Ar−CH_4 complex from close-coupling calculations. These authors applied the semiempirical potential of Buck et al.[86] (BKPS potential) and found bound-state levels that are 4−5 cm^{-1} lower than in the work of ref 98. The cause of this deviation is that the SAPT potential has a shallower well than the BKPS potential. This is illustrated by the well depth of the isotropic part, which is 104.3 cm^{-1} for the SAPT potential, 12 cm^{-1} less than for the BKPS potential. From the A levels listed in Table 1, the stretching frequency of Ar−CH_4 is estimated to be 29 cm^{-1}. This is approximately 4 cm^{-1} lower than the value reported in ref 104.

In Figure 4 we show the lowest bound-states levels with $J = 1$ for the ground state and with $J = 2$ for the case where the CH_4 monomer is in the ν_3 vibrationally excited state. Since this ν_3 mode is triply degenerate, the number of levels per interval is about three times as large as that for the ground state, as is clearly shown in Figure 4. Given that the ν_3 mode is of F_2 symmetry, all symmetry labels Γ change according to the direct product $\Gamma \times F_2$ of the group T_d. For $\Gamma = A_1$ (or A_2) and E, this direct product results in one and two F states, respectively, while for the F states the coupling with the ν_3 mode gives one A, one E, and two F levels. We see the symmetry labels for the total wave function and the dominant j component in Figure 4. Particularly for the higher levels, states with van der Waals components of different symmetry are mixed. As was also the case for the ground state, j, $|K|$, and n are approximately good quantum numbers. The only exception is formed by the two states of F symmetry near −57.6 and −57.0 cm^{-1} with $|K| = 0$ and 1, respectively, which are mixed to a great extent. Note that the van der Waals parts of these two states are of different symmetry, viz. F and E, respectively. The Coriolis coupling with the vibrational angular momentum of CH_4 affects the levels only by a relatively small amount. Splittings are typically 1−2 cm^{-1} or less.

3.2. The Spectrum and Its Assignment

As described in the previous section, one has to compute the square of transition dipole moments in order to obtain spectral intensities. In the present case, the transitions are from the ground vibrational to the ν_3 excited mode of the methane simultaneous with excitations of the intermolecular modes. The laser field is by definition in the space-fixed (SF) frame, and since the wave functions are expressed in molecule-fixed (MF) basis functions, we must transform

$$\mu_0^{\mathrm{SF}} = \sum_{m',m''} D^{(1)}_{0m'}(\alpha, \beta, 0)^* D^{(1)}_{m'm''}(\boldsymbol{\omega})^* \mu^{\mathrm{MF}}_{m''}(\boldsymbol{Q}) \quad (12)$$

where $\boldsymbol{Q}$ stands for the normal modes of methane. The assumption here is that $\boldsymbol{\mu}^{\mathrm{MF}}$ does not depend on the interaction, i.e.,

$$\langle v_3 = 1,\, m_l | \mu^{\mathrm{MF}}_{m''}(\boldsymbol{Q}) | v = 0 \rangle = \delta_{m l, m''} \mu_{10} \quad (13)$$

The reduced matrix element μ_{10} is independent of m_l, and since one is usually only interested in relative intensities, it is taken to be unity. The matrix elements of the operator in eq 12 in the basis of eq 10 follow easily from the Wigner−Eckart theorem.[37] As usual, the transition dipole matrix elements are inserted into an expression for the intensities, see ref 10. The temperature of the beam was taken to be 1 K. In addition, the spin statistical weights[105] enter this expression and have been included in all the calculated spectra, namely, 5, 5, 2, 3, and 3 for A_1, A_2, E, F_1, and F_2, respectively. The dipole selection rules are $A_1 \leftrightarrow A_2$, $E \leftrightarrow E$, and $F_1 \leftrightarrow F_2$, i.e., the nuclear spin species A, E, and F are conserved under dipole transitions. The theoretical infrared spectrum of Ar−CH_4, calculated from the ab initio SAPT potential, is presented in Figure 5b in the same frequency range as the experimental spectrum shown in Figure 5a.

All of the bands observed in the experimental spectrum are reproduced in the theoretical spectrum and were considered one at a time in ref 99. For this purpose the various bands were labeled I−VII, see Figure 5. The corresponding transitions are indicated in Figure 4. From the theoretical calculations, we find that the most intense feature in the spectrum,

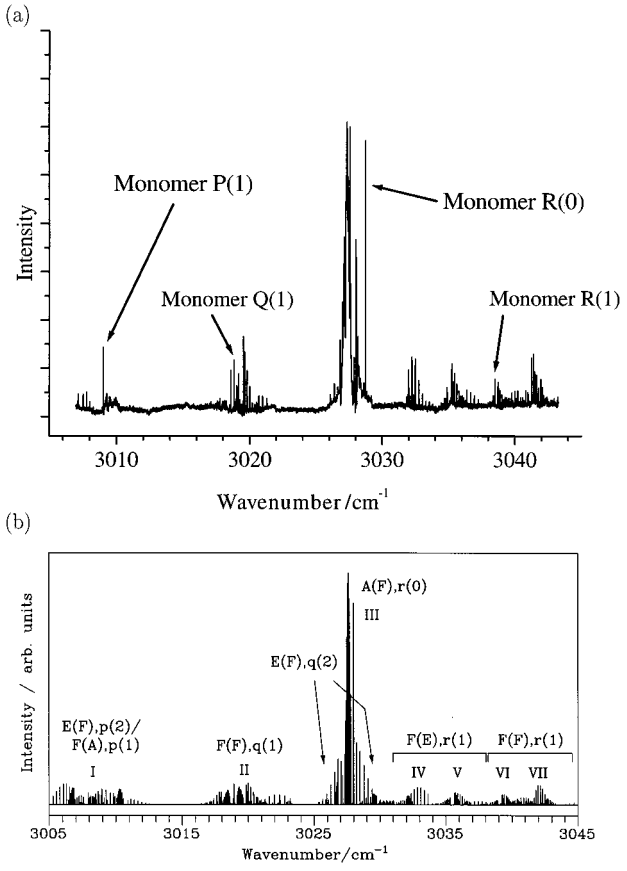

Figure 5. (a) Broad scan of experimental infrared spectrum of Ar−methane. (b) Ab initio calculated spectrum at $T = 1$ K. The symmetry species is indicated; initial and final states are of the same symmetry. Between parentheses is the symmetry of the van der Waals component of the final state. The symbols $p(j)$, $q(j)$, and $r(j)$ refer to transitions from an initial state of certain j, the angular momentum of the methane monomer.

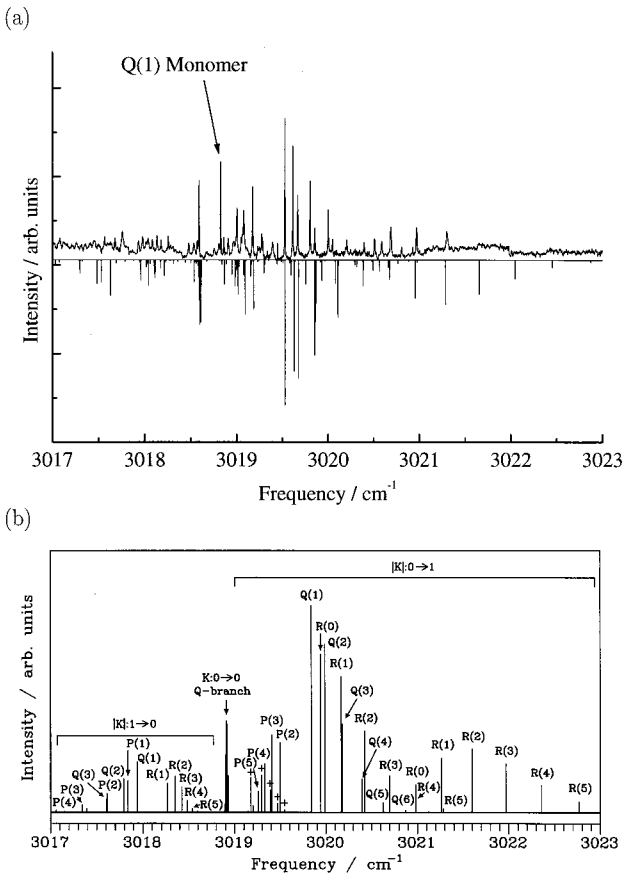

Figure 6. (a) Experimental spectrum of Ar−methane in the region 3017−3023 cm^{-1}. The inverted stick spectrum is the theoretical spectrum of Figure 5b, red shifted by −0.311 cm^{-1}. (b) Calculated spectrum (F states) in this region (band II). Lines indicated by + symbols correspond to $|K|:1 \rightarrow 1$ transitions with $\Delta J = +1$, the leftmost one being the $R(1)$ line.

namely, the broad band near the $R(0)$ transition of the monomer, primarily arises from the A states ($j = 0$). As noted in the figure, there are also some weaker transitions in this region, assigned to the E states ($j = 2$). Most of the other bands in the spectrum are associated with the F states ($j = 1$).

As an example of a more detailed comparison between theory and experiment, we refer to Figure 6. It shows an expanded view of band II from 3017 to 3023 cm^{-1}. This band is assigned to F states corresponding to $j'' = 1$ and $\Delta j = 0$, correlating with the Q branch of the methane monomer. The lower panel shows the theoretical spectrum, obtained directly from the potential surface, along with the assignments given above the individual lines. In the upper panel, the experimental spectrum is compared with the same calculated spectrum (inverted) that has been shifted in absolute frequency to give the best agreement with experiment. In this case, the calculated spectrum had to be shifted by −0.311 cm^{-1} to match the experiment. Overall, the resulting agreement is excellent, certainly sufficient to assign most of the transitions in the experimental spectrum. The frequency offsets needed to bring experiment and theory into agreement and the line width data are summarized in Table 1 of ref 99, also for the other subbands. The offsets vary for the different subbands between −0.11 and −0.68 cm^{-1}. The other subbands are detailed in ref 99.

It may be concluded that a detailed comparison between the experimental near-infrared spectrum of argon−methane and the results of a theoretical calculation led to a definite assignment of many of the bands. The spectrum is highly sensitive to the anisotropy of the argon−methane potential surface, and the agreement with the ab initio spectrum, although not quantitative, is very good.

4. Water Pair Potential and Dimer Spectrum

Thirty years of classical Monte Carlo (MC) and molecular dynamics (MD) simulations have provided much insight into the microscopic behavior of liquid water and ice. Yet, a quantitative statistical mechanical description which explains the anomalous properties of water is still lacking. There are good reasons to believe that this is mainly due to an insufficient knowledge of the intermolecular potential needed for the simulations. Ab initio calculations[106−114] have shown that the deviations of this potential from pairwise additivity are substantial and that, in particular, the three-body interactions are important. Most of the simulations used 'effective' pair potentials: simple empirically parametrized model poten-

tials in which the many-body interactions are represented implicitly. Some authors[115,116] used so-called polarizable potentials, which explicitly include the many-body polarization (induction) effects. Even the latter are based on simplified models, however. Moreover, it was found in some of the ab initio calculations[107,113,114] that, in addition to the polarization effects, also the nonadditive exchange forces are significant. It is therefore not surprising that the results of simulations with these model potentials are usually valid only for a restricted set of properties—often those to which the empirical parameters have been fit—in a limited range of temperatures and pressures. Simulations of more general validity will have to start from the *real* water pair potential and explicitly include the important three-body interactions.

Very precise information about the pair and many-body interactions can be extracted, in principle, from the spectra of small water clusters. Such clusters have been prepared in supersonic molecular beams and extensively studied by microwave and (far-)-infrared spectroscopy.[117−147] Especially through the work of the Saykally group at Berkeley, a systematic set of high-resolution spectral data on water clusters, from the dimer to the hexamer, has recently been collected. The spectra of these very cold clusters correspond directly to the transitions between their quantum levels, without the statistical−thermodynamical averaging that complicates the interpretation of experimental data for the condensed phases. It was evident from the vibration−rotation−tunneling (VRT) level patterns observed in the spectra that the dynamical processes found in liquid water,[148−150] which involve the breaking and reconstruction of hydrogen bonds, also occur in these clusters. Because of the absence of thermal motions in the clusters, the bond breaking is solely due to quantum mechanical tunneling through the barriers in the potential that separate multiple equivalent hydrogen-bonded equilibrium structures. While the equilibrium geometries of small water clusters can be reasonably well predicted from fairly simple model potentials, it was demonstrated[144,151,152] that the VRT level splittings form an extremely sensitive probe of the detailed shape of the intermolecular potential surface. Hence, the most critical test of the pair potential—especially in the physically important attractive region—is the dimer spectrum, while the trimer spectrum probes both the pair potential and the three-body forces. The actual use of dimer spectroscopic data to test and improve the water pair potential, and the methods needed to perform such tests, form the subjects of the present section of this review.

4.1. Tunneling Processes in the Water Dimer

The water dimer, along with the HF dimer, is a textbook[15] example of tunneling in hydrogen-bonded systems. In such dimers, the monomers are free to find orientations that maximize the strength of the hydrogen bond and the dimer equilibrium geometries may be considered as ideal hydrogen-bonded structures. The water dimer equilibrium structure was predicted by ab initio calculations[153−156] and experimentally determined in 1974 by molecular beam electric resonance spectroscopy.[117] The first full water pair potential obtained through ab initio calculations[157] dates back to 1976, see ref 158 for a review of the extensive ab initio literature.

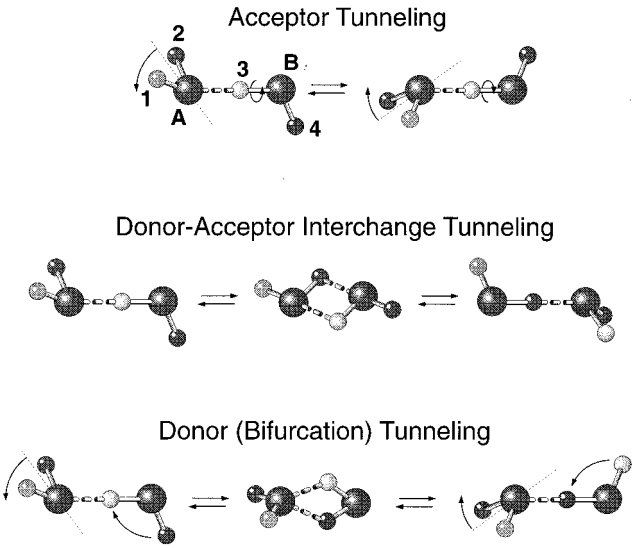

Figure 7. Three different hydrogen-bond rearrangement processes in the water dimer which connect the eight equivalent, permutationally distinct, equilibrium structures: acceptor tunneling with PI operation (12), donor−acceptor interchange tunneling with PI operation (*AB*) (1423), and bifurcation (or donor) tunneling with PI operation (12) (34).

It was shown by the now classical work of Dyke and co-workers[117,159] and in a large number of more recent papers[118−123,126−129,144,147] that the 6-dimensional intermolecular potential surface of the water dimer has eight equivalent—permutationally distinct—global minima which are all connected by tunneling. The equilibrium structure has reflection symmetry, and its point group is isomorphic to the permutation−inversion group $G_2 = \{E, (12)^*\}$, with 1 and 2 labeling the two 'free' acceptor protons. Also, the PI symmetry group G_{16} associated with the tunneling processes was discussed[159] already in 1977. The VRT levels of the water dimer can be labeled by the irreducible representations (irreps) of this PI group. Three different tunneling processes allow the dimer to interconvert between the eight minima, see Figure 7. The first process, acceptor tunneling, does not require complete breaking of the hydrogen bond and has the lowest barrier: 156 cm^{-1} in the SAPT-5s potential of ref 114 and 152. (This potential was named SAPT-5s because it is the analytic representation of a large number of data points computed ab initio by symmetry-adapted perturbation theory (SAPT) in the form of a site−site model with eight sites per molecule, five of which are symmetry distinct.) The permutation made feasible by acceptor tunneling is (12), but note that the minimum energy pathway for this process is not simply the rotation of the acceptor about its C_2 axis. Acceptor tunneling yields a relatively large splitting between the $A_1^{\pm}$, $E^{\pm}$, $B_1^{\pm}$ levels, on the one hand, and the $A_2^{\mp}$, $E^{\mp}$, $B_2^{\mp}$ levels, on the other. The magnitude of this splitting is about 10 cm^{-1} in $(H_2O)_2$ and about 2 cm^{-1} in $(D_2O)_2$ but depends strongly on the value of the rotational

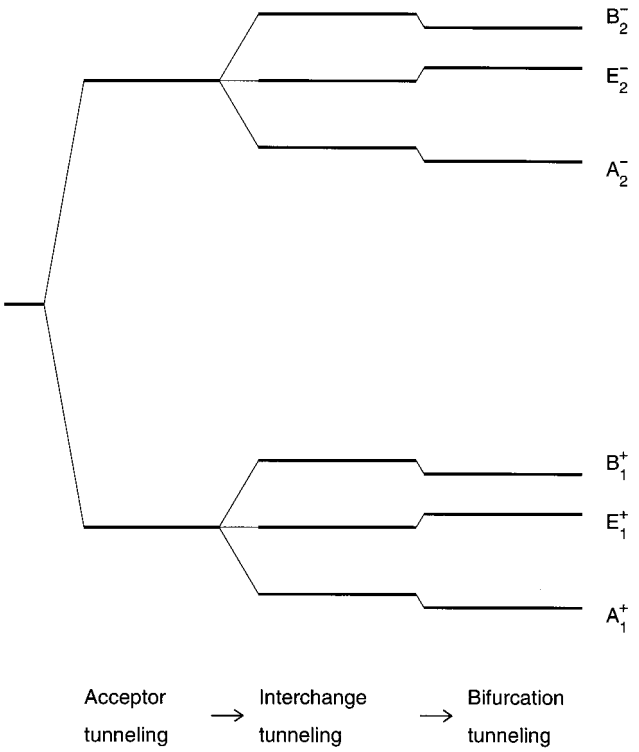

Figure 8. Tunneling splitting pattern of the rovibrational levels of the water dimer for $J = 0$ by the mechanisms shown in Figure 7.

quantum number K. The water dimer is a prolate near-symmetric rotor, and K is the projection of the total angular momentum $\boldsymbol{J}$ on the long axis—the a axis. The second and third processes, donor−acceptor interchange and bifurcation tunneling, involve hydrogen-bond breaking with higher barriers: 185 and 636 cm^{-1}, respectively, in the same SAPT-5s potential. The permutation associated with donor−acceptor interchange tunneling is $(AB)(1423) = (AB)(13)(24)(12)$, i.e., the simultaneous interchange of the oxygen nuclei A and B and the protons 1, 2 and 3, 4 of the monomers A and B, combined with the acceptor tunneling permutation (12). This process leads to splittings between the A, E, and B levels which are typically 0.3 cm^{-1} in $(H_2O)_2$ and 0.02 cm^{-1} in $(D_2O)_2$. The permutation associated with bifurcation tunneling is (12)(34), where (34) exchanges the bound and free proton of the donor. This process does not cause a further splitting of the rovibrational levels but leads to a shift of the E levels relative to the A and B levels. This shift is very small: about 0.02 $cm^{-1} \approx 700$ MHz for $(H_2O)_2$ and 7 MHz for $(D_2O)_2$. The three tunneling pathways are illustrated in Figure 7, and the typical level splitting pattern is shown in Figure 8.

A detailed qualitative model that explains the tunneling splitting pattern of the water dimer levels in terms of a number of empirical parameters was developed by Coudert and Hougen.[160,161] They used the water pair potential of Coker and Watts[162] to determine the three tunneling paths and the internal-axis method (IAM)[163] to determine the amount of angular momentum generated by the tunneling motions and the J, K dependence of the splittings. This model was used as a basis to fit tunneling levels to the measured spectra;[121−123] the result of this fit is a set of empirically determined parameters which completely determine all the tunneling levels for arbitrary J and K.

4.2. Dynamics Calculations

After a more approximate 5-dimensional treatment by Althorpe and Clary[164,165] in 1994 and some rigid-body quantum Monte Carlo calculations[166] giving estimates of the tunneling splittings, Leforestier et al.[167] were the first in 1997 to calculate nearly exactly the VRT levels of the water dimer from a 6-dimensional potential. They implemented a split Wigner pseudospectral method.[168] Somewhat later, the same problem was solved by Chen and Light[151] with the use of a sequential diagonalization−truncation method and by Groenenboom et al.,[152,169] who developed a very efficient implementation of a conventional variational method. All these methods start from the Hamiltonian for two rigid monomers in body-fixed dimer coordinates

$$H = T_A + T_B + \frac{1}{2\mu_{AB}R^2}\left[-\hbar^2\frac{\partial}{\partial R}R^2\frac{\partial}{\partial R} + J^2 + j^2 - 2\boldsymbol{j}\cdot\boldsymbol{J}\right] + V(R, \boldsymbol{\omega}_A, \boldsymbol{\omega}_B) \quad (14)$$

This expression may be considered a generalization of the Hamiltonian used for atom−molecule complexes such as Ar−CH_4, see eq 8 of section 3. The two-angle embedded dimer frame $\vec{\boldsymbol{f}}$ is the same, and the monomer frames $\vec{\boldsymbol{g}}_A$ and $\vec{\boldsymbol{g}}_B$ are similar to the monomer frame $\vec{\boldsymbol{g}}$ used in that section. R is the distance between the centers of mass of the monomers, and $\boldsymbol{\omega}_A$ and $\boldsymbol{\omega}_B$ with $\boldsymbol{\omega} \equiv (\omega_1, \omega_2, \omega_3)$ are the Euler angles describing the orientations of $\vec{\boldsymbol{g}}_A$ and $\vec{\boldsymbol{g}}_B$ with respect to the dimer frame $\vec{\boldsymbol{f}}$. The potential $V(R, \boldsymbol{\omega}_A, \boldsymbol{\omega}_B)$ contains five angular coordinates, because it depends on ω_{1A} and ω_{1B} only through the difference $\omega_{1A} - \omega_{1B}$. The operator $\boldsymbol{J}$ represents the total angular momentum, $\boldsymbol{j} = \boldsymbol{j}_A + \boldsymbol{j}_B$ is the sum of the monomer angular momenta, and μ_{AB} is the dimer reduced mass. The kinetic-energy operator of monomer X (= A or B) is given by

$$T_X = A_X(j_{Xx}^{\mathrm{BF}})^2 + B_X(j_{Xy}^{\mathrm{BF}})^2 + C_X(j_{Xz}^{\mathrm{BF}})^2 \quad (15)$$

with the rotational constants A_X, B_X, and C_X. The Hamiltonian in eq 14 has been derived by Brocks et al.[23] with the use of chain rules. An alternative derivation is given in Appendix A-4 of ref 10.

Another common feature of the implementations of refs 167 and 152 is the use of a coupled product basis of symmetric rotor functions—Wigner D-functions[37]—for the angular coordinates

$$|j_A, k_A, j_B, k_B, j_{AB}, K; J, M\rangle = \left[\frac{(2j_A+1)(2j_B+1)(2J+1)}{256\pi^5}\right]^{1/2} \times \sum_{m_A m_B} D^{(jA)}_{m_A k_A}(\boldsymbol{\omega}_A)^* D^{(jB)}_{m_B k_B}(\boldsymbol{\omega}_B)^* \langle j_A m_A; j_B m_B | j_{AB} K\rangle \times D^{(J)}_{MK}(\alpha, \beta, 0)^* \quad (16)$$

in which $\langle j_A m_A; j_B m_B | j_{AB} K \rangle$ is a Clebsch−Gordan coupling coefficient[37] and α, β are the polar angles of the intermolecular vector $R \equiv R_{AB}$ with respect to the space-fixed frame. Reference 151 uses a similar, but uncoupled, basis. Various DVR schemes were applied for the radial coordinate R. In each of the implementations, the basis was adapted to the G_{16} symmetry and the calculations were performed for each G_{16} irrep separately. Large values of j_A and j_B (up to 12), leading to basis sizes of more than a hundred thousand, were required to converge the bound states of $(H_2O)_2$ and, especially, $(D_2O)_2$. The reasons for this slow convergence are the rather sharp minima in the potential surface at the hydrogen-bonded geometries and the occurrence of very small tunneling splittings and shifts. This made these calculations much more demanding than those for the NH_3 dimer,[63,64] which used the same Hamiltonian and basis, and were described in the 1994 *Chemical Reviews* issue on van der Waals molecules.[10]

In the split-Wigner pseudospectral method,[167] the kinetic energy is computed with the analytic basis of eq 16 while the potential is calculated on a 6-dimensional grid. The grid for the Euler angles consists of Gauss−Legendre quadrature points for the colatitudinal angles and evenly spaced points for the azimuthal angles. In the first version of this method,[167] the radial basis consisted of sine functions, with the corresponding equidistant DVR points. Later,[144] this sine function basis was contracted and the radial points were optimized by means of a variation[170] of the scheme proposed by Harris et al.[171] The eigenvalue problem is solved by the iterative Lanczos algorithm, avoiding the storage of the full Hamilton matrix. In each cycle of the iteration the matrix elements of the potential are first transformed to an uncoupled Wigner D-function product basis and next to the G_{16} symmetry-adapted and coupled angular basis. The dimension of the eigenvalue problem is determined by the latter basis.

The sequential diagonalization−truncation method[151] diagonalizes the angular part of the Hamiltonian and then the radial part in successive steps, with truncation of the intermediate eigenfunction basis. A potential-optimized DVR is used for the radial coordinate R. At each radial DVR point the 5-dimensional angular Hamiltonian is constructed with a symmetry-adapted basis of uncoupled Wigner D-function products. The kinetic energy is simple in this basis. The potential matrix elements over the angular basis are computed by numerical integration. Also, this is done in a stepwise procedure, first integrating over the three azimuthal angles and then over the two colatitudinal angles, with partial storage of the intermediate results. The primitive potential matrix elements are computed only once and saved. Up to now, this method has been restricted to $J = 0$.

In the variational method of Groenenboom et al.,[152,169] both the potential and the kinetic energy are calculated in the symmetry-adapted and coupled angular D-function basis. The potential is expanded in the same type of angular functions as the basis in eq 16. Since the potential is invariant under overall rotations, only the functions with $J = M = K = 0$ occur in its expansion. High angular functions, with j_A and j_B values up to 8 inclusive, are required to converge the expansion of the strongly anisotropic water pair potential. The angular integrals can then be reduced to products of 3-j and 9-j symbols, see our earlier review.[10] In the implementation of Groenenboom et al., these are precomputed and stored, not from the start, but at some intermediate level. For the radial basis they use a contracted sinc function DVR[172,173] obtained by solving the 1-dimensional radial Schrödinger equation. The radial potential in this equation corresponds to a fixed-angles cut of the 6-dimensional surface through the global minimum. The eigenvalues and eigenvectors are obtained by the Davidson algorithm which, just as the Lanczos scheme, avoids storage of the full Hamilton matrix.

Both Leforestier et al.[144,167] and Chen and Light[151] used their method to test several ab initio and empirical water potentials against the dimer spectrum. Although these potentials had been selected in the belief that they are the best available, they produced VRT transition frequencies which deviate from experiment by factors of 2 or 3, or even by an order of magnitude, cf. Figures 4−6 in ref 144 and Figure 12 in ref 151. Fellers et al.[34] implemented the method of Leforestier et al.[167] as part of a fitting program and obtained a 'spectroscopic' water pair potential. They started from the ab initio-based ASP−W potential of Millot and Stone[174] and optimized some of the parameters in this potential through a fit of the dimer spectrum.[34] Groenenboom et al.[152,169] used their program to test and improve a new water pair potential[114,175] obtained from extensive ab initio calculations applying symmetry-adapted perturbation theory (SAPT).[30,176]

4.3. Pair Potential and Dimer VRT Levels

As an illustration of the H_2O dimer results, we show in Figure 9 the VRT levels for J, $K \leq 2$ which Groenenboom et al.[152] calculated from the SAPT-5s ab initio pair potential of ref 114 and compare them with the experimental data.[123] The smaller splittings resulting from the donor−acceptor interchange and bifurcation tunneling are in remarkably good—within 0.03 cm^{-1}—agreement with experiment for each J, K. Also, the end-over-end rotational constant $B + C$, which is a measure for the average intermolecular distance R, and even the rotational constant A, which depends sensitively on the average orientations of the molecules in the dimer, are close to the measured values. The frequency of the 22.3 cm^{-1} transition observed between the lowest $K = 1$ and 2 levels agrees with experiment to 0.1 cm^{-1}. The larger acceptor tunneling splittings $a(K)$ have not been directly measured, but the sum $a(K = 0) + a(K = 1)$ is known. This is the only quantity that was not so well reproduced by the ab initio calculations: it is overestimated by about 40%. From a comparison with the VRT levels obtained[144,151] from previously available water pair potentials, it was concluded that the SAPT-5s potential represents a significant improvement.

The corresponding levels of the D_2O dimer are displayed in Figure 10. The acceptor tunneling split-

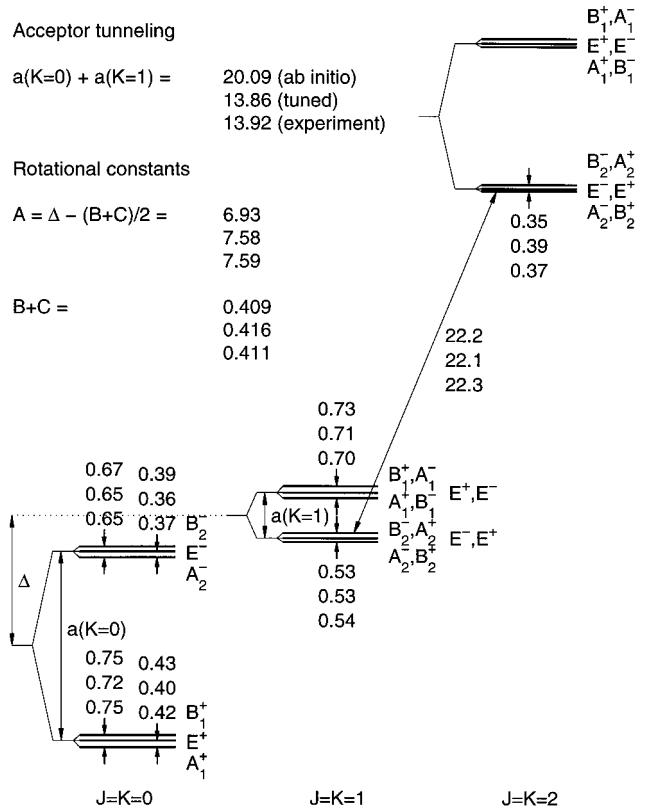

Figure 9. VRT levels of the H_2O dimer (in cm^{-1}) from converged calculations[152,169] with the SAPT-5s ab initio potential (upper numbers) and the tuned version of this potential (middle numbers) in comparison with experimental data[123] (lower numbers). The labels $A_{1,2}^{\pm}$, $B_{1,2}^{\pm}$, $E^{\pm}$ correspond to the irreducible representations of the PI group G_{16}; J and K are the dimer rotational quantum numbers. The rotational constant A is defined here (also for the experimental levels) as the difference between the average energy of all the tunneling components of the $K = 1$ levels and the average energy of the $K = 0$ levels for $J = 1$.

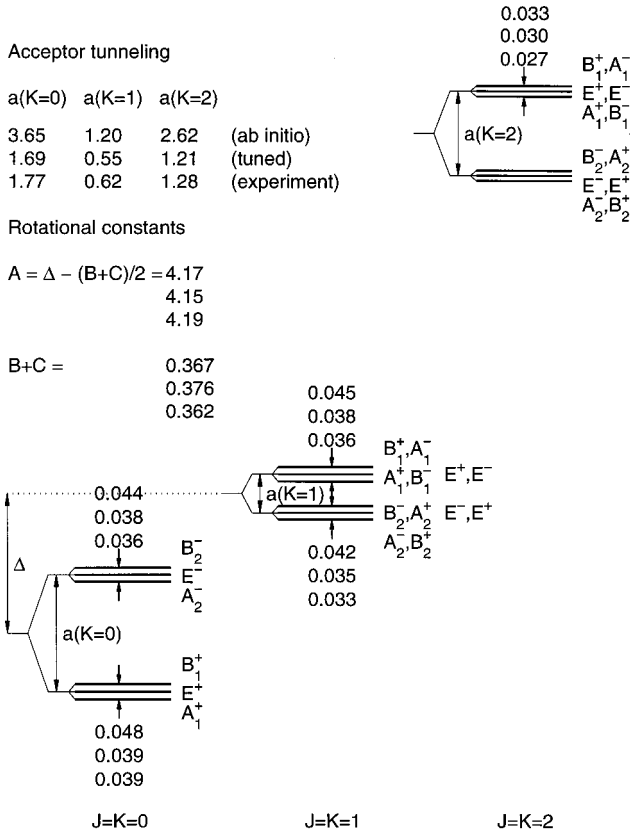

Figure 10. VRT levels of the D_2O dimer calculated[152,169] from the SAPT-5s ab initio potential (upper numbers) and from the tuned version of this potential (middle numbers) in comparison with experimental data[129] (lower numbers). The energies are drawn to scale, except for the small interchange splittings which are enlarged by a factor of 10.

tings are about 6 times smaller than those in the H_2O dimer, and the interchange splittings are smaller by factors of 10−20. Nevertheless, it was found that the SAPT-5s potential produced interchange splittings that overestimate the experimental values only by about 20%. Also, the rotational constants $B + C$ and A agreed well with experiment,[129] but the acceptor tunneling splittings deviated more strongly, just as in the H_2O dimer. Here they were overestimated by a factor of 2. However, one must keep in mind that the smaller the splittings, the more sensitive they are to the shape of the barriers in the potential.

Groenenboom et al. developed an efficient procedure[152,169] to use the spectra to improve the ab initio SAPT potential. The levels and transition frequencies of $(H_2O)_2$ were analyzed with respect to their sensitivity to changes in the linear parameters in the SAPT-5s potential. Then, these parameters were altered in such a way that—in a first-order estimate—the only quantity which deviates substantially from experiment, i.e., the acceptor tunneling splitting, becomes equal to the experimental value. Constraints in this parameter variation were that the (already accurate) interchange splittings do not change and that the parameter modification leaves the potential as close as possible to the ab initio potential. Possible small effects of the nonrigidity of the water molecules are implicitly included by this procedure. With this reparametrized SAPT-5s potential (referred to as SAPT-5s-tuned), the VRT levels of $(H_2O)_2$ were recomputed and excellent agreement with experiment was obtained, see Figure 9. The tuned potential was then used to compute the energy levels of $(D_2O)_2$ without any further reparametrization. As can be seen in Figure 10, also the results for $(D_2O)_2$ agreed very well with experiment. The 100% deviation from experiment for the acceptor tunneling splitting was reduced to 6%, and the smaller (20%) deviations of the interchange tunneling splittings were diminished to about 5%. The VRT levels of $(D_2O)_2$ calculated from the SAPT-5s-tuned potential agree equally well with the experimental data as the results obtained from the VRT(ASP−W) potential,[34] which was fit to these levels, while the representation of the $(H_2O)_2$ levels is better with the SAPT-5s-tuned potential.

Recently, a beautiful collection of spectroscopic data has been gathered[147,177,178] on the intermolecular vibrations of both $(H_2O)_2$ and $(D_2O)_2$, with frequencies up to 150 cm^{-1}. An interesting observation is that the harmonic model fails rather badly in representing these vibrations: the harmonic frequencies[179] are typically 50% larger than the experimental values. Part of the experimental data were used in the fit of the VRT(ASP−W) potential—Figure 3 in ref 34. In ref 169 it is shown that all of the measured vibra-

tional frequencies are reproduced by the SAPT-5s-tuned potential to within 3.6 cm^{-1} on average (i.e., to better than 5%). This is quite remarkable since this potential was *not* tuned to any $(D_2O)_2$ data or to any vibrationally excited levels. The second virial coefficients computed with both SAPT-5s potentials[114] are in good agreement with the best experimental data. The well depth D_e is 4.86 kcal/mol for SAPT-5s and 5.03 kcal/mol for SAPT-5s-tuned. The most reliable estimate, from the ab initio work of Klopper and Lüthi,[180] is $D_e = 5.0 \pm 0.05$ kcal/mol. See ref 114 for a discussion of the comparison of the interaction energy obtained for monomers in their (relaxed) equilibrium geometries[180] with those obtained for vibrationally averaged monomer structures.[114] The dimer dissociation energy D_0 with SAPT-5s-tuned is 3.08 kcal/mol = 1077 cm^{-1} for $(H_2O)_2$ and 3.47 kcal/mol = 1214 cm^{-1} for $(D_2O)_2$. The best experimental value[181] of D_0 for $(H_2O)_2$ is 1250 ± 175 cm^{-1}. The Fortran code that generates the SAPT-5s(-tuned) potential is deposited as AIP Document No. EPAPS: EPRLTAO-84-060018. An advantage of this potential over the potentials based on the ASP model[174] is that its analytic representation in the form of a site−site model[114,152] is considerably simpler and, hence, much cheaper to evaluate.

The work of Groenenboom et al.[152,169] has also provided a more complete characterization of the VRT levels of the water dimer. The experimentally determined transitions are sufficient to fix most but not all of the levels. In $(H_2O)_2$, for example, the sum $a(K = 0) + a(K = 1) = 13.9$ cm^{-1} has been measured but the individual values $a(K = 0)$ and $a(K = 1)$ of the acceptor tunneling splittings for $K = 0$ and $K = 1$ were not known. The value of $a(K = 0) = 9.4$ cm^{-1} first given in the experimental paper of Zwart et al.,[123] and later quoted[144,151,167] as the 'experimental' value, was actually extracted from a fit of the spectroscopic data with the approximate model of Coudert and Hougen.[160,161] A more precise value, $a(K = 0) = 11.2$ cm^{-1}, has been obtained from full 6-dimensional calculations with the SAPT-5s-tuned potential which reproduce the measured quantity $a(K = 0) + a(K = 1) = 13.9$ cm^{-1}. While one must conclude that the Coudert−Hougen model is not so reliable for the large acceptor tunneling splittings, the smaller splittings originating from donor−acceptor interchange and the shifts from bifurcation tunneling turn out to be accurately represented by this model. Also, for $(D_2O)_2$ the 'experimental' value of $a(K = 0) = 1.77$ cm^{-1} was not directly measured; it was based on the assumption[129] that the value of $a(K = 0)$ for the acceptor antisymmetric O−D stretch excited state of $(D_2O)_2$ is equal to the ground-state value. The calculations[152] demonstrated that this assumption is justified.

Summarizing this section, it may be concluded that the use of high-resolution spectroscopic data has shown that a number of the best available water pair potentials currently applied in simulations of liquid water fail to provide a good quantitative description of the intermolecular vibrations and tunneling processes occurring in the dimer. This is perhaps not so surprising for empirical 'effective' pair potentials adjusted to the properties of liquid water and ice that implicitly include the many-body interactions. However, potentials derived from ab initio calculations on the water dimer such as MCY,[157] NEMO,[182] ASP−S, and ASP−W[174] and semiempirical potentials partly based on dimer properties such as RWK[183] also emerged from this spectroscopic test rather poorly. Fellers et al.[34] obtained a 'spectroscopic' pair potential from a fit to the dimer spectrum. Groenenboom et al.[152] have shown that it is possible to obtain a water pair potential from ab initio calculations by SAPT[114] which, after some tuning, passed the very critical test of quantitatively reproducing detailed dimer spectroscopic data. In the next section, we will show how these potentials can be further evaluated by considering the water trimer spectrum and discuss the important three-body interactions.

5. Three-Body Interactions; Water Trimer Spectrum

Since the first experimental characterization of the water trimer in 1992 with high-resolution laser spectroscopy in the terahertz region,[125] a great deal of experimental results have been obtained for this complex. Four torsional bands[145] of $(D_2O)_3$ and two torsional bands[146] of $(H_2O)_3$ have been added to the first observations.[131,132] The standard procedure to use high-resolution spectral information is to make a fit of—and simultaneously assign—the raw data to extract the molecular properties: vibrational frequencies, rotational and distortion constants, etc. For 'normal' molecules, the detailed rotational structure present in the high-resolution spectra can be represented by the semirigid rotor model. This, in fact, could be taken as the definition of a 'normal' molecule. But also for the much floppier van der Waals molecules, this model—implemented in the standard spectroscopic fitting programs—is commonly used. Sometimes—we presented the example of $Ar-CH_4$ in section 3—this standard procedure fails completely. In the case of the water trimer, the spectra could be partly fit with the use of this model if many different parameters were introduced for different bands and subbands. However, even then, the accuracy of the fit remained much lower than usual and no physical meaning could be attributed to several of the terms that had to be introduced into the rotational model Hamiltonian and to the parameters extracted from such a fit. A much more satisfactory fit of the water trimer spectrum has been obtained via the derivation of a new model Hamiltonian which directly takes into account the large-amplitude internal motions and the occurrence of tunneling between multiple minima in the potential surface. This derivation, and the fit of the water trimer spectrum with the use of this rotational−tunneling model Hamiltonian, are outlined below. This has led to a complete characterization[145,146] of the torsional states of $(D_2O)_3$ and $(H_2O)_3$ up to energies near 100 cm^{-1}.

Also, the theoretical investigation of the water trimer has made much progress. Ab initio calculations[179,184] have predicted the triple hydrogen-bonded equilibrium structure of this trimer, evaluated the barriers of different rearrangement processes,[113,185]

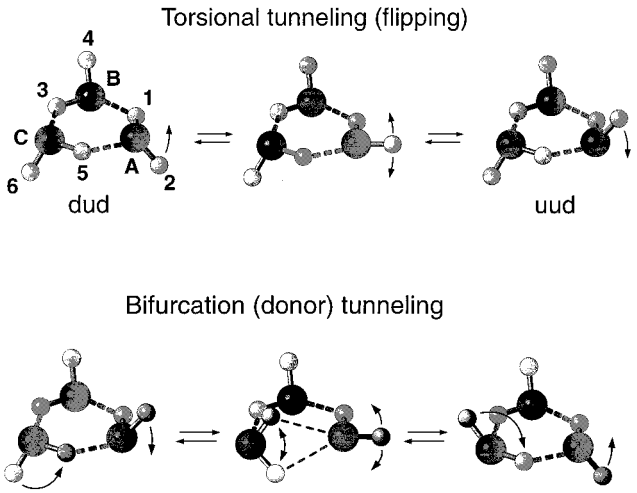

Figure 11. Hydrogen-bond rearrangement processes observed in the water trimer: torsional flips of the free hydrogens approximately about the hydrogen bonds, PI operation (*ACB*) (153) (264)*, and bifurcation tunneling, where the roles of the free and bound hydrogens of a molecule in the cluster are switched, PI operation (56)*. Each of the VRT bands reported arises from the transitions between the levels created through the torsional vibration. Bifurcation tunneling gives rise to the quartet splitting of the rovibrational lines in the spectrum.

investigated tunneling pathways,[186] and determined 3-[109,187] and 4-dimensional[188] potential surfaces. Several calculations of the VRT levels and spectrum of the water trimer[22,188−198] have been performed on these surfaces. Also, the rigid-body quantum Monte Carlo method has been applied[166,199,200] to estimate the tunneling splittings in the water trimer with the use of the ASP−W potential,[174] which includes nonadditive polarization effects. Recently, the trimer spectrum has been used, via 3-dimensional calculations of the VRT levels,[152,201] to test global water potentials. The spectrum probes both the pair potential and the three-body forces, in a much more direct and sensitive way than the data collected for liquid water and ice. The dynamical models and their application are described below.

5.1. Torsion and Bifurcation Tunneling

The minimum energy structure of the water trimer, the asymmetric ring shown in Figure 11, has been established by many ab initio calculations.[179,184,185] It is a classic example of a frustrated equilibrium. Two nonbonded ('free') hydrogens are on the same side of the oxygen plane. Experimentally it has been demonstrated that this nonplanar asymmetric structure vibrationally averages to a planar symmetric top via the torsional (flipping) motion,[124,131] illustrated in Figure 11. This large-amplitude hydrogen torsional motion creates a degenerate rearrangement mechanism, predicted as early as 1975 by Owicki, Shipman, and Scheraga.[202] All ab initio calculations performed thus far[109,113,114,185−187] indicate that this process is a very facile one. Such low-barrier rearrangement mechanisms naturally give rise to large tunneling splittings. In light of the understanding gained at present, it is perhaps more appropriate to consider the torsional (also termed 'pseudorotational') large-amplitude motions involving six equivalent minima as giving rise to a set of vibrational energy levels rather than to a genuine tunneling splitting. Experiments and theory on mixed isotope water trimers,[142,194,196,203] where the symmetry of the system is broken, confirm this analysis.

The torsional quantum levels of the water trimer have been considered at various levels of theory. The first, and simplest, was a 1-dimensional treatment by Schütz et al. who used an adjustable cosine wave as the potential.[189,190] Their calculation obtained the correct ordering of the energy levels but gave poor quantitative results. A Hückel-like treatment of the water trimer by Wales[186] gave an improved description of the energy level structure but required fitting a tunneling parameter (β_1) to the experimental data. Model torsional potential-energy surfaces fit to ab initio-calculated points were created by Bürgi et al.[187] and by van Duijneveldt-van de Rijdt and van Duijneveldt.[109] Two-dimensional[191] and 3-dimensional[192] dynamics calculations have been performed on these potential surfaces. Three-dimensional calculations that include the coupling of the torsional motions to the overall rotation of the trimer were made by van der Avoird et al.[22,193] A 4-dimensional ab initio potential which includes the symmetric intermolecular stretch coordinate has been calculated by Sabo et al.[188,197,198] and applied in a (3 + 1)-dimensional dynamical model.

The second type of internal large-amplitude motion in the water trimer is bifurcation tunneling (also called donor tunneling). This is a rearrangement process wherein a single water monomer exchanges its hydrogen-bonded and free hydrogen atoms by tunneling through a bifurcated transition state, as shown in Figure 11. It could be observed experimentally[131] and unambiguously identified, since it gives rise to a splitting of the torsional levels and transitions into quartets. The splitting between the lines in these quartets, typically about 300 MHz for $(H_2O)_3$ and about 2 MHz for $(D_2O)_3$, is much smaller than the energy gaps between the torsional levels. This is because the corresponding barrier height, calculated by Fowler and Schaefer[185] as 525 cm^{-1} (corrected for zero point effects), is substantially higher than the torsional barrier,[109,113,114,185−187] which is about 90 cm^{-1}. The splitting of the levels due to the combined effect of torsional flips and bifurcation tunneling is shown in Figure 12.

The construction of the torsional states of the water trimer, including a group theoretical treatment, has been detailed in several papers.[22,131,186,193,195] Also, the bifurcation tunneling splitting of the levels was considered in these references. Even without breaking any chemical bonds, i.e., considering a 12-dimensional intermolecular potential surface, the water trimer may, in principle, interconvert between 96 equivalent equilibrium structures. This corresponds with the permutation−inversion (PI) symmetry group G_{96}, generated by the three transpositions (12), (34), and (56) that exchange the protons (or deuterons) in the same molecule, the six permutations that permute the three molecules as a whole, and inversion, E^*. In the first pathway shown in

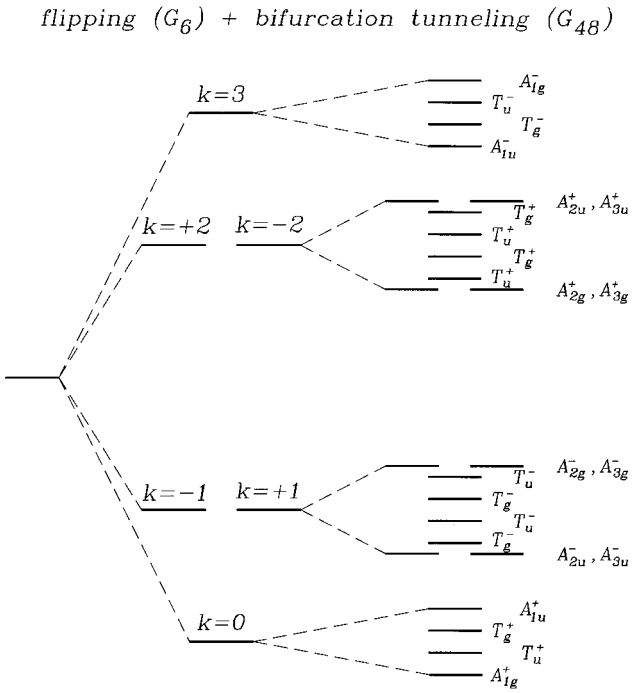

Figure 12. Tunneling splitting pattern of the rovibrational levels of the water trimer for $J = 0$ by the mechanisms shown in Figure 11. The G_{48} selection rules for dipole transitions between these levels are $\Gamma^+ \leftrightarrow \Gamma^-$.

Figure 11, a hydrogen is flipped from one side of the oxygen framework to the other through a simple low-barrier process. This connects two of the equivalent minima in the potential: the 'down−up−down' (*dud*) and the 'up−up−down' (*uud*) minimum. The endpoints of this pathway correspond to the permutation−inversion operation $F = (ACB)\ (153)\ (264)^*$, where (*ACB*) cyclically permutes the oxygen nuclei *A*, *B*, and *C* of the different monomers and (153) (264) simultaneously permutes their protons. Extending this pathway, one ultimately visits six equivalent minima through a cyclic process. The PI symmetry group associated with the torsional flipping between these six minima is the cyclic group G_6, generated by the operation F and isomorphic to the point group C_{3h}. The torsional energy levels are conveniently labeled by the quantum number $k = 0, \pm1, \pm2, 3$, which corresponds to the 1-dimensional complex irreducible representations (irreps) of the Abelian group G_6. A diagram showing the six lowest energy torsional levels is given in Figure 12. The symmetry of these levels may be compared to a Hückel treatment of the π-electron system of benzene: The levels with $k = 0$ and $k = 3$ are nondegenerate, as the *A* and *B* levels in benzene, while those with $k = \pm1$ and $k = \pm2$ are 2-fold degenerate, similarly to the benzene *E* levels.

Next we consider the bifurcation tunneling process shown in Figure 11. This rearrangement mechanism, along with the 'flipping' process discussed above, allows the water trimer to access 48 equivalent minima. The molecular symmetry group G_{48} is obtained by extending the torsional flipping symmetry group G_6 with the operations $(12)^*$, $(34)^*$, and $(56)^*$, which represent the bifurcation tunneling pathways of monomers A, B, and C, respectively. The only permutation lacking to generate the full intermolecular PI group G_{96} is the operation that inverts the directions of all three hydrogen bonds simultaneously or, alternatively, interchanges two of the three whole water molecules. This process, which would require a concerted breaking of more than one hydrogen bond, has not been observed.[131] Hence, the feasible PI group[15] is G_{48}, rather than G_{96}. The group theory for these rearrangement processes has been examined extensively in a number of papers.[22,131,186] A model has been proposed[186] and elaborated[22] which explicitly expresses the bifurcation splitting of the torsional levels in terms of two parameters β_2 and β_3, associated with two different possible bifurcation tunneling pathways (see Table 2 of ref 22). Figure 12 illustrates that the resulting splitting pattern becomes rather complicated, especially for the degenerate levels with $k = \pm1$ and $k = \pm2$.

In refs 22 and 193 the theory was further extended to include the overall rotation of the trimer, by introduction of the basis $|\Phi_k\rangle|JKM\rangle$. The functions $|\Phi_k\rangle$ represent the internal torsional motions and the symmetric rotor functions $|JKM\rangle \equiv D^{(J)}_{MK}(\alpha, \beta, \gamma)^*$ the overall rotation. The total angular momentum quantum number *J* and its space-fixed *z*-component *M* are exact constants of the motion. Functions with different *K*, the total angular momentum component along the trimer (symmetric rotor) *c*-axis, are mixed by Coriolis coupling of the internal motions with the overall rotation, see eq 23. Below we will show that this Coriolis coupling splits the $-|k|$ and $+|k|$ substates of degenerate torsional levels with $k = \pm1$ and $k = \pm2$ by a relatively large amount $\mp2\zeta CK$, linear in *K*. Another observation is that the bifurcation−rotation splitting patterns of the *A* levels are essentially different from those of the *T* levels, cf. Figures 2 and 3 in ref 22 and Tables 3 and 4 in ref 193. Both these effects will be discussed in section 5.3. By *A* levels we mean here the levels that carry the $A^{\pm}_{1g,1u}$, $A^{\pm}_{2g,2u}$, and $A^{\pm}_{3g,3u}$ irreps of G_{48} and by *T* levels those that carry the $T^{\pm}_{g,u}$ irreps of the same group. The A_2, A_3 irreps are complex conjugate irreps; the corresponding energy levels are always degenerate. Torsion−rotation functions $|\Phi_k\rangle|JKM\rangle$ carry the G_6 irrep $k - K$ (modulo 6). Transitions between the energy levels follow the dipole selection rule

$$\Delta(k - K) = 3(\text{modulo } 6) \qquad (17)$$

This rule permits the allowed transitions to be easily determined, as well as the band polarization. Parallel transitions correspond by definition to $\Delta K = 0$ and hence $\Delta k = \pm3$. Perpendicular transitions show two distinct subbands, as $\Delta k = +2$ is only allowed when $\Delta K = -1$ while $\Delta k = -2$ requires $\Delta K = +1$. The gap between these two subbands is relatively large, because of the linear Coriolis splitting $\mp2\zeta CK$ of the $+|k|$ and $-|k|$ sublevels. The G_{48} selection rules are easily expressed in terms of the irreps $A^{\pm}_{1g,1u}$, $A^{\pm}_{2g,2u}$, $A^{\pm}_{3g,3u}$, and $T^{\pm}_{g,u}$ labeling the torsion−bifurcation levels. Dipole transitions are allowed only between levels carrying the same irrep Γ except for the $\pm$ parity which must be opposite, i.e., $\Gamma^+ \leftrightarrow \Gamma^-$.

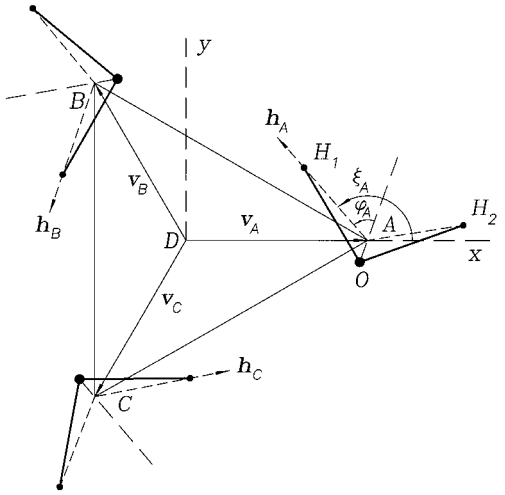

Figure 13. Planar reference geometry of the water trimer, with rotation angles $\chi_A = \chi_B = \chi_C = 0$, in the torsional model of refs 22 and 193. The fixed vectors $\boldsymbol{v}_v$ point from the trimer center of mass to the monomer mass centers, and the vectors $\boldsymbol{h}_v$ are the fixed monomer rotation axes. The x and y axes describe the rotating BF frame.

5.2. Torsional Model Hamiltonian

For the 12 intermolecular degrees of freedom of the water trimer, it is presently not possible to perform calculations as accurate as for the dimer. Both from experiment[142,145,146] and theory[22,188,193,196] it became evident, however, that there is a good adiabatic separation between the relatively fast vibrations of the triangular hydrogen-bonded—fairly rigid—framework and the slower torsional motions of the three water monomers about their hydrogen bonds. A model Hamiltonian for the torsional motions of the three monomers in a rotating water trimer was rigorously derived in ref 22. We will briefly summarize this derivation, because it refers to a constrained curvilinear internal motion in three coupled degrees of freedom and forms a nice illustration of the general theory outlined in section 2.1. It was based on the assumption that the trimer has a rigid equilateral triangular framework, held together by three hydrogen bonds, and that each of the monomers v = A, B, and C can only rotate about a single fixed axis $\boldsymbol{h}_v$, with rotation angle χ_v, see Figure 13. These internal rotations (or torsions) are hindered by a potential $V(\chi_A, \chi_B, \chi_C)$ which has minima for the external, i.e., non-hydrogen-bonded, protons (or deuterons) lying above or below the plane through the molecular centers of mass. There are six equivalent global minima, and the torsional motions involve 'flips' of the external protons between these minima. The derivation of the Hamiltonian starts with the definition of a rotating body-fixed (BF) frame, with Euler angles α, β, and γ defining the orientation of this frame with respect to a space-fixed (SF) system of axes, and the coordinate transformation

$$\boldsymbol{d}^{\mathrm{SF}}_{v,i} = \mathrm{R}_z(\alpha)\mathrm{R}_y(\beta)\mathrm{R}_z(\gamma)\boldsymbol{d}^{\mathrm{BF}}_{v,i} \qquad (18)$$

The rotation matrices R_z, etc., are defined in Appendix B, and $\boldsymbol{d}_{v,i}$ denotes the Cartesian coordinate vector of nucleus i in molecule v. Then the explicit transformation is introduced which relates the BF Cartesian coordinates to the three torsional angles χ_v

$$\boldsymbol{d}^{\mathrm{BF}}_{v,i} = \boldsymbol{v}_v + \mathrm{R}_{\boldsymbol{h}_v}(\chi_v)\mathrm{R}_z(\xi_v - \varphi_v)\boldsymbol{x}_{v,i} \qquad (19)$$

The fixed vectors $\boldsymbol{v}_v$ and $\boldsymbol{h}_v$ and fixed angles $(\xi_v - \varphi_v)$ appearing in this expression are shown in Figure 13. Also, since the model uses rigid monomers, the vectors $\boldsymbol{x}_{v,i}$ are fixed; they are the Cartesian coordinates of the nuclei in monomer v with respect to the principal axes system of this monomer. The rotation matrix $\mathrm{R}_{\boldsymbol{h}}(\chi)$, which describes the rotation about a fixed axis $\boldsymbol{h}$ over the angle χ, is defined by eq 27 in Appendix B. From this coordinate transformation, eqs 18 and 19, follows the expression for the metric tensor G corresponding to the six angular coordinates $(\alpha, \beta, \gamma, \chi_A, \chi_B, \chi_C)$. This tensor is substituted into the Podolsky form of the kinetic-energy operator, cf. eq 4. The resulting operator is rewritten by introducing internal angular momentum operators $\boldsymbol{j} = \boldsymbol{j}_A + \boldsymbol{j}_B + \boldsymbol{j}_C$ associated with the torsional motions of the monomers

$$T = \frac{1}{2}(\boldsymbol{J}^\dagger - \boldsymbol{j}^\dagger)\boldsymbol{\mu}(\chi_A, \chi_B, \chi_C)(\boldsymbol{J} - \boldsymbol{j}) + \frac{1}{2}\sum_{v=A,B,C}\Lambda_v^{-1}p_v^\dagger p_v \qquad (20)$$

Almost all the complexity of this kinetic-energy operator is hidden in the definition of the non-Hermitian operators $\boldsymbol{j}$. The operator $\boldsymbol{j}_v$ is not a vector operator but rather the generator of rotations about a single axis $\boldsymbol{h}_v$. Nevertheless, it is convenient to introduce the operators $j_\pm = j_x \pm ij_y$ which shift the quantum number k, the G_6 irrep label. Explicit expressions for $j_\pm$ and j_z in terms of the torsional angles χ_A, χ_B, χ_C are given in eqs A44 and B5 of ref 22. The operator $\boldsymbol{J}$ with components J_x, J_y, J_z is the usual body-fixed total angular momentum operator, depending on the Euler angles α, β, γ, and $\boldsymbol{\mu}(\chi_A, \chi_B, \chi_C)$ is the inverse inertia tensor. The operator p_v is defined as $-i\hbar\partial/\partial\chi_v$, and the constant Λ_v—see eq 3 of ref 22—is the moment of inertia of monomer v about its fixed axis of rotation.

Because of the non-Hermiticity of the operators $\boldsymbol{j}$, the operator in eq 20 and also the Hamiltonians in eqs 23 and 24 below contain the Hermitian conjugate operators $\boldsymbol{j}^\dagger$. Hence, they are examples of writing the Podolsky kinetic-energy operator as in eq 4. As noted there, we do not need the explicit form—given in eq A50 of ref 22—of the operators $\boldsymbol{j}^\dagger$ because in basis set or DVR calculations one can always apply the turnover rule to replace matrix elements of the Hermitian conjugate operators by the corresponding expressions with the original operators, see Appendix A.

The inertia tensor $\boldsymbol{\mu}^{-1}$ consists of a large constant contribution of the hydrogen-bonded framework and a small ($\approx$1%) term which depends on the torsional angles χ_A, χ_B, χ_C. The latter may safely be neglected. For identical monomers, with their centers of mass forming an equilateral triangle, the constant part of $\boldsymbol{\mu}$ is diagonal and contains the rotational constants of the trimer: $A = B = \mu_{xx}/2 = \mu_{yy}/2$ and $C = \mu_{zz}/2$.

The Hamiltonian resulting from eq 20 can be split into three terms

$$H = H^{\mathrm{rot}} + H^{\mathrm{Cor}} + H^{\mathrm{int}} \tag{21}$$

The first term

$$H^{\mathrm{rot}} = B(J_x^2 + J_y^2) + CJ_z^2 \tag{22}$$

is simply the oblate symmetric rotor Hamiltonian for the overall rotation of the complex. The second term

$$H^{\mathrm{Cor}} = -\frac{1}{2}B[(j_+ + j_-^\dagger)J_+ + (j_- + j_+^\dagger)J_-] - C(j_z + j_z^\dagger)J_z \tag{23}$$

represents the Coriolis coupling between the overall angular momentum $\boldsymbol{J}$, with $J_\pm = J_x \mp iJ_y$, and the torsional angular momentum $\boldsymbol{j}$. The last, internal motion, term

$$H^{\mathrm{int}} = -\frac{\hbar^2}{2\Lambda_v}\sum_{v=A,B,C}\frac{\partial^2}{\partial\chi_v^2} + \frac{1}{2}B(j_+^\dagger j_+ + j_-^\dagger j_-) + Cj_z^\dagger j_z + V(\chi_A, \chi_B, \chi_C) \tag{24}$$

describes the torsional motions, with the (model) potential $V(\chi_A, \chi_B, \chi_C)$ defined by fixing all other internal coordinates of the trimer. This model is justified for the ground vibrational state of the hydrogen-bonded framework, since the hydrogen-bond stretch/bend vibrations have considerably higher frequencies than the torsional motions,[179,189,190] but it might break down at higher torsional energies. The above Hamiltonian was used by Olthof et al.[193] in quantitative calculations of the torsional levels of $(H_2O)_3$ and $(D_2O)_3$ for $J = 0$, 1, and 2. The potential $V(\chi_A, \chi_B, \chi_C)$ was taken from the ab initio calculations by Bürgi et al.[187] (the BGLK potential) and by van Duijneveldt-van de Rijdt and van Duijneveldt[109] (the DD potential). A sinc function DVR[172,173] was used for each of the torsional coordinates χ_A, χ_B, χ_C. The results with the DD potential agree fairly well with the experimentally measured transition frequencies[145,146] for the lower torsional levels, while for the higher levels the results with the BGLK potential are slightly better. Later, Geleijns and van der Avoird[196] returned to the more general kinetic-energy operator in eq 20 to derive slightly generalized versions of eqs 22−24 for water trimer isotopomers with less symmetry than $(H_2O)_3$ and $(D_2O)_3$. The latter were used in quantitative DVR calculations for H/D mixed isotopomers. Again, the results from the ab initio potentials are in fair agreement with the experimental data.[142] Also, the intensities of the torsional transitions were computed,[196] which led to the reassignment of one of the observed bands.

5.3. Effective Rotational and Tunneling Hamiltonian

To interpret the complex rotational and bifurcation tunneling structure in the observed torsional bands of $(H_2O)_3$ and $(D_2O)_3$, one needs an effective Hamiltonian which describes the rotational energy levels for each torsional state. Such an effective Hamiltonian must take into account the large-amplitude motions in the water trimer. In particular, it must correctly include the effects of the Coriolis coupling between the overall rotations of the water trimer and its internal torsional or 'flipping' motions. The model Hamiltonian derived in section 5.2 includes these effects and, therefore, forms a good starting point.

In various textbooks[12,204−206] it is shown how an effective rotational Hamiltonian for each vibrational state of a molecule can be derived with the help of Van Vleck perturbation theory or 'contact transformations'. Hershbach[207] used this formalism to obtain the effective rotor Hamiltonian for each torsional state in a molecule with a single internal rotation. An effective rotational Hamiltonian for the water trimer, with its three coupled torsional motions, has been obtained[145] by the application of Van Vleck perturbation theory to the Hamiltonian of eq 21. The effective Hamiltonian for a torsional state with quantum number k—an eigenstate of the internal Hamiltonian in eq 24—was derived by including the perturbation H^{Cor} of eq 23 to second order. For the nondegenerate torsional levels with $k = 0$ and 3, one simply obtains a standard symmetric rotor Hamiltonian

$$H_{\mathrm{eff}}^{(k)} = E_0^{(k)} + B^{(k)}J^2 + [C^{(k)} - B^{(k)}]J_z^2 \tag{25}$$

where $E_0^{(k)}$ is the energy of torsional level k for $J = 0$, i.e., the 'vibrational origin'. The rotational constants $B^{(k)}$ and $C^{(k)}$ contain second-order Coriolis coupling terms, defined in ref 145. For the 2-fold-degenerate torsional levels with $k = \pm1$ and ±2, the effective Hamiltonian is more complex

$$H_{\mathrm{eff}}^{(k',k)} = \delta_{k',k}[\mathrm{E}_0^{|k|} + B^{|k|}J^2 + (C^{|k|} - B^{|k|})J_z{}^2 \mp 2\zeta^{|k|}C^{|k|}J_z] + \delta_{k',k-2(\mathrm{modulo}\ 6)}\mu_{--}^{(k)}J_-J_- + \delta_{k',k+2(\mathrm{modulo}\ 6)}\mu_{++}^{(k)}J_+J_+ + \delta_{k',-k}\delta_{\Gamma,\mathrm{T}}\delta \tag{26}$$

Expressions for the Coriolis coupling parameters $\zeta^{|k|}$ and $\mu_{++}^{|k|} = (\mu_{--}^{|k|})^*$ are given in ref 145, while δ is a constant bifurcation splitting parameter defined in ref 146. The Kronecker delta $\delta_{\Gamma,T}$ implies that the term δ does not appear for all G_{48} irreps Γ but only for the levels carrying the T_g and T_u irreps. This follows from the theory in ref 22.

The occurrence of the linear Coriolis term, $\mp2\zeta^{|k|}C^{|k|}J_z$, giving rise to diagonal terms linear in K, is quite remarkable. Normally the occurrence of such a linear term implies that at least one component of the vibrational angular momentum of some degenerate vibration must have a nonzero expectation value. In this case, however, the expectation value of the torsional angular momentum operator $j_z + j_z^\dagger$ vanishes and the linear Coriolis term originates completely from second-order perturbation theory, through the commutation relation $J_+J_- - J_-J_+ = 2J_z$. A similar effect was found in earlier work on benzene−Ar,[26,208] where the degenerate van der Waals bending mode carries first-order vibrational angular momentum but also a substantial second-order contribution. In light of the standard theory for normal semirigid

molecules,[12,205] this seems a strange phenomenon but one should remember that the vibrational angular momentum for such molecules—which perform small amplitude vibrations about a single equilibrium structure—is defined with respect to a body-fixed frame fixed by the Eckart conditions. This choice minimizes the Coriolis coupling between the vibrations and rotations. We already pointed out that it does not make sense to define such a frame for the water trimer, because the torsional motions involve tunneling flips between six equivalent equilibrium structures.

Another remarkable observation is the occurrence of J_-J_- and J_+J_+ terms. Normally the presence of such terms implies that the molecule is an asymmetric rotor with $B \neq A$. Here, they occur only for the degenerate levels with $k = \pm 1$ and ± 2, and in contrast with the asymmetric rotor, they appear in the off-diagonal blocks of the rotational Hamiltonian with $k' = -k$, which automatically obey the rule that $k' = k \pm 2$ (modulo 6).

Finally, we note the presence of the constant bifurcation splitting term δ in the off-diagonal $k' = -k$ blocks, on the diagonal of these blocks. This extra interaction term appears only for the T irreps of G_{48}, not for the A irreps. It gives rise to a strong interference between the effects of Coriolis coupling and bifurcation tunneling and is the origin of a very irregular structure of the levels and spectra. Actually, it is important only for $(H_2O)_3$, not so much for $(D_2O)_3$, because the magnitude of the bifurcation splitting in $(H_2O)_3$ is about 100 times larger. This puts this splitting on the same scale as the linear Coriolis splitting. Moreover, there is always a simple additive effect of bifurcation tunneling, both in $(H_2O)_3$ and $(D_2O)_3$, which gives rise to the observed quartet splittings of the rovibrational levels.

The effective Hamiltonian (26) for degenerate torsional levels with $k = \pm 1$ and ± 2, which operates in the space of functions $|k\rangle|JKM\rangle$ with fixed $|k| = 1$ or 2, is diagonal in J and M but not in K. It is easy to build the diagonalization of the $2(2J + 1)$ dimensional matrices of this effective Hamiltonian into a fitting program that analyzes the rotational and tunneling structure of the torsional bands. Before the actual analysis of the experimental spectra, the theory was checked by comparison of the energy levels obtained from the effective Hamiltonian with the results of full 3-dimensional DVR calculations of the torsional levels for $J = 0$, 1, 2, and 3, cf. Tables 3 and 4 of ref 193. The latter were based on the full Hamiltonian of eq 21. It turned out that the effective Hamiltonian gives an accurate representation of the level splittings and shifts from the full numerical computations and nicely reflects the irregularities in the degenerate states with $k = \pm 1$ and ± 2.

5.4. Experimental Results and Analysis

A summary of all the torsional bands observed for $(D_2O)_3$ and $(H_2O)_3$ and their assignment is given in Table 2. This assignment has been unambiguously confirmed by the analysis of the detailed rotational and bifurcation tunneling structure of each band, with the aid of the effective Hamiltonian in section 5.3. Especially the transitions involving 2-fold degenerate torsional levels with $k = \pm 1$ and ± 2 were difficult to assign line by line because of the strong perturbations in these levels. Parallel transitions involving such perturbations both in the initial and final state are the bands at 89.6 cm^{-1} observed for $(D_2O)_3$ and the band at 42.9 cm^{-1} for $(H_2O)_3$. In the first instance, the observation that the spectrum at 89.6 cm^{-1} exhibited far too many transitions to be accounted for by a single well-behaved band led to the assumption that the spectrum arose from an asymmetric rotor and thus exhibited asymmetry doublets. However, the corresponding analysis did not account for the strongly perturbed spectrum. It is now evident that the observed spectrum consists of two parallel ($\Delta K = 0$) subbands: the $k = -2 \leftarrow +1$ and $k = +2 \leftarrow -1$ torsional transitions. Also, the band at 42.9 cm^{-1} has two such subbands. The perturbations in this band are even stronger, because the relatively large bifurcation splittings in $(H_2O)_3$ interfere with the Coriolis coupling effects. Without the effective Hamiltonian described in section 5.3, it is unlikely that this band could have been fit to any reasonable degree of accuracy. The relatively large separation between the two subbands is caused by the linear Coriolis splitting $\mp 2\zeta CK$ of the $+|k|$ and $-|k|$ sublevels. A stick-figure representation of the Q-branch of the $(H_2O)_3$ band at 42.9 cm^{-1} is presented in Figure 14. The two repelling Q-branches are characteristic of a 'first-order' linear Coriolis perturbation.[209] The observation of this transition was a surprise, as the $k = \pm 1$ torsional levels in $(H_2O)_3$ are 23 cm^{-1} above the ground state, suggesting that the expansion is not nearly as cold vibrationally as it is rotationally.

Also, the perpendicular bands at 28.0 and 98.1 cm^{-1} for $(D_2O)_3$ and at 65.6 cm^{-1} for $(H_2O)_3$ consist of two subbands, assigned to the $k = +2 \leftarrow 0$ ($\Delta K = -1$) and $k = -2 \leftarrow 0$ ($\Delta K = +1$) torsional transitions. Similarly, the perpendicular band at 81.8 cm^{-1} for $(D_2O)_3$ consists of two subbands corresponding to the $k = 3 \leftarrow 1$ ($\Delta K = -1$) and the $k = 3 \leftarrow -1$ ($\Delta K = +1$) transitions.

By far the simplest and strongest spectra are the 41.1 cm^{-1} band of $(D_2O)_3$ and the 87.1 cm^{-1} band of $(H_2O)_3$, both assigned to the parallel ($\Delta K = 0$) transition between nondegenerate torsional levels with $k = 0$ and 3. The only perturbation observed in

Table 2. Principal Characteristics of the Torsional Transitions Observed in $(D_2O)_3$ and $(H_2O)_3$[a]

frequency/ cm^{-1}	band type	assignment	relative intensity	ref
		$(D_2O)_3$		
28.0	perpendicular	$k = \pm 2^l \leftarrow 0$	5.0	145
41.1	parallel	$k = 3^l \leftarrow 0$	125.0	133, 142
81.8	perpendicular	$k = 3^u \leftarrow \pm 1^l$	1.0	145
89.6	parallel	$k = \mp 2^u \leftarrow \pm 1^l$	1.5	124
98.1	perpendicular	$k = \pm 2^u \leftarrow 0$	5.0	131
		$(H_2O)_3$		
42.9	parallel	$k = \mp 2^l \leftarrow \pm 1^l$	weak	146
65.6	perpendicular	$k = \pm 2^l \leftarrow 0$	weak	146
87.1	parallel	$k = 3^l \leftarrow 0$	strong	131

[a] The superscripts l and u refer to the lower and upper set of levels with $k = 0, \pm 1, \pm 2, 3$, see Figure 16.

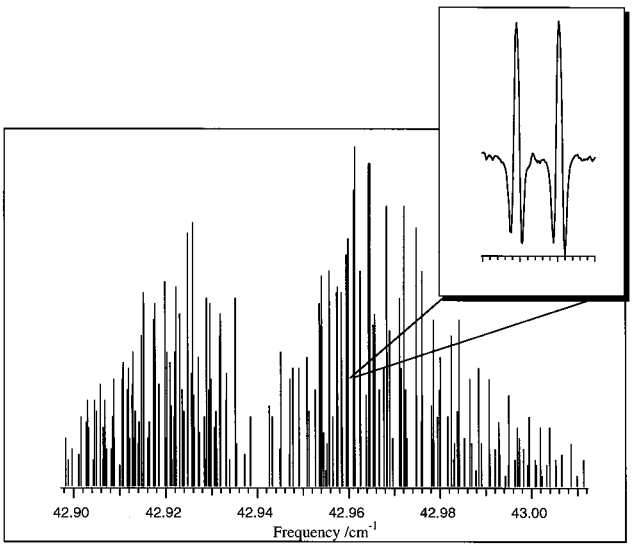

Figure 14. Repelling *Q*-branches of the 42.9 cm^{-1} band of $(H_2O)_3$ measured by Brown et al.[146] The two subbands correspond to the $k = -2 \leftarrow +1$ and $k = +2 \leftarrow -1$ transitions, both obeying $\Delta K = 0$. The *Q*-branch to the left is shifted to lower energy by the $-2\zeta CK$ pseudo-first-order Coriolis interaction, while the *Q*-branch to the right is shifted to higher energy by $+2\zeta CK$. The inset shows a representative spectrum in a 10 MHz scan.

the 87.1 cm^{-1} band for $(H_2O)_3$ is a small doublet splitting of each *T*-state component arising from $|K| = 1$ transitions. This additional splitting, a Coriolis-induced bifurcation tunneling effect explained by van der Avoird et al.,[22,193] is absent for the *A* components. Specifically, it was observed that only the *P*- and *R*-branches of the *T* lines are split, but not the *Q*-branch, and that the splitting is proportional to J^2. This pattern is similar to the effects of 'axis switching' in a slightly asymmetric rotor. With the aid of the appropriate selection rules, it could be deduced[193] from the J^2 dependence and other characteristics of this splitting that, among two possibilities,[186] bifurcation tunneling in $(H_2O)_3$ prefers the pathway represented by the PI operations (12)*, (34)*, and (56)*.

Also, the quartet splitting of the rovibrational transitions by bifurcation tunneling is very regular in these $k = 3 \leftarrow 0$ bands, as depicted in Figure 15. In the $(H_2O)_3$ band at 87.1 cm^{-1}, each quartet component is separated from the other by a constant 289 MHz; only at high values of the rotational quantum number *J* does this splitting become slightly smaller. The nuclear spin intensity ratios for the bifurcation pattern agree with theory:[22,131,186] 11:9:3:1 when $K = 3n$ and 8:9:3:0 when $K \neq 3n$. The tunneling components that have weight zero when $K \neq 3n$ are clearly missing in the spectrum. Similar quartets in the 41.1 cm^{-1} band of $(D_2O)_3$ show a bifurcation splitting of 1.5 MHz.

The irregularities in the rotational structure of the bands caused by transitions to or from degenerate torsional levels with $k = \pm 1$ and ± 2 are also manifest in the bifurcation splitting patterns. For example, in the 81.8 cm^{-1} band of $(D_2O)_3$, most quartets have a normal intensity pattern 1:5:10:7, consistent with the group theoretical (G_{48}) nuclear spin statistics of 11:54:108:76 and 2.7 MHz spacings between each of the

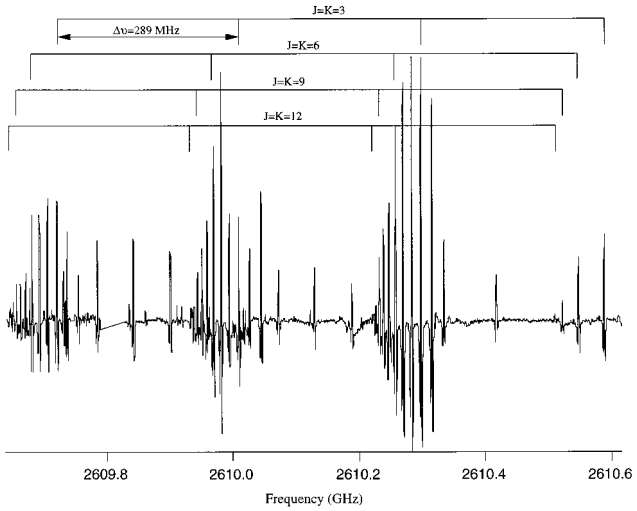

Figure 15. *Q*-branch of the 87.1 cm^{-1} (2610 GHz) parallel $k = 3 \leftarrow 0$ band of $(H_2O)_3$ measured by Brown et al.[146] The quartet tunneling splitting is evident as four *Q*-branches separated by a tunneling splitting of 289 MHz. Notice that the fourth component (A_g symmetry) has a nonzero nuclear spin weight only when *K* is a multiple of three.

lines. Anomalous quartet intensity patterns were observed for the $|K| = 0 \leftarrow 1$ transitions, with approximate intensity ratios of 5:3:5:2. In the $(D_2O)_3$ band at 28.0 cm^{-1}, the quartet intensity ratios observed, for example, in the $|K| = 3 \leftarrow 2$ *Q*-branch (approximately 1:5:10:7) are consistent with the G_{48} nuclear spin statistics, with spacings of 0.9 MHz between each of the four lines. However, again, anomalous quartet intensity patterns were observed for the $|K| = 0 \leftarrow 1$ *P*-, *Q*-, and *R*-branch transitions, with approximate intensity ratios of 2:9:4:6. For these quartets the individual lines exhibit an uneven spacing with a small *J* dependence. Similar anomalous quartets were observed in the $|K| = 0 \leftarrow 1$ transitions in the 98.1 cm^{-1} $(D_2O)_3$ band.[131] All of these findings were explained by the theory in refs 22 and 193. A perturbation not observed in any of the other water trimer bands was found in the 65.6 cm^{-1} band of $(H_2O)_3$. In this band the T_g and T_u levels, the two middle levels in the quartets, are separated by a constant 255 MHz and the outer A_u and A_g components by a constant tunneling splitting of 765 MHz, i.e., 3 times the 255 MHz spacing. However, it was noticed that the *T* components shift considerably relative to the *A* components, resulting in separations between the *A* and *T* components that vary from 200 to 300 MHz. This perturbation caused considerable difficulty in the rotational assignment of the band.

A global fit of the entire experimental $(D_2O)_3$ data set, 554 rovibrational transitions, can be found in ref 145. The quality of the fit is reflected by a root-mean-square of the frequency residuals of 1.36 MHz, which is even less than the typical experimental frequency precision of 2 MHz. Table 3 in ref 145 summarizes the optimized parameters (torsional energies, rotational and distortion constants, and Coriolis parameters) obtained from the final fit. A total of 361 rovibrational transitions was observed and assigned[146] in the three torsional bands of $(H_2O)_3$. Despite the strong perturbations in the spectrum, a global fit of all these transitions with the effective

Hamiltonian of section 5.3 gave a root-mean-square deviation of only 0.93 MHz. The *A* tunneling components in each band were fit separately from the *T* tunneling components, because of the different tunneling splitting patterns predicted by the theory. Tables 2 and 3 in ref 146 summarize the optimized parameters (torsional energies, rotational, distortion, and Coriolis coupling constants, and bifurcation splitting parameters) obtained from the final fit. The overall result of these fits of the measured torsional spectra of $(H_2O)_3$ and $(D_2O)_3$ is a very precise description of the energies and other characteristics of the torsional states of both these water trimer isotopomers, up to about 100 cm^{-1}. The rotational constants $A = B$ and C associated with the different torsional states of the trimer show an interesting nonmonotonic dependence on the amount of torsional excitation energy. This has been quantitatively explained by Sabo et al.,[188,197,198] with the aid of a (3 + 1)-dimensional dynamical model which includes the symmetric intermolecular stretch coordinate. Calculations of the vibrationally averaged moments of inertia of the different torsional states show that the variations of $A = B$ and C are the effect of both the averaging over the torsional angles and a change of the intermolecular distances accompanying torsional excitation.

5.5. Three-Body Interactions; Trimer VRT Levels

Next, let us describe the use of water trimer spectra to further test the pair potential and check the accuracy of ab initio-calculated water three-body interactions.[152] The explicit calculation[113,114] of these nonadditive interactions was made possible by the recent extension of SAPT.[210−214] It turned out that the three-body interactions contribute about 15% of the water trimer binding energy at the hydrogen-bonded equilibrium geometry and 30% or more to the hydrogen-bond rearrangement barriers. The dominant three-body interactions are the second- and third-order polarization effects, but the nonadditive exchange effects are not negligible, especially for the rearrangement barriers.

In section 5.2 we outlined the 3-dimensional model which was employed[193] in DVR calculations of the torsional energy levels, with two different ab initio potentials, DD and BGLK. These are not global water potentials, however, in the sense that they do not depend on all of the $6N - 6$ intermolecular degrees of freedom for an *N*-molecule system. The DD potential[109] is a polynomial fit of ab initio data in the three torsional coordinates of the trimer, only valid for a limited range of angles. The BGLK (also called modEPEN) potential is a modified form of the empirical EPEN potential of Scheraga and co-workers[202] reparametrized by Bürgi et al.[187] on the basis of the same type of 3-dimensional ab initio data as the DD potential. In principle, this modEPEN potential—a site−site model—is a global potential but if used as such it exhibits unphysical behavior in some important regions of the 12-dimensional configuration space of the trimer.[195,201] Groenenboom et al.[152] applied the dynamical model of van der Avoird et al.[22,193] in calculations with the SAPT pair and three-body

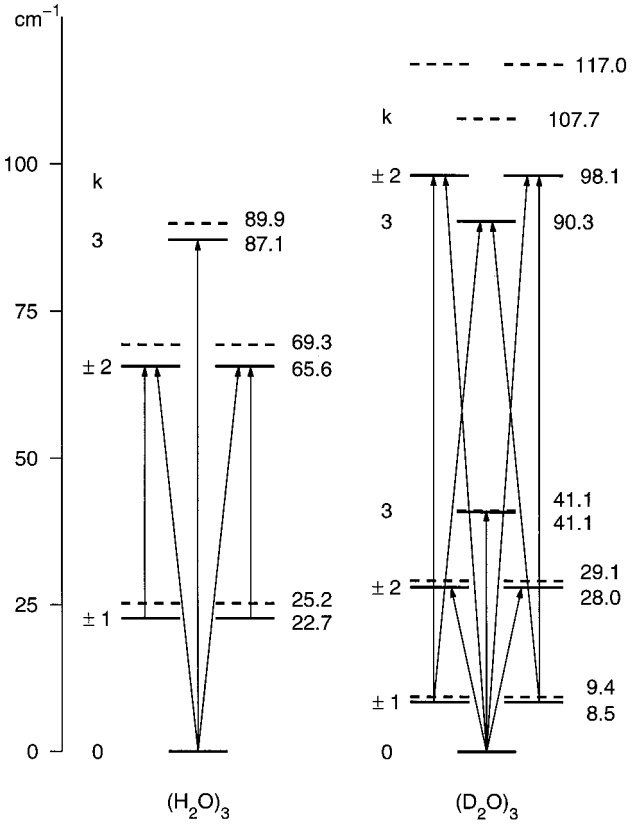

Figure 16. Torsional levels (in cm^{-1}) of the H_2O and D_2O trimers for $J = 0$. The labels $k = 0, \pm1, \pm2, 3$ correspond to the irreducible representations of the (cyclic) permutation−inversion group G_6. The dashed levels are calculated[152,169] from the SAPT-5s pair and three-body potential; the solid levels are experimental data.[145,146] Arrows indicate the observed transitions. If the three-body interactions were omitted the torsional flipping barrier would be substantially lower and the torsional levels would be higher by about 10% for $(H_2O)_3$ and 20% for $(D_2O)_3$.

potential. The separations of $R = 5.37$ bohr between the centers of mass of the water molecules and the angles $\alpha = 21.2°$ describing the nonlinearity of the hydrogen bonds correspond to the trimer equilibrium structure and were kept fixed. The three-body contributions to the potential were directly calculated[114] on the 3-dimensional grid with 568 symmetry-distinct points used in the DVR calculations.[22,152,193,196] In similar calculations of the torsional levels in the water trimer for $J = 0$, Wales[201] tested the popular TIP4P water potential,[215] employed in many simulations of liquid water, and the ab initio-based modEPEN[187] and polarizable ASP−W[174] potentials. The modEPEN (or BGLK) potential already tested by Olthof et al.[193] gave reasonable torsional frequencies but, as we just mentioned, unfortunately fails as a global potential.[195] For the other potentials it was found, just as in the tests on the dimer spectrum,[144,151] that the calculated transition frequencies deviate from the measured spectra by factors of 2 or 3, at least, cf. Figure 6 in ref 201.

Figure 16 shows the torsional levels of the normal and fully deuterated water trimer calculated from the SAPT-5s potential for the pair interactions and additional three-body interactions computed by SAPT on the 3-dimensional DVR grid. The agreement of the lower ($k = 0, \pm1, \pm2, 3$) levels with experiment is

excellent. For the higher levels—measured in $(D_2O)_3$—the deviations are larger but there are several indications[145,188,197,198] that the separation between the torsional motions and other vibrations of the trimer starts breaking down at these higher energies. The torsional levels of both $(H_2O)_3$ and $(D_2O)_3$ in Figure 16 agree considerably better with experiment than those from any of the previously tested global water potentials.[201] The replacement of the SAPT-5s pair potential by the 'spectroscopic' VRT(ASP−W) potential[34] gave a substantial quality degradation: the resulting torsional levels became much too dense, as a consequence of the flipping barrier becoming too high by nearly a factor of 3. The torsional levels computed with the SAPT-5s-tuned potential (not shown in Figure 16) are about 14% too low, due to a 30% increase of the flipping barrier. However, it follows from the analytic pair and three-body SAPT potential generated by Mas et al.[114] that the flipping barrier in the full 12-dimensional trimer potential surface is nearly 30% lower than in the 3-dimensional surface obtained by freezing the center-of-mass separations R and the angles α. The compensation of these two 30% effects will probably bring the levels from SAPT-5s-tuned into equally good agreement with experiment as those from SAPT-5s in Figure 16.

Concluding this section, we may say that the comparison between theory and experiment for the torsional spectrum of the water trimer clearly confirms the conclusion of section 4 that the water potentials currently in use in simulations of liquid water and ice are not able to provide a good quantitative description of the intermolecular vibrations and tunneling processes in water clusters. Two water pair potentials were recently developed or improved with the aid of dimer spectroscopic data: the VRT-(ASP−W) pair potential and the SAPT-5s-tuned potential. The trimer test indicates, more clearly than the dimer spectrum, that the SAPT-5s-tuned potential is to be preferred over the 'spectroscopic' VRT-(ASP−W) pair potential. This is probably related to the fact that the ab initio calculations by SAPT are of higher quality—containing a higher and more consistent level of electron correlation in the monomer wave functions—than the calculations on which the ASP−W potential is based. Furthermore, the use of the trimer spectrum has demonstrated that the three-body nonadditive interactions in water, which were also calculated by SAPT, are of comparable accuracy as the pair potential. Simulations with the use of this more realistic pair and three-body SAPT potential will hopefully lead to a better understanding of the anomalous properties of water and ice. Although its functional form is more complicated than that of the model potentials commonly used in such simulations, computations with this potential are very feasible on modern computers.

6. Other Recent Developments

Since the appearance of the 1994 issue of *Chemical Reviews* devoted to van der Waals molecules, many papers—theoretical as well as experimental—were published in this field. We will summarize the work on some systems that have been investigated most intensively since then. We do not strive for complete coverage of the literature but rather select a number of examples that illustrate the progress which was recently made by theory, experiment, and, especially, by the two in collaboration.

6.1. Complexes of Nonpolar Molecules

6.1.1. Atom–Linear Molecule Dimers

The argon−N_2 system has been revisited by several workers during the past few years. Dham et al.[216] developed an exchange-Coulomb (XC) model potential-energy surface for this system. It is based upon results for the Heitler−London interaction energy, long-range dispersion energies, the temperature dependencies of interaction second virial, binary diffusion, and mixture shear viscosity coefficients, microwave spectra of the van der Waals complex, and collision broadening of the depolarized Rayleigh light scattering spectrum. The potential gives good overall agreement with many different experiments for the N_2−Ar mixture but is still open for improvement, as appears from simulations of infrared spectra of the $^{14}N_2$−Ar complex by Wang et al.[217] The latter authors performed exact quantum mechanical calculations using a modified Morse−Morse−spline−van der Waals potential and the XC model potential. The spectrum simulated from the modified Morse-type potential surface shows distinctly better agreement with experiment than does the spectrum simulated from the XC model.

Two sets of ab initio calculations on the argon−N_2 system appeared recently. The first publication was by Naumkin[218] and the second by Fernández et al.,[219] who evaluated the potential by the CCSD(T) model (coupled cluster singles and doubles with noniterative triples) in a very good atomic orbital basis set. Fernández et al. determined the rovibrational spectroscopic properties from their ab initio potential and compared them with the available experimental data. Considerable improvement was obtained when four of the potential parameters were refined based on the Ar−$^{14}N_2$ rotational transition frequencies. Thus, it was shown that the CCSD(T) method can be used to predict the spectroscopic properties of van der Waals complexes but that fine-tuning to experiment remains necessary.

Roche et al.[220] considered two new empirical potential surfaces[221] for the van der Waals molecule CO_2−Ar, which, just as N_2−Ar, consists of two nonpolar monomers. Pressure broadening of both infrared and Raman lines was tested against measurements. Thermally averaged infrared and Raman cross sections at different temperatures showed good agreement with the experimental data available. Transport properties, such as diffusion, viscosity, and nuclear spin relaxation, provided a different test of the surfaces and agreed well with experiment. Very recently, ab initio rovibrational spectra were published for CO_2−Ar.[222] These were obtained from a fairly low-level SAPT potential. Surprisingly enough, the higher level SAPT potentials did not perform as well.

The Nijmegen−Warsaw collaboration resulted, apart from the work on Ar−CH_4 reviewed above, in SAPT

potentials for He−CO,[223] Ne−CO,[224] He−C_2H_2,[225] and Ne−C_2H_2.[226] Although, strictly speaking, CO is a polar molecule, it has such a small dipole that the Rg−CO dimers (Rg = rare gas atom) have the characteristics of nonpolar complexes. The 3-dimensional He−CO potential of Heijmen et al.[223] was used by Simpson and co-workers[227] in the calculation of vibrational relaxation cross-sections and rate constants for the deactivation of CO($v = 1$) by ^{3}He and ^{4}He. The surface was found to resolve the qualitative discrepancy between theory and experiment which existed in earlier theoretical calculations. The same He−CO potential was used to compute cross sections for state-to-state rotationally inelastic scattering, which gave results[228] agreeing very well with measured relative integral cross sections for rotational excitation of CO at energies of 72 and 89 meV. Heck and Dickinson[229] performed classical trajectory calculations of diffusion, viscosity, thermal conductivity, and thermal diffusion in first-order kinetic theory using the He−CO SAPT potential. For diffusion and viscosity, their results are consistent with experiment. The results for thermal diffusion, on the other hand, suggest that the repulsive part of the SAPT potential may be too anisotropic.

The Ne−CO SAPT potential[224] was used to generate the infrared spectrum corresponding to the simultaneous excitation of vibration and internal rotation in the CO subunit within the complex.[224] The computed frequencies were in good agreement with the experimental data.[230,231] Later a new ab initio 2-dimensional potential-energy surface for the Ne−CO interaction was described.[232] This surface was obtained by the supermolecule method at the CCSD(T) level of theory. This new surface gave modestly better predictions of scattering cross sections that depend on close approach of Ne to CO than the SAPT potential but does not describe the ground-state geometry as well as the SAPT surface.

Jansen[233] computed a potential for Ar−CO using the coupled pair functional supermolecule method and subsequently applied it in rovibrational calculations.[234] Tao and co-workers[235] used the supermolecule Møller−Plesset fourth-order method to obtain a surface for rovibrational calculations[236] on the same system. The *A*-rotational constant of Ar−CO was (re)measured by double-resonance microwave−millimeter-wave spectroscopy,[237] and its infrared spectrum was scanned in the $v_{CO} = 2$ overtone region.[238] Brookes and McKellar[239] recently measured the rotationally resolved infrared spectra of Kr−CO and Xe−CO in the region of the CO stretching vibration, both in a long-path (200 m) low-temperature (76 K) gas cell and in a pulsed supersonic jet expansion. van der Waals bending frequencies and other parameters were extracted from these spectra through the use of a simple empirical Hamiltonian. Thus, the properties of the entire series of rare gas−carbon monoxide complexes, from He−CO to Xe−CO, are now characterized.

Total differential cross sections and differential energy loss spectra for He−C_2H_2 were computed[240] from the ab initio SAPT potential mentioned above. The results were in excellent agreement with the earlier experimental values of Buck et al.[241] The same He−C_2H_2 potential was recently employed[242] to obtain state-to-state rate constants for the collisional rotational (de)excitation of acetylene by He and pressure broadening coefficients. The computed pressure broadening coefficients and rate constants agree well with the experimental data. In fact, the theory revealed that the interpretation of the experimental data required accounting for the influence of multiple collisions.

The Ne−acetylene SAPT points were fit to an analytic form and applied in calculations of the rovibrational energy levels of Ne−C_2H_2 and Ne−C_2HD.[226] From these levels and calculated transition intensities the near-infrared spectra of these complexes were generated in the region of the ν_3 band, which is the C−H stretching vibrational band lying around 3300 cm^{-1}. For Ne−C_2H_2, the results obtained from the ground-state surface gave semiquantitative agreement with the measured spectrum. For Ne−C_2HD, all of the (much sharper) lines in the experimental spectrum could be assigned. The ν_3 excited-state interaction potential was obtained from a fit of the calculated spectrum to the experimental one. The ground-state ab initio potential was not altered in this fit; the excellent agreement between the calculated and measured infrared spectrum for Ne−C_2HD demonstrated that the Ne−acetylene SAPT potential is quite accurate.

6.1.2. Ar–Benzene

Much attention has been given to another nonpolar system, namely, the Ar−benzene dimer. Brupbacher et al.[243,244] measured the rotational spectra of normal and deuterated benzene−Ar complexes. They modeled the intermolecular motions with a potential containing three adjustable parameters. These parameters, one of which represents the equilibrium distance of the rare gas atom from the plane of benzene, were obtained by a fit of the observed rotational transition frequencies.

Riedle et al.[245] measured rotationally resolved vibronic spectra of C_6H_6−Ar and C_6D_6−Ar. The lowest energy van der Waals band of both complexes displayed a completely unexpected rotational structure. This could neither be explained by a genuine perpendicular nor by a parallel transition. This situation was analyzed in detail by Riedle and van der Avoird,[208] who deduced the final vibronic assignments. To that end they performed calculations of the van der Waals states of electronically excited benzene−Ar and included the coupling to the vibronic angular momentum of the excited state of benzene. A detailed analysis of the degenerate intermolecular bending fundamentals in the experimental UV spectra of C_6H_6−Ar was given and found to agree with the theory.

Recently, two experimental studies appeared that report accurate measurements of a number of intermolecular vibrational transitions of ground-state benzene−Ar. Kim and Felker[246] reported the results of nonlinear Raman spectroscopy on the intermolecular transitions of C_6H_6−Ar and C_6D_6−Ar. They assigned unambiguously the five lowest vibrational

transitions. Neuhauser et al.[247] were able to measure by coherent ion-dip spectroscopy rotationally resolved spectra of high-lying overtones of the intermolecular vibrations of the benzene−Ar complex. The small isotope shifts upon deuteration of the benzene molecule could be measured and compared with the simple classical harmonic oscillator and with anharmonic 3-dimensional quantum calculations. By comparing the latter calculations with the experimental results, the quality of several benzene−Ar interaction potentials could be discussed.

Very recently a stringent upper limit of 316 cm^{-1} for the value of the dissociation energy D_0 of the neutral C_6D_6−Ar complex was found by Meijer and co-workers.[248] This limit was extracted from infrared absorption spectra of C_6D_6 cations, complexed with Ar, throughout the 450−1500 cm^{-1} region via IR-laser-induced vibrational dissociation spectroscopy.

Koch et al.[249] calculated by an ab initio coupled cluster method the equilibrium dissociation energy D_e of the benzene−argon van der Waals complex in the ground state S_0. They quote a dissociation energy $D_e = 389 \pm 2$ cm^{-1} for the ground state S_0. Later they extended the calculations to obtain the ground-state potential-energy surface[250] and performed full 3-dimensional vibrational calculations. They find $D_0 =$ 328.1 cm^{-1} for C_6H_6 and $D_0 = 330.6$ cm^{-1} for C_6D_6. The latter number is 14.6 cm^{-1} higher than the recent experimental (upper bound) value of Meijer et al.[248] The S_0-S_1 excitation energies were computed by determining poles of a coupled cluster linear response function.[251] Thus, they were able to obtain a potential-energy surface for the excited S_1 state as well.

Work that is similar to that on benzene−Ar has recently been performed on jet-cooled neutral and ionized aniline−Ar,[252] on aniline−Ne[253] (vibrational predissociation studies), on complexes of Ar and Ne bound with 4-fluorostyrene[254] and on *p*-difluorobenzene−Ar[255] (UV spectra with rotational resolution including several van der Waals modes), on dimers of 1- and 2-fluoronaphthalene with Ar and CH_4[256] and indole−Ar[257] (high-resolution UV spectra), and on *o*-xylene−Ar[258] and some dimethylnaphthalene complexes with Ar and Ne[259,260] (two-color resonant two-photon ionization spectra). For several of these complexes the measurements were accompanied by 3-dimensional quantum calculations[254,258−261] of the intermolecular vibrations and rotational constants.

6.1.3. Trimers and Larger Clusters

The experimental and theoretical work on trimers and three-body interactions up to 1994 has been reviewed by Elrod and Saykally[262] and by Chalasiński and Szczęśniak.[31] Much relevant work has appeared since then. Since we already discussed the three-body interactions in the water trimer in section 5.5, here we will concentrate on some nonpolar systems.

In contrast with the water trimer and other hydrogen-bonded systems, where classical polarization effects provide the dominant nonadditive interaction, the situation in clusters composed of nonpolar molecules is much more complex. At least two of the monomers in a trimer or larger cluster need to be polar to obtain important second-order nonpairwise−additive polarization interactions. Prototype trimers which have been studied intensively are the argon trimer and Ar_2−HX (with X = F or Cl). The latter system is more easily accessible to spectroscopy than the former because the HX with its strong dipole plays the role of an infrared chromophore. In both of these trimers there is a subtle balance between nonadditive interactions[210,211,263,264] of different origin: second-order induction (which is merely due to charge cloud penetration and hence is relatively small), third-order dispersion (including the well-known Axilrod−Teller triple dipole interaction), third-order induction and mixed induction−dispersion, first-order triple-exchange effects, and mixed electrostatic-exchange, induction−exchange, and dispersion−exchange contributions. An example of an important mixed electrostatic−exchange contribution in Ar_2−HF is the electrostatic interaction of the permanent multipoles of HF with the quadrupole caused by electron exchange between the two Ar atoms as they overlap. This contribution was modeled by Ernesti and Hutson[265,266] in their attempts to extract the nonadditive intermolecular forces in Ar_2−HF and Ar_2−HCl from the spectra of these van der Waals trimers.

Ab initio supermolecule studies of the nonadditive interactions in Ar_2−HF and Ar_2−HCl have been made by Chalasiński and collaborators.[267−270] Recently, the explicit and direct ab initio calculation of each of the above-mentioned three-body components of the interaction energy became possible by the extension of SAPT.[210−212] Moszynski et al.[271] applied this three-body SAPT method to study Ar_2−HF, while Lotrich et al.[263,264] applied it both to Ar_3 and to Ar_2−HF. In the Ar_2−HF studies, it was concluded that the anisotropy of the nonadditive interactions is determined by a subtle balance between the various attractive and repulsive contributions. All of the above-mentioned exchange, induction, dispersion, and mixed terms occurring in first, second, third, and even fourth order of perturbation theory are important. Some of these are—implicitly—included already by Hartree−Fock calculations; others involve electron correlation effects. Some of the terms, such as the second- and third-order (penetration) induction, are nearly canceled by the corresponding exchange contributions, for most—but not all—geometries. Furthermore, it was shown that the semiempirical exchange quadrupole model of Ernesti and Hutson,[265,266] describing the nonadditive mixed electrostatic−exchange contributions, can be given a theoretical basis. The ab initio data will be useful for modeling the geometry dependence of these three-body interactions. Also, for Ar_3 it was concluded from the SAPT analysis[263] that there are several three-body contributions of nearly equal importance. The geometry dependence of the total three-body interaction in Ar_3 follows that of the Axilrod−Teller dispersion term. This is not because other terms are less important, but rather because they cancel each other to a large extent.

With regard to the computation of rovibrational states, we mention that González-Lezana et al.[272,273]

used a variational method in terms of atom−atom distance coordinates and a basis of distributed Gaussians to investigate the stability and geometrical properties of He, Ne, and Ar trimers. Wright and Hutson[274] presented a new method for calculating the energy levels and wave functions of rare gas trimers, based upon a potential-optimized DVR. This method was applied to Ar_3, while for several mixed rare gas trimers Ernesti and Hutson[275] used the older method of Cooper et al.[276] The latter calculations investigate the effects of different rare gas pair potentials and of the Axilrod−Teller three-body interactions on the rotational constants of the mixed rare gas trimers. Some of these have been measured by Xu et al.[277] using microwave spectroscopy. In their experiment to confirm the existence of a stable He dimer by diffraction through a grating, Schöllkopf and Toennies[278] found a stable He trimer as well.

Four intermolecular vibrational states of the weakly bound trimers Ar_2−HF and Ar_2−DF have been studied via high-resolution infrared spectroscopy.[279] These van der Waals vibrational states, accessed as combination bands built on the $v = 1$ HF or DF intramolecular stretch, correlate adiabatically with $j = 1$ motion of a hindered HF/DF rotor and correspond to a librational motion either in or out of the molecular plane. Ernesti and Hutson[265,266] calculated the vibrational frequencies and rotational constants of these trimers including all five intermolecular degrees of freedom. The intramolecular vibrational states of the HX molecules were separated out adiabatically, so that the calculations could be carried out on effective intermolecular potentials for each HX vibrational state. The calculations were performed both on pairwise additive potentials, derived from well-known Ar−Ar and Ar−HF potentials, and on nonadditive potentials incorporating different three-body forces. On a pairwise additive surface, the intermolecular vibrational frequencies are found to be as much as 11% higher than the experimental values; this indicates the presence of repulsive three-body contributions to the angular potential. Inclusion of the conventional three-body induction and Axilrod−Teller dispersion terms can only account for 30% of the observed discrepancies. The other 70% of the vibrational shifts can be attributed to three-body exchange effects, i.e., the strongly anisotropic interaction of the HF/DF dipole with the exchange quadrupole formed by Ar−Ar. Inclusion of all three nonadditive terms (dispersion, induction, and exchange) improves the agreement with experiment by up to an order of magnitude. The in-plane and out-of-plane bending vibrations of HF in the Ar_2−HF cluster were also investigated by Chuang et al.,[280] who recorded infrared spectra in the $v_{HF} = 3$ overtone region.

Xu et al.[281] determined rotational spectra of four different H/D, $^{20}Ne/^{22}Ne$, and $^{35}Cl/^{37}Cl$ isotopomers of the Ne−Ar−HCl trimer by means of pulsed molecular beam Fourier transform microwave spectrometry. Nuclear quadrupole hyperfine structures due to the $^{35}Cl/^{37}Cl$ and D nuclei were observed, assigned, and used to provide information about the angular anisotropy of the Ne−Ar−HCl potential-energy surface. Structural parameters of the trimer were determined from the rotational constants obtained, and a pseudo-triatomic harmonic force field analysis was performed to provide qualitative frequency predictions of the heavy atom van der Waals vibrational motions.

Also, clusters of HF and DF with up to 14 Ar atoms were investigated, both experimentally and theoretically. Particular attention was given to the (deviations from) additivity of the 'matrix' or 'solvation' shift of the HF stretch frequency with the increase of the number of Ar atoms. Some earlier studies[282,283] on Ar_n−HF clusters with $n = 1, ..., 14$ in which the Ar cage was frozen at the equilibrium geometry have shown that a coordination number of $n = 12$, which completes the first solvation shell of HF, produces a red shift close to the value observed for a solid argon matrix. Both Lewerenz[284] and Niyaz et al.[285] treated the zero-point motions of Ar_n−HF clusters with $n = 1, ..., 4$ by means of diffusion quantum Monte Carlo (DQMC) calculations, and Dykstra[286] applied the same method for clusters with n up to 12. Niyaz et al. used the best available Ar−Ar and Ar−HF pair potentials and concluded from small but systematic differences between the calculated and measured red shifts that nonadditive interactions need to be included. Lewerenz used the same pair potentials, as well as a nonadditive potential that includes a simple isotropic Axilrod−Teller dispersion contribution. Dykstra used simple model pair potentials, again with only Axilrod−Teller nonadditive terms. Hutson et al.[287] employed a more complete nonadditive potential in their theoretical studies of Ar_n−HF clusters with $n = 2, 3, 4$, and 12. Just as in the earlier studies,[282,283] they used a fixed Ar_n cage which was first optimized by simulated annealing and solved the resulting 5-dimensional Schrödinger equation for the hindered rotational and translational motion of the ground-state and excited HF molecule in the field of the Ar atoms. The nonadditive potentials, which include dispersion, induction, and exchange distortion effects, are found to account remarkably well for the observed frequency shifts. Even larger Ar_n−HF clusters with $n = 62$ were theoretically investigated[288] by classical molecular dynamics simulations with the use of a model potential based on the diatomics-in-molecules (DIM) approximation. Also, these studies concentrated on the effect of many-body interactions on the red shift in the HF frequency. The infrared spectroscopic data for Ar_n−HF with $n = 1, 2, 3, 4$ and for Ar_n−DF with $n = 1, 2, 3$ to which the results of theoretical studies have been compared were provided by Nesbitt and co-workers.[289,290]

6.2. Hydrogen-Bonded Complexes

6.2.1. HF and HCl Dimers

Not only the water dimer discussed in section 4, but also the hydrogen halide dimers $(HCl)_2$ and $(HF)_2$ have been the focus of a growing body of experimental and theoretical research, because they are prototypes of hydrogen-bonded systems. Quack and Suhm[291] and Bačić and Miller[292] may be consulted for a summary of experimental and theoretical information on the

HF dimer available up to 1996. We will review the work on the HF dimer performed since then. This four-atom complex is planar at equilibrium and has two equivalent minima distinguished by an interchange of proton acceptor and donor. The experimental splitting[293,294] due to tunneling from the one minimum to the other is 0.658 690 cm^{-1} in the ground state. The stretch frequency of 3961.57 cm^{-1} of free HF is downshifted by 31 cm^{-1} for the acceptor HF (v_1) and by 93 cm^{-1} for the donor (v_2). The donor−acceptor interchange splittings of the excited states are reduced with respect to the ground state; they are −0.215 and +0.234 cm^{-1} for the v_1 and v_2 states, respectively.

Peterson and Dunning[295] performed high-level ab initio calculations to obtain the binding energy and structure of the HF dimer. They find as best estimates for the equilibrium properties $D_e = 4.60$ kcal/mol, $R_{FF} = 2.73$ Å, $r_{donor} = 0.922$ Å, $r_{acceptor} = 0.920$ Å, a slightly bent hydrogen bond (7°), and an angle of the free HF bond with R_{FF} of 111°. These computations were confirmed by Schaefer and co-workers.[296] The latter workers also gave the harmonic vibrational frequencies and IR intensities for $(HF)_2$. Later Schaefer et al.[297] improved their basis set and found $D_e = 4.91$ kcal/mol and $D_0 = 3.07$ kcal/mol, where the last number is within the harmonic approximation. Klopper et al.[298] performed explicitly correlated coupled cluster calculations on $(HF)_n$ for $n = 2, 3, 4, 5$ and found $D_e = 4.6$ kcal/mol for $(HF)_2$, in exact agreement with the value of Peterson and Dunning.

In the calculation of the VRT states of the dimer one needs full potential-energy surfaces, either 4D (HF bond lengths frozen) or 6D (all internal coordinates included). A 6D $(HF)_2$ potential-energy surface often used is the semiempirical SQSBDE potential of Quack and Suhm.[299] This potential was obtained by adjusting an older ab initio (coupled pair functional) potential such that the dimer rotational constant B and the dimer binding energy D_0 are reproduced by quantum Monte Carlo calculations. Recently Stone and co-workers[300] presented a new ab initio 4D potential for the HF dimer. This potential is extended to larger clusters, the induction energy accounting for many-body contributions to the energy. A few months after Stone's potential appeared, Quack and co-workers[301] reported a new 6D potential based on a large number of ab initio explicitly correlated second-order Møller−Plesset points. Again, they adjusted the potential to experiment obtaining two semiempirical pair potentials labeled SC-2.9 and SO-3. These intermolecular potentials are combined with a four-parameter intramonomer potential of generalized Poschl−Teller type.

The SQSBDE surface mentioned above was used by Zhang et al.[302] in 6D quantum calculations of the vibrational levels of $(HF)_2$, $(DF)_2$, and HF−DF, for total angular momentum $J = 0$. The ground-state tunneling splitting for the HF dimer from converged 6D calculations, 0.44 cm^{-1}, agrees exactly with the result of a 6D bound-state calculation for $(HF)_2$ by Necoechea and Truhlar.[303,304] Zhang et al., again using the SQSBDE potential, also computed $J = 0$ energy levels with excited monomer stretches; they considered $(v_1v_2) = (01)$, (10), (02), (20), and (11). These states are narrow resonances in the dissociation continuum. The calculated fundamental transition frequencies are $v_1 = 3940.6$ cm^{-1} and $v_2 = 3896.4$ cm^{-1}. These values are 10 and 28 cm^{-1} higher than the corresponding experimental values. Also, vibrational predissociation lifetimes were computed for $v_{HF} = 1$ states by means of a 4D golden rule method.[305] Similar calculations were performed by Truhlar and co-workers,[306] who obtained converged energies and tunneling splittings of the intramolecular stretching fundamentals and high-frequency, low-frequency combination levels on three different potential-energy surfaces, one of which was the SQSBDE surface. Wu et al.,[307,308] also using the SQSBDE potential, were the first to consider total $J > 1$ in 6D computations on $(HF)_2$. They computed the lowest 40 states for $0 \leq J \leq 4$ and parity $(-1)^J$. They found that for these low J values, Coriolis couplings are unimportant.

Very recently the SO-3 potential[301] was used by Vissers et al.[309] in 6D calculations. It gives a ground-state tunneling splitting of 0.59 cm^{-1}, significantly closer to the experimental value of 0.66 cm^{-1} than the splitting of 0.44 cm^{-1} obtained with the SQSBDE potential. Also, the acceptor and donor HF stretch frequencies are much better: $v_1 = 3929.2$ cm^{-1} and $v_2 = 3867.1$ cm^{-1}, close to the experimental values of $v_1 = 3930.90$ cm^{-1} and $v_2 = 3868.08$ cm^{-1}. Even the small excited-state interchange splittings are reproduced fairly well: −0.18 and +0.17 cm^{-1} for v_1 and v_2, respectively, while the values obtained[302] from the SQSBDE potential are −0.13 and +0.09 cm^{-1}. Clearly, the SO-3 potential of Klopper et al.[301] is an improvement over the SQSBDE potential.

Chang and Klemperer measured the vibrational second overtones of HF dimer[310] and introduced a phenomenological model[311] for the vibrational dependence of hydrogen interchange tunneling in this dimer.

We conclude this brief review on the HF dimer by mentioning a series of four recent near-infrared studies by Nesbitt and collaborators,[312−315] which characterize all four intermolecular modes of both $(HF)_2$ and $(DF)_2$. A large number of bands has been observed and assigned in which the low-frequency intermolecular modes: the van der Waals stretch (v_4), the geared and anti-geared bend (v_5 and v_3), and the torsional mode (v_6) are excited in combination with both of the high-frequency intramolecular HF stretches v_1 and v_2 of the hydrogen-bond acceptor and donor. This very complete experimental data set, which in addition to the vibrational frequencies includes the tunneling splittings, rotational constants, and predissociation rates of each of the excited states, may serve as a benchmark for testing 6D potentials.

Experimental studies have revealed that $(HCl)_2$ differs from $(HF)_2$ in several respects. The dissociation energy of the HCl dimer,[316] $D_0 = 431 \pm 22$ cm^{-1}, is much smaller than the D_0 of 1062 ± 1 cm^{-1} for $(HF)_2$.[317] The distance between the two HCl subunits of HCl dimer is about 40% larger than the separation of the HF subunits in $(HF)_2$. The ground-state tunneling splitting[318,319] of $(HCl)_2$ is 15.5 cm^{-1}, more than

20 times that of $(HF)_2$, indicating that $(HCl)_2$ is much floppier than $(HF)_2$.

Elrod and Saykally[320,321] calculated the VRT states of $(HCl)_2$ while keeping the HCl bond lengths fixed at 1.278 Å. They obtained an intermolecular potential-energy surface, the ES1 surface, from an earlier 6D ab initio potential[322,323] by performing a direct non-linear least-squares fit of eight of the ab initio parameters to 33 microwave, far-infrared, and near-infrared spectroscopic quantities. The global minimum ($D_e = 692$ cm^{-1}) is located near the planar hydrogen-bonded L-shaped geometry ($R = 3.746$ Å, $\Theta_1 = 9°$, $\Theta_2 = 89.8°$). The tunneling splitting obtained from this 6D potential in a 4D calculation is 15.66 cm^{-1}.

Qiu and Bačić[324] used the ES1 potential in 6D quantum calculations and found by comparison of the results with experimental data that the ES1 potential is indeed substantially more accurate than the earlier ab initio surface[322,323] but also that there is room for further refinement. In a later paper[24] Qiu et al. presented 6D computations of the vibrational levels of the v_1 and v_2 HCl stretch excited $(HCl)_2$ for $J = 0$. The ab initio potential[322,323] as well as the ES1 potential were found to give tunneling splittings for the vibrational eigenstates of the v_1/v_2 excited dimer that are 2 orders of magnitude smaller than the corresponding experimental values. To fix this problem, a 6D electrostatic interaction potential was added to the ES1 potential; the resulting potential is designated ES1-EL. Calculations on the ES1-EL surface yield v_1/v_2 tunneling splittings that are about 75% of the corresponding experimental values. Finally, we mention a recent $(HCl)_2$ potential[325] that to our knowledge has not yet been applied in VRT calculations.

We wish to end the review on $(HCl)_2$ by referring to two recent experimental papers on the dimer and its isotopomers. The first regards the dipole moment of the complex: By focusing of HCl and DCl dimers in an electrostatic hexapole field, the electric dipole moments for both $(D^{35}Cl)_2$ and $(D^{37}Cl)_2$ were determined to be 1.5 ± 0.2 D, which is the same value as that observed for $(HCl)_2$.[326] Second, Liu et al.[327] report overtone spectra of $(H^{35}Cl)_2$ and its Cl isotope mixed dimers obtained by using IR cavity ringdown laser absorption spectroscopy. Their findings indicate that the $H^{35}Cl-H^{37}Cl$ and $H^{37}Cl-H^{35}Cl$ heterodimers are distinguishable at the eigenstate level in the first overtone excited state ($2v_1$), which—as we just discussed—is not the case for the ground and HCl stretch fundamental eigenstates because of tunneling.

Also, trimers and larger clusters of HF, DF, and HCl were studied experimentally and theoretically, see the review by Bačić and Miller[292] and the recent work of Quack et al.[328] The measured properties of these, mostly cyclic, hydrogen-bonded clusters will serve as a testing ground for the many-body interactions calculated ab initio.[298]

6.2.2. Water Clusters

In section 4 we mentioned that high-resolution infrared spectra have been taken of water clusters up to the hexamer,[119,124−126,129−147] but so far we have only discussed the dimer and the trimer. The equilibrium structures of the tetramer and pentamer correspond to a cyclic hydrogen-bonded geometry, just like the trimer, with each water molecule acting simultaneously as proton donor and proton acceptor. The tetramer has a square-planar system of hydrogen bonds, and the pentamer has a slightly puckered pentagonal hydrogen-bonded framework. In both cases the external, non-hydrogen-bonded, protons lie above and below the planes of the hydrogen-bonded 'skeletons' (denoted 'up' and 'down' or *u* and *d*). For $(H_2O)_4$ the *u* and *d* protons alternate and the symmetry group of the equilibrium structure is the point group S_4. Two equivalent minima of this type exist, *udud* and *dudu*. From the spectra[137−139] it is known that they are connected by a tunneling process which involves a concerted $u-d$ flip of all four external protons and leads to a feasible permutation−inversion group G_8 isomorphic to C_{4h}. This rather high-barrier process was theoretically studied by Wales and Walsh[329] and, in 4D quantum calculations, by Leutwyler and co-workers.[330,331] The tunneling splittings calculated[331] for $(H_2O)_4$ and $(D_2O)_4$ with the use of a high-quality 4D ab initio potential[330] do not agree at all with the experimental values.[137−139] Three different possible explanations are given for this discrepancy,[331] but the problem has not been resolved yet.

In some respects, the water pentamer is more similar to the trimer than the tetramer. Just as in the trimer, it has a 'frustrated' equilibrium structure, *uudud*, with two neighboring protons on the same side of a nearly planar hydrogen-bonded framework and no spatial symmetry. It is connected to another global minimum, *dudud*, by the up−down flip of one of these two protons. In the pentamer this proton flip is accompanied by a wagging motion of one of the flaps of the puckered hydrogen-bonded framework.[332] There are 10 equivalent global minima interconnected by this tunneling process, and G_{10}, isomorphic to C_{5h}, is the feasible PI group. Just as in the trimer, there is also a bifurcation tunneling process, which increases the number of accessible minima by a factor of 2^5 and yields the PI group G_{320} in this case. Both Wales and Walsh[333] and Graf et al.[332] performed 1D model calculations for the flipping motions with the use of an ab initio potential and compared their results with the experimental data.[135,140,143]

The high-resolution far-infrared studies of water clusters up to the hexamer[134−141,143] have been both preceded and succeeded by ab initio calculations[110,112,179,334−336] and by rigid-body diffusional QMC studies.[136,337,338] The ab initio calculations predicted the equilibrium geometries and harmonic vibrational frequencies. The QMC calculations of Clary and co-workers[136,337] made use of the ASP model potential[174] and focused on the effect of the strongly anharmonic zero-point motions on the rotational constants. Especially for the hexamer, this has led to an interesting result: it is the smallest cluster that does not have the cyclic hydrogen-bonded ring structure as the lowest energy minimum. The rotational constants from QMC calculations in con-

junction with the experimental data[136,141] established that it has a cage-like structure.[136] An interesting observation is that without the inclusion of the zero-point vibrational energy, this cage-like structure would probably not be the most stable one. Also, Severson and Buch[338] applied the rigid-body QMC method to the water hexamer and obtained rotational constants. After developing a nodal optimization scheme in which the fundamental excited-state nodes are constructed from harmonic normal coordinates, they could study 10 low-lying intermolecular excited vibrational states of the cage form of $(H_2O)_6$, in addition to the ground state. They found substantial anharmonic effects and assigned the band observed by Liu et al.[136] to a transition involving primarily flipping motions of the free O−H bonds on the doubly bound monomers. A more generally applicable way to obtain anharmonic excited states from QMC calculations is by the projector Monte Carlo method of Blume and Whaley. This method has recently been tested[339] on the torsional excitations in the water trimer, extensively discussed in section 5. Also, the water heptamer and octamer were studied by ab initio methods,[340−346] while the isomerization and melting behavior of the hexamer and octamer were simulated by classical Monte Carlo (MC) and molecular dynamics (MD) methods.[347,348] Dang[349] employed a classical MD method with a polarizable model potential to find the equilibrium geometry of the nonamer and decamer.

Clusters larger than the hexamer, with $n = 7$, 8, 9, and 10, have been studied experimentally by looking at the O−H and O−D stretch vibrations. Recent developments are: infrared cavity ringdown laser absorption spectroscopy with rotational resolution[130] and the combination of infrared spectroscopy with size selection by He beam deflection and mass spectrometry.[350−352] This work is summarized in the review article of Buck and Huisken in the present issue of *Chemical Reviews*. References to older work are given in the papers cited. In the discussion of the HF dimer in section 6.2.1, we observed that the red shift of the H−F stretch frequency is much larger for the proton donor than for the acceptor. In the water dimer, the donor O−H (or O−D) shift is much larger for the bound proton than for the free proton. From ab initio calculations[341,353,354] it follows that for larger clusters this shift depends also on the involvement of the water monomers in other hydrogen bonds. One can distinguish so-called single-donor and double-donor, as well as single-acceptor and double-acceptor, molecules by their different shifts of the O−H stretch frequency. In this manner it was possible, with the help of ab initio and model potential calculations,[351,352] to derive the structure of these larger water clusters from their O−H vibrational spectra, without the use of rotationally resolved spectra. It was thus established that the water octamer has a cubic structure with two isomers of D_{2d} and S_4 symmetry existing simultaneously.[351] These are the same forms of the water octamer cube as found in a water octamer−benzene complex by resonant ion-dip infrared spectroscopy.[355,356] Also, the assignment of the latter spectra employs the O−H frequency shift as a signature; these shifts were computed by a density functional method. The pure water heptamer has two isomers as well,[352] which are derived from the S_4 cubic octamer by removal of either a double-donor or a double-acceptor water molecule. The nonamer is derived from the octamer by insertion of a two-coordinated molecule into one of the cube edges; the decamer structure is obtained by a second similar insertion.[351]

Also, the hydrogen bonding of water to other species such as methanol,[357−359] phenol, indole,[360−363] and benzyl alcohol[364] has received attention through the spectroscopic and theoretical study of mixed dimers and larger clusters. In particular, the phenol−water dimer has been studied in great detail by UV spectroscopy with rotational resolution,[365,366] by mass-resolved UV spectral hole burning,[367] by infrared-UV and stimulated Raman-UV double resonance techniques,[368] and by microwave spectroscopy,[369] as well as theoretically.[370]

6.2.3. Benzene–Water, π-Electron Hydrogen Bonding

The hydrophobic interaction between water and aromatic molecules which stabilizes water cluster−benzene complexes[344,355,356] has been studied in detail in a series of spectroscopic papers on the water−benzene dimer. The water−benzene interaction may be conceived as bonding of the positive hydrogen side of a water molecule to the negative π-electron cloud of benzene. Its binding energy $D_0 = 855 \pm 32$ cm^{-1} for $C_6H_6-H_2O$ and 936 ± 40 cm^{-1} for $C_6H_6-D_2O$ deduced from measurements of ionization thresholds by Courty et al.[371] is not much lower than the dissociation energy of a normal hydrogen bond in the water dimer, $D_0 = 1077$ cm^{-1} for $(H_2O)_2$ and 1214 cm^{-1} for $(D_2O)_2$ (see section 4.3), and substantially higher than that of the nonpolar Ar−benzene complex, $D_0 = 328$ cm^{-1} for C_6H_6 and 331 cm^{-1} (or 316 cm^{-1}) for C_6D_6.[248,250] Structural information has been obtained from the microwave spectra of several isotopomers of benzene−water.[372,373] The C_6H_6 to H_2O center-of-mass distance R is 3.329 Å, and the oxygen is on the 6-fold axis of benzene. The hydrogens of H_2O are closer to the benzene plane than the oxygen by 0.48 Å. The 6-fold axis of benzene coincides with the *a*-axis of the complex; hence, there is little or no tilt of the benzene molecule. The C_2 axis of H_2O is not coincident with the *a*-axis but is at an angle of 37° to it. It is evident from the spectra that the complex is not nearly rigid: the dimers of the parent C_6H_6 benzene with H_2O, HDO, D_2O, and $H_2{}^{18}O$ have symmetric top spectra characteristic of two coaxial rotors with a symmetric top frame and a very low effective 6-fold barrier. The dimers of H_2O and D_2O with ^{13}C and D monosubstituted benzenes have asymmetric top spectra, with a 2-fold term of only $\approx$0.5 MHz in their barriers. The hyperfine structure from the proton−proton magnetic dipole interaction and the deuterium quadrupole interaction demonstrates effective nuclear equivalence in dimers with H_2O and D_2O. The symmetries found for their nuclear spin functions correlate with the lowest rotational levels of free water, the $m = 0$ internal

rotor state with 0_{00} and the $m = 1$ state with 1_{01} and 1_{11}. For the $m = 1$, $K = 0$ transitions of $C_6H_6-H_2O$, the correlation is with 1_{11} and for the $K = 1$ with 1_{01}. These assignments are reversed for $C_6H_6-D_2O$.

Also, by resonant ion-dip infrared spectroscopy[374,375] of benzene−H_2O and benzene−HOD, it was found that there is nearly free internal rotation of H_2O about benzene's 6-fold axis in both ground and vibrationally excited states. A 2-dimensional model involving free internal rotation and torsion of HOD in its plane is used[374,375] to account for the qualitative appearance of the spectrum. The O−H ($v = 0$) and O−H ($v = 1$) torsional potentials which reproduce the qualitative features of the spectrum are slightly asymmetric double-minimum potentials which allow large-amplitude excursions of HOD over nearly 180°. Reference 376 presents a theoretical investigation of benzene−water by diffusion QMC methods. Simulations were performed for four isotopomers of $C_6H_6-H_2O$ with two different site−site model potentials: one of Lennard−Jones plus Coulomb type and one that was obtained from a fit of 153 ab initio data points.[377] Although the minimum energy structure can be considered to have only a single hydrogen bond, vibrational averaging renders the hydrogens indistinguishable, a prediction in agreement with the experimental observation that the complex is a symmetric top. The results include zero-point energies, vibrationally averaged structures, rotational constants and wave functions. By calculating transition states and rearrangement mechanisms, it is possible to characterize the tunneling dynamics and calculate the associated tunneling splittings. Kim et al.[378] performed 6-dimensional DVR calculations of the $J = 0$ intermolecular states in the benzene−H_2O complex up to about 110 cm^{-1} by a filter diagonalization method. They used the same site−site model potential from ref 377 as the QMC study of ref 376. The results are interpreted in terms of five internal rotation states, a doubly degenerate bending mode and a nondegenerate stretching mode, the latter two modes involving the relative translation of the monomers in the complex. The internal rotation states are discussed in terms of the model of Pribble et al.[375] It is shown that this model is largely successful in identifying the important features of the low-energy benzene−H_2O states that involve rotation and/or libration of water.

Benzene−water clusters with more than one water molecule have been investigated experimentally by Zwier and co-workers[344,355,356] and by Maxton et al.[379] It was mentioned already in section 6.2.2 that Zwier and co-workers used resonant ion-dip infrared spectroscopy to measure shifts of the O−H stretch vibrations. Maxton et al. report species-selective spectra of intermolecular vibrational transitions in $C_6H_6-(H_2O)_n$ clusters with $n = 1, ..., 5$, measured by mass-selective, ionization-loss stimulated Raman spectroscopy. The spectra exhibit prominent Raman activity in the range of 35−65 cm^{-1}. In addition, Raman bands at less than 10 cm^{-1} are found for the $n = 1$ and 3 species, and rotational Raman features are observed for all of the clusters. It is argued that much of the Raman activity is due to intermolecular vibrations in which water moieties move collectively across the plane of the benzene. Sorenson and Clary[380] performed a rigid-body QMC study of the vibrationally averaged structure, binding energy, and rotational constants of benzene−$(H_2O)_2$. Estimates of some rearrangement tunneling splittings were given as well.

6.3. Conclusion

This selection from the recent literature shows that impressive progress has been made since 1994, both in theory and experiment. Since this is mostly a theoretical paper, we will not try to summarize the experimental developments. Instead, we refer to the experimental papers in this *Chemical Reviews* issue. On the theoretical side, one observes that high-quality intermolecular pair potentials can now be obtained from ab initio calculations for molecules of size up to benzene, either by the use of supermolecule methods or by symmetry-adapted perturbation theory (SAPT). Still, some systems, like the CO dimer,[381] appear to resist the computation of a reliable potential and require a level of electron correlation that is even higher than the CCSD(T) method. Also, three-body interactions can be reliably computed by ab initio methods, although the large number of coordinates needed to describe a full three-body potential surface makes it difficult to obtain good analytic representations of these interactions. Quantum dynamical methods to treat large-amplitude motions have now arrived at six fully coupled degrees of freedom, except for the quantum Monte Carlo method which is applicable to more complex systems. In general, however, QMC methods have problems with vibrationally excited states. Other methods that allow the treatment of larger systems are based on some kind of decoupling scheme, such as the time-dependent Hartree or self-consistent field method. In the multiconfiguration versions of these methods,[382−384] the coupling is partially restored. If, in the future, these methods will reach a sufficiently high level of accuracy, they will become a tool for the spectroscopic probing of intermolecular potentials for more complex systems. Despite the high quality of the ab initio potentials that have become available for quite a few systems, we saw several examples where the use of cluster spectroscopic data, due to their extremely high precision and sensitive dependence on the potential surface, made it possible to improve the ab initio potential. Most progress is made in the study of van der Waals molecules by the intensive and stimulating collaboration between theoreticians and experimentalists. Future theoretical work will involve the extension to closed-shell systems of ever increasing size and the explicit inclusion of the intramolecular degrees of freedom and the coupling between the intermolecular motions and the molecular vibrations. Future developments will also concentrate more on open-shell systems, electronic excitations, and chemical reactions in van der Waals complexes, for which work is still rather scarce at present.

7. Acknowledgment

We thank Richard J. Saykally and Roger E. Miller for stimulating collaborations and for making available the experimental spectra shown in this review. We gratefully acknowledge the permission of Eric M. Mas, Robert Bukowski, Krzysztof Szalewicz, and Gerrit C. Groenenboom to present the water dimer and trimer results obtained with the SAPT-5s water pair potential and three-body interactions before publication. Gerrit Groenenboom is also thanked for valuable discussions and for critically reading the manuscript.

8. Appendix A

We will prove eq 3 of the main text. First we note that $\sqrt{g} \equiv w(\boldsymbol{q})$ is the volume element belonging to the coordinates $\boldsymbol{q}$. Since G is Hermitian and positive definite, the weight function $w(\boldsymbol{q})$ is real and positive. For the sake of argument we restrict our attention to the 1-dimensional case. We consider

$$\left\langle \phi \middle| \frac{d\psi}{dq} \right\rangle \equiv \int_{q_1}^{q_2} \phi^*(q)\psi(q)'w(q)dq \text{ with } \psi(q)' = \frac{d\psi(q)}{dq}$$

and assume that $[\phi^*(q)\psi(q)w(q)]_{q_1}^{q_2} = 0$. This gives

$$0 = \int_{q_1}^{q_2} \frac{d(\phi^*\psi w)}{dq} dq = \int_{q_1}^{q_2} \phi^*\psi' w dq + \int_{q_1}^{q_2} \psi(\phi^* w)' dq = \int_{q_1}^{q_2} \phi^*\psi' w dq + \int_{q_1}^{q_2} w^{-1}(\phi^* w)'\psi w dq$$

Hence

$$\int \phi^* \frac{d\psi}{dq} w dq = -\int w^{-1} \frac{d(w\phi)^*}{dq} \psi w dq \equiv -\left\langle w^{-1} \frac{d(w\phi)}{dq} \middle| \psi \right\rangle$$

and thus

$$\left(\frac{d}{dq}\right)^\dagger = -w^{-1}\frac{d}{dq}w$$

Multiplying by $i\hbar$ we find eq 3. Similarly, we can derive

$$\int \phi^* w^{-1} \frac{d(w\psi)}{dq} w dq = -\int \frac{d\phi^*}{dq} \psi w dq$$

so that

$$\left(w^{-1}\frac{d}{dq}w\right)^\dagger = -\frac{d}{dq}$$

and $(p^\dagger)^\dagger = p$.

9. Appendix B

In this Appendix we define the Euler angles in an algebraic manner and show that exactly three Euler angles are needed to describe a rotation. In the usual definition ('rotate around the *z*-axis, then around the new *y*-axis', etc.) this fact relies on geometrical insight and is strictly speaking not proved.

Consider the linear transformation from one orthonormal right-handed frame to another:

$$(\vec{f}_x, \vec{f}_y, \vec{f}_z) = (\vec{e}_x, \vec{e}_y, \vec{e}_z)\,\mathrm{R}$$

The matrix R is orthogonal: $\mathrm{R} = \mathrm{R}^T$ and proper: det = 1. Write $\mathrm{R} = (\boldsymbol{r}_1, \boldsymbol{r}_2, \boldsymbol{r}_3)$ and the properties of R imply that the columns $\boldsymbol{r}_i$, $i = 1, 2, 3$, form a right-handed orthogonal set of unit vectors. We define the rotation matrices:

$$\mathrm{R}_z(\varphi) \equiv \begin{pmatrix} \cos\varphi & -\sin\varphi & 0 \\ \sin\varphi & \cos\varphi & 0 \\ 0 & 0 & 1 \end{pmatrix}$$

$$\mathrm{R}_y(\varphi) \equiv \begin{pmatrix} \cos\varphi & 0 & \sin\varphi \\ 0 & 1 & 0 \\ -\sin\varphi & 0 & \cos\varphi \end{pmatrix}$$

Any proper orthogonal matrix R can be factorized as a 3-fold product of these matrices:

$$\mathrm{R} = \mathrm{R}_z(\alpha)\,\mathrm{R}_y(\beta)\,\mathrm{R}_z(\gamma)$$

The angles α, β, and γ are the *Euler angles* of the frame $(\vec{f}_x, \vec{f}_y, \vec{f}_z)$ with respect to the frame $(\vec{e}_x, \vec{e}_y, \vec{e}_z)$.

To prove the factorization we consider

$$\mathrm{R}_z(\alpha)\,\mathrm{R}_y(\beta) = \begin{pmatrix} \cos\alpha\cos\beta & -\sin\alpha & \cos\alpha\sin\beta \\ \sin\alpha\cos\beta & \cos\alpha & \sin\alpha\sin\beta \\ -\sin\beta & 0 & \cos\beta \end{pmatrix} \equiv (\boldsymbol{a}_1, \boldsymbol{a}_2, \boldsymbol{a}_3)$$

The spherical polar angles β and α ($0 \le \beta \le \pi$, $0 \le 2\pi$) of $\boldsymbol{r}_3$ are determined in the usual way; from the definition of the spherical polars follows that $\boldsymbol{r}_3 = \boldsymbol{a}_3$. With α and β uniquely determined, also the orthogonal unit vectors $\boldsymbol{a}_1$ and $\boldsymbol{a}_2$ are given uniquely.

Since $\boldsymbol{a}_1$, $\boldsymbol{a}_2$, and $\boldsymbol{a}_3$ are the columns of a proper rotation matrix, they form an orthonormal right-handed system. The plane spanned by $\boldsymbol{a}_1$ and $\boldsymbol{a}_2$ is orthogonal to $\boldsymbol{a}_3 = \boldsymbol{r}_3$ and hence contains $\boldsymbol{r}_1$ and $\boldsymbol{r}_2$. Thus,

$$(\boldsymbol{r}_1, \boldsymbol{r}_2) = (\boldsymbol{a}_1, \boldsymbol{a}_2) \begin{pmatrix} \cos\gamma & -\sin\gamma \\ \sin\gamma & \cos\gamma \end{pmatrix}.$$

As $\boldsymbol{a}_1$, $\boldsymbol{a}_2$, and $\boldsymbol{r}_1$ are known unit vectors, we can compute

$$\boldsymbol{a}_1 \cdot \boldsymbol{r}_1 = \cos\gamma \text{ and } \boldsymbol{a}_2 \cdot \boldsymbol{r}_1 = \sin\gamma$$

These equations give γ, $0 \le \gamma \le 2\pi$. Finally, because of the block structure of $\mathrm{R}_z(\gamma)$

$$\mathrm{R} \equiv (\boldsymbol{r}_1, \boldsymbol{r}_2, \boldsymbol{r}_3) = (\boldsymbol{a}_1, \boldsymbol{a}_2, \boldsymbol{a}_3)\,\mathrm{R}_z(\gamma) = \mathrm{R}_z(\alpha)\,\mathrm{R}_y(\beta)\,\mathrm{R}_z(\gamma)$$

Often one defines

$$\mathrm{R}_{z''}(\gamma) \equiv [\mathrm{R}_z(\alpha)\,\mathrm{R}_y(\beta)]\,\mathrm{R}_z(\gamma)[\mathrm{R}_z(\alpha)\,\mathrm{R}_y(\beta)]^{-1}$$

and

$$\mathrm{R}_{y'}(\beta) \equiv \mathrm{R}_z(\alpha)\,\mathrm{R}_y(\beta)\,\mathrm{R}_z(\alpha)^{-1}$$

It is easy to see then that

$$R = R_{z''}(\gamma)\, R_{y'}(\beta)\, R_z(\alpha)$$

The latter factorization corresponds to the geometric definition of the Euler angles.

Another parametrization often used to describe rotations uses a normalized vector $\boldsymbol{h} = (h_x, h_y, h_z)$ as the rotation axis. The two polar angles of $\boldsymbol{h}$ give two of the three required parameters. The third parameter is the angle χ over which the molecule is rotated. It is easy to prove[205] that

$$R_{\boldsymbol{h}}(\chi) = E + \sin\chi\, H + (1 - \cos\chi)\, H^2 \qquad (27)$$

where

$$H = \begin{pmatrix} 0 & -h_z & h_y \\ h_z & 0 & -h_x \\ -h_y & h_x & 0 \end{pmatrix}.$$

It is easily shown that

$$H\boldsymbol{r} = \boldsymbol{h} \times \boldsymbol{r}$$

for any arbitrary vector $\boldsymbol{r}$, where the expression on the right-hand side denotes the cross product of two vectors.

10. References

(1) Verhoeve, P.; Zwart, E.; Versluis, M.; Drabbels, M.; ter Meulen, J. J.; Meerts, W. L. *Rev. Sci. Instrum.* **1990**, *61*, 1612.
(2) Blake, G. A.; Laughlin, K. B.; Cohen, R. C.; Busarow, K. L.; Gwo, D.-H.; Schmuttenmaer, C. A.; Steyert, D. W.; Saykally, R. J. *Rev. Sci. Instrum.* **1991**, *62*, 1693.
(3) Blake, G. A.; Laughlin, K. B.; Cohen, R. C.; Busarow, K. L.; Gwo, D.-H.; Schmuttenmaer, C. A.; Steyert, D. W.; Saykally, R. J. *Rev. Sci. Instrum.* **1991**, *62*, 1701.
(4) Cohen, R. C.; Saykally, R. J. *J. Phys. Chem.* **1992**, *96*, 1024.
(5) Linnartz, H.; Meerts, W. L.; Havenith, M. *Chem. Phys.* **1995**, *193*, 327.
(6) Miller, R. E. Infrared Spectroscopy. In *Atomic and Molecular Beam Methods*; Scoles, G., Ed.; Oxford University Press: Oxford, 1992; Vol. 2.
(7) Nesbitt, D. J. *Faraday Discuss. Chem. Soc.* **1994**, *97*, 1.
(8) Neusser, H. J.; Krause, H. *Chem. Rev.* **1994**, *94*, 1829.
(9) McKellar, A. R. W. *Faraday Discuss. Chem. Soc.* **1994**, *97*, 69.
(10) van der Avoird, A.; Wormer, P. E. S.; Moszynski, R. *Chem. Rev.* **1994**, *94*, 1931.
(11) van der Avoird, A.; Wormer, P. E. S.; Moszynski, R. Theory and Computation of Vibration, Rotation and Tunneling Motions of van der Waals Complexes and their Spectra. In *Molecular Interactions: From van der Waals to Strongly Bound Complexes*; Scheiner, S., Ed.; Wiley: New York, 1997.
(12) Papoušek, D.; Aliev, M. R. *Molecular Vibrational−Rotational Spectra*; Elsevier: Amsterdam, 1982.
(13) Louck, J. D.; Galbraith, H. W. *Rev. Mod. Phys.* **1976**, *48*, 69.
(14) Wilson, E. B.; Decius, J. C.; Cross, P. C. *Molecular Vibrations*; McGraw-Hill: New York, 1955.
(15) Bunker, P. R.; Jensen, P. *Molecular Symmetry and Spectroscopy*, 2nd ed.; NRC Research Press: Ottawa, 1998.
(16) Makarewicz, J.; Bauder, A. *Mol. Phys.* **1995**, *84*, 853.
(17) Justum, Y.; Menou, M.; Nauts, A.; Chapuisat, X. *Chem. Phys.* **1997**, *223*, 211.
(18) Spiegel, M. R. *Vector Analysis and an Introduction to Tensor Analysis*; Schaum's outline series; Mc-Graw-Hill: New York, 1959.
(19) Podolsky, B. *Phys. Rev.* **1928**, *32*, 812.
(20) Chapuisat, X.; Belafhal, A.; Nauts, A. *J. Mol. Spectrosc.* **1991**, *149*, 274.
(21) Wei, H.; Carrington, T., Jr. *J. Chem. Phys.* **1994**, *101*, 1343.
(22) van der Avoird, A.; Olthof, E. H. T.; Wormer, P. E. S. *J. Chem. Phys.* **1996**, *105*, 8034.
(23) Brocks, G.; van der Avoird, A.; Sutcliffe, B. T.; Tennyson, J. *Mol. Phys.* **1983**, *50*, 1025.
(24) Qiu, Y.; Zhang, J. Z. H.; Bačić, Z. *J. Chem. Phys.* **1998**, *108*, 4804.
(25) Brocks, G.; van Koeven, D. *Mol. Phys.* **1988**, *63*, 999.
(26) van der Avoird, A. *J. Chem. Phys.* **1993**, *98*, 5327.
(27) Mitchell, K. A.; Littlejohn, R. G. *Mol. Phys.* **1999**, *96*, 1305.
(28) Mladenović, M. *J. Chem. Phys.* **2000**, *112*, 1070.
(29) Mladenović, M. *J. Chem. Phys.* **2000**, *112*, 1082.
(30) Jeziorski, B.; Moszynski, R.; Szalewicz, K. *Chem. Rev.* **1994**, *94*, 1887.
(31) Chalasiński, G.; Szczęśniak, M. M. *Chem. Rev.* **1994**, *94*, 1723.
(32) van Duijneveldt, F. B.; van Duijneveldt-van der Rijdt, J. G. C. M.; van Lenthe, J. H. *Chem. Rev.* **1994**, *94*, 1873.
(33) Chuaqui, C. E.; Roy, R. J. L.; McKellar, A. R. W. *J. Chem. Phys.* **1994**, *101*, 39.
(34) Fellers, R. S.; Leforestier, C.; Braly, L. B.; Brown, M. G.; Saykally, R. J. *Science* **1999**, *284*, 945.
(35) Meuwly, M.; Hutson, J. M. *J. Chem. Phys.* **1999**, *110*, 8338.
(36) Cohen, R. C.; Saykally, R. J. *Ann. Rev. Phys. Chem.* **1991**, *42*, 369.
(37) Brink, D. M.; Satchler, G. R. *Angular Momentum*, 3rd ed.; Clarendon: Oxford, 1993.
(38) Tennyson, J.; Sutcliffe, B. T. *J. Chem. Phys.* **1982**, *77*, 4061.
(39) Tennyson, J.; Sutcliffe, B. T. *J. Chem. Phys.* **1983**, *79*, 43.
(40) Bačić, Z.; Light, J. C. *J. Chem. Phys.* **1986**, *85*, 4594.
(41) Clary, D. C.; Nesbitt, D. J. *J. Chem. Phys.* **1989**, *90*, 7000.
(42) Le Roy, R. J.; van Kranendonk, J. *J. Chem. Phys.* **1974**, *61*, 4750.
(43) Arthurs, A. M.; Dalgarno, A. *Proc. Royal Soc. (London) A* **1960**, *256*, 540.
(44) Child, M. S. *Molecular Collision Theory*; Academic: New York, 1974.
(45) Hutson, J. M. *Adv. Mol. Vib. Collision Dyn.* **1991**, *1*, 1.
(46) Light, J. C.; Hamilton, I. P.; Lill, J. V. *J. Chem. Phys.* **1985**, *82*, 1400.
(47) Choi, S. E.; Light, J. C. *J. Chem. Phys.* **1990**, *92*, 2129.
(48) Mladenović, M.; Bačić, Z. *J. Chem. Phys.* **1991**, *94*, 4988.
(49) Mandziuk, M. M.; Bačić, Z. *J. Chem. Phys.* **1993**, *98*, 7165.
(50) Cohen, R. C.; Saykally, R. J. *J. Phys. Chem.* **1990**, *94*, 7991.
(51) Peet, A. C.; Yang, W. *J. Chem. Phys.* **1989**, *90*, 1746.
(52) Peet, A. C.; Yang, W. *J. Chem. Phys.* **1989**, *91*, 6598.
(53) Yang, W.; Peet, A. C.; Miller, W. H. *J. Chem. Phys.* **1989**, *91*, 7537.
(54) Block, P. A.; Pedersen, L. G.; Miller, R. E. *J. Chem. Phys.* **1993**, *98*, 3754.
(55) Friesner, R. A. *Ann. Rev. Phys. Chem.* **1991**, *42*, 341.
(56) Martinez, T. J.; Carter, E. A. Pseudospectral Methods Applied to the Electronic Correlation Problem. In *Modern Electronic Structure Theory, Part II*; Yarkony, D. R., Ed.; World Scientific: Singapore, 1995.
(57) Anderson, J. B. *Ann. Rev. Phys. Chem.* **1995**, *14*, 85.
(58) Buch, V. *J. Chem. Phys.* **1992**, *97*, 726.
(59) Gregory, J. K.; Clary, D. C. *Chem. Phys. Lett.* **1994**, *228*, 547.
(60) Gregory, J. K.; Clary, D. C. *J. Phys. Chem.* **1996**, *100*, 18014.
(61) Hougen, J. T. *J. Chem. Phys.* **1962**, *37*, 1433.
(62) Longuet-Higgins, H. C. *Mol. Phys.* **1963**, *6*, 445.
(63) van Bladel, J. W. I.; van der Avoird, A.; Wormer, P. E. S.; Saykally, R. J. *J. Chem. Phys.* **1992**, *97*, 4750.
(64) Olthof, E. H. T.; van der Avoird, A.; Wormer, P. E. S. *J. Chem. Phys.* **1994**, *101*, 8430.
(65) van Bladel, J. W. I.; van der Avoird, A.; Wormer, P. E. S. *J. Phys. Chem.* **1991**, *95*, 5414.
(66) Heijmen, T. G. A.; Moszynski, R.; Wormer, P. E. S.; van der Avoird, A. *Mol. Phys.* **1996**, *89*, 81.
(67) Lovejoy, C. M.; Hutson, J. M.; Nesbitt, D. J. *J. Chem. Phys.* **1992**, *97*, 8009.
(68) Block, P. A.; Miller, R. E. *Chem. Phys. Lett.* **1994**, *226*, 317.
(69) Cohen, R. C.; Saykally, R. J. *J. Chem. Phys.* **1993**, *98*, 6007.
(70) Weida, M. J.; Nesbitt, D. J. *J. Chem. Phys.* **1997**, *106*, 3078.
(71) Schmuttenmaer, C. A.; Cohen, R. C.; Saykally, R. J. *J. Chem. Phys.* **1994**, *101*, 146.
(72) Jacobs, T.; Peeters, L.; Vermant, J. *Bull. Soc. Chim. Belges* **1970**, *79*, 337.
(73) Trengove, R. D.; Robjohns, H. L.; Dunlop, P. J. *Ber. Bunsen-Ges. Phys. Chem.* **1982**, *86*, 951.
(74) Dunlop, P. J.; Bignell, C. M. *Physica A* **1987**, *145*, 584.
(75) Rakshit, A. B.; Roy, C. S.; Barua, A. K. *J. Chem. Phys.* **1973**, *59*, 3633.
(76) Kestin, J.; Ro, S. T. *Ber. Bunsen-Ges. Phys. Chem.* **1974**, *78*, 20.
(77) Kestin, J.; Ro, S. T. *Ber. Bunsen-Ges. Phys. Chem.* **1976**, *80*, 619.
(78) Strein, K.; Lichtenthaler, R. N.; Schramm, B.; Schäfer, K. *Ber. Bunsen-Ges. Phys. Chem.* **1971**, *75*, 1308.
(79) Hahn, R.; Schäfer, K.; Schramm, B. *Ber. Bunsen-Ges. Phys. Chem.* **1974**, *78*, 287.
(80) Bellm, J.; Reineke, W.; Schäfer, K.; Schramm, B. *Ber. Bunsen-Ges. Phys. Chem.* **1974**, *78*, 282.
(81) Martin, M. L.; Trengove, R. D.; Harris, K. R.; Dunlop, P. J. *Aust. J. Chem.* **1982**, *35*, 1525.
(82) Heintz, A.; Lichtenthaler, R. N.; Schäfer, K. *Ber. Bunsen-Ges. Phys. Chem.* **1975**, *79*, 426.
(83) Shahin, F.; Abdel-Latif, B. T.; Farag, N. *J. Chem. Phys.* **1980**, *73*, 2465.
(84) Behrens, R., Jr.; Freedman, A.; Herm, R. R.; Parr, T. P. *Chem. Phys. Lett.* **1975**, *36*, 446.

(85) Buck, U.; Schleusener, J.; Malik, D. J.; Secrest, D. *J. Chem. Phys.* **1981**, *74*, 1707.
(86) Buck, U.; Kohlhase, A.; Phillips, T.; Secrest, D. *Chem. Phys. Lett.* **1983**, *98*, 199.
(87) Brooks, J. R.; Grosser, A. E. *Physica* **1974**, *78*, 340.
(88) Kistemaker, P. G.; Hanna, M. M.; de Vries, A. E. *Physica* **1972**, *60*, 459.
(89) Kistemaker, P. G.; Hanna, M. M.; de Vries, A. E. *Physica* **1974**, *78*, 457.
(90) Chapman, W. B.; Schiffman, A.; Hutson, J. M.; Nesbitt, D. J. *J. Chem. Phys.* **1996**, *105*, 3497.
(91) Chapman, W. B.; Kulcke, A.; Blackmon, B. W.; Nesbitt, D. J. *J. Chem. Phys.* **1999**, *110*, 8543.
(92) Miller, R. E. *Faraday Discuss. Chem. Soc.* **1994**, *97*, 177.
(93) Nesbitt, D. J. *Faraday Discuss. Chem. Soc.* **1994**, *97*, 175.
(94) Fowler, P. W.; Lazzeretti, P.; Zanasi, R. *Mol. Phys.* **1989**, *68*, 853.
(95) Szczęśniak, M. M.; Chalasiński, G.; Cybulski, S. M. *J. Chem. Phys.* **1992**, *96*, 463.
(96) Heijmen, T. G. A.; Korona, T.; Moszynski, R.; Wormer, P. E. S.; van der Avoird, A. *J. Chem. Phys.* **1997**, *107*, 902.
(97) Heijmen, T. G. A.; Moszynski, R.; Wormer, P. E. S.; van der Avoird, A.; Buck, U.; Steinbach, C.; Hutson, J. M. *J. Chem. Phys.* **1998**, *108*, 4849.
(98) Heijmen, T. G. A.; Wormer, P. E. S.; van der Avoird, A.; Miller, R. E.; Moszynski, R. *J. Chem. Phys.* **1999**, *110*, 5639.
(99) Miller, R. E.; Heijmen, T. G. A.; Wormer, P. E. S.; van der Avoird, A.; Moszynski, R. *J. Chem. Phys.* **1999**, *110*, 5651.
(100) Tarrago, G.; Dang-Nhu, M.; Poussigue, G.; Guelachvili, G.; Amiot, C. *J. Mol. Spectrosc.* **1975**, *57*, 246.
(101) Gray, D. L.; Robiette, A. G.; Pine, A. S. *J. Mol. Spectrosc.* **1979**, *77*, 440.
(102) *Handbook of Chemistry and Physics*; Weast, R. C., Asth, M. J., Eds.; Chemical Rubber: Boca Raton, 1981.
(103) Bukowski, R.; Jankowski, P.; Jeziorski, B.; Jeziorska, M.; Kucharski, S. A.; Moszynski, R.; Rybak, S.; Szalewicz, K.; Williams, H. L.; Wormer, P. E. S. *SAPT96: An Ab Initio Program for Many-Body Symmetry-Adapted Perturbation Theory Calculations of Intermolecular Interaction Energies*; University of Delaware and University of Warsaw, 1996.
(104) Hutson, J. M.; Thornley, A. E. *J. Chem. Phys.* **1994**, *100*, 2505.
(105) Hougen, J. T. Methane Symmetry Operations. In *International Review of Science*; Ramsay, D. A., Ed.; Butterworth: London, 1976; Vol. 3 (Spectroscopy).
(106) Kistenmacher, H.; Lie, G. C.; Popkie, H.; Clementi, E. *J. Chem. Phys.* **1974**, *61*, 546.
(107) Chalasiński, G.; Szczęśniak, M. M.; Cieplak, P.; Scheiner, S. *J. Chem. Phys.* **1991**, *94*, 2873.
(108) van Duijneveldt-van de Rijdt, J. G. C. M.; van Duijneveldt, F. B. *Chem. Phys.* **1993**, *175*, 271.
(109) van Duijneveldt-van de Rijdt, J. G. C. M.; van Duijneveldt, F. B. *Chem. Phys. Lett.* **1995**, *237*, 560.
(110) Xantheas, S. *J. Chem. Phys.* **1994**, *100*, 7523.
(111) Klopper, W.; Schütz, M.; Lüthi, H.-P.; Leutwyler, S. *J. Chem. Phys.* **1995**, *103*, 1085.
(112) Hodges, M. P.; Stone, A. J.; Xantheas, S. *J. Phys. Chem. A* **1997**, *101*, 9163.
(113) Milet, A.; Moszynski, R.; Wormer, P. E. S.; van der Avoird, A. *J. Phys. Chem. A* **1999**, *103*, 6811.
(114) Mas, E. M.; Bukowski, R.; Szalewicz, K.; Groenenboom, G. C.; Wormer, P. E. S.; van der Avoird, A. *J. Chem. Phys.* **2000**, in press.
(115) Svishchev, I. M.; Kusalik, P. G.; Wang, J.; Boyd, R. J. *J. Chem. Phys.* **1996**, *105*, 4742.
(116) Kozack, R. E.; Jordan, P. C. *J. Chem. Phys.* **1992**, *96*, 3120.
(117) Dyke, T. R.; Muenter, J. S. *J. Chem. Phys.* **1974**, *60*, 2929. Dyke, T. R.; Mack, K. M.; Muenter, J. S. *J. Chem. Phys.* **1977**, *66*, 498.
(118) Odutola, J. A.; Hu, T. A.; Prinslow, D.; O'dell, S. E.; Dyke, T. R. *J. Chem. Phys.* **1988**, *88*, 5352.
(119) Huang, Z. S.; Miller, R. E. *J. Chem. Phys.* **1988**, *88*, 8008.
(120) Busarow, K. L.; Cohen, R. C.; Blake, G. A.; Laughlin, K. B.; Lee, Y. T.; Saykally, R. J. *J. Chem. Phys.* **1989**, *90*, 3937.
(121) Fraser, G. T. *Intern. Rev. Phys. Chem.* **1991**, *10*, 189.
(122) Zwart, E.; ter Meulen, J. J.; Meerts, W. L. *Chem. Phys. Lett.* **1990**, *173*, 115.
(123) Zwart, E.; ter Meulen, J. J.; Meerts, W. L.; Coudert, L. H. *J. Mol. Spectrosc.* **1991**, *147*, 27.
(124) Pugliano, N.; Saykally, R. J. *J. Chem. Phys.* **1992**, *96*, 1832.
(125) Pugliano, N.; Saykally, R. J. *Science* **1992**, *257*, 1937.
(126) Pugliano, N.; Cruzan, J. D.; Loeser, J. G.; Saykally, R. J. *J. Chem. Phys.* **1993**, *98*, 6600.
(127) Karyakin, E. N.; Fraser, G. T.; Suenram, R. D. *Mol. Phys.* **1993**, *78*, 1179.
(128) Karyakin, E. N.; Fraser, G. T.; Lovas, F. J.; Suenram, R. D.; Fujitake, M. *J. Chem. Phys.* **1995**, *102*, 1114.
(129) Paul, J. B.; Provencal, R. A.; Saykally, R. J. *J. Phys. Chem. A* **1998**, *102*, 3279.
(130) Paul, J. B.; Provencal, R. A.; Chapo, C.; Petterson, A.; Saykally, R. J. *J. Chem. Phys.* **1998**, *109*, 10201.
(131) Liu, K.; Loeser, J. G.; Elrod, M. J.; Host, B. C.; Rzepiela, J. A.; Saykally, R. J. *J. Am. Chem. Soc.* **1994**, *116*, 3507.
(132) Liu, K.; Elrod, M. J.; Loeser, J. G.; Cruzan, J. D.; Pugliano, N.; Brown, M.; Rzepiela, J.; Saykally, R. *Faraday Discuss. Chem. Soc.* **1994**, *97*, 35.
(133) Suzuki, S.; Blake, G. A. *Chem. Phys. Lett.* **1994**, *229*, 499.
(134) Liu, K.; Cruzan, J. D.; Saykally, R. J. *Science* **1996**, *271*, 929.
(135) Liu, K.; Brown, M. G.; Cruzan, J. D.; Saykally, R. J. *Science* **1996**, *271*, 62.
(136) Liu, K.; Brown, M. G.; Carter, C.; Saykally, R. J.; Gregory, J. K.; Clary, D. C. *Nature* **1996**, *381*, 501.
(137) Cruzan, J. D.; Braly, L. B.; Liu, K.; Brown, M. G.; Loeser, J. G.; Saykally, R. J. *Science* **1996**, *271*, 59.
(138) Cruzan, J. D.; Brown, M. G.; Liu, K.; Braly, L. B.; Saykally, R. J. *J. Chem. Phys.* **1996**, *105*, 6634.
(139) Cruzan, J. D.; Viant, M. R.; Brown, M. G.; Saykally, R. J. *J. Phys. Chem. A* **1997**, *101*, 9022.
(140) Liu, K.; Brown, M. G.; Cruzan, J. D.; Saykally, R. J. *J. Phys. Chem. A* **1997**, *101*, 9011.
(141) Liu, K.; Brown, M. G.; Saykally, R. J. *J. Phys. Chem. A* **1997**, *101*, 8995.
(142) Viant, M. R.; Cruzan, J. D.; Lucas, D. D.; Brown, M. G.; Liu, K.; Saykally, R. J. *J. Phys. Chem. A* **1997**, *101*, 9032.
(143) Brown, M. G.; Keutsch, F. N.; Saykally, R. J. *J. Chem. Phys.* **1998**, *109*, 9645.
(144) Fellers, R. S.; Braly, L. B.; Saykally, R. J.; Leforestier, C. *J. Chem. Phys.* **1999**, *110*, 6306.
(145) Viant, M. R.; Brown, M. G.; Cruzan, J. D.; Saykally, R. J.; Geleijns, M.; van der Avoird, A. *J. Chem. Phys.* **1999**, *110*, 4369.
(146) Brown, M. G.; Viant, M. R.; McLaughlin, R. P.; Keoshian, C. J.; Michael, E.; Cruzan, J. D.; Saykally, R. J.; van der Avoird, A. *J. Chem. Phys.* **1999**, *111*, 7789.
(147) Braly, L. B. *The intermolecular vibrations of the water dimer*; Thesis, University of California at Berkeley, 1999.
(148) Luzar, A.; Chandler, D. *Phys. Rev. Lett.* **1996**, *76*, 928.
(149) Luzar, A.; Chandler, D. *Nature* **1996**, *379*, 55.
(150) Woutersen, S.; Emmerichs, U.; Bakker, H. J. *Science* **1997**, *278*, 658.
(151) Chen, H.; Liu, S.; Light, J. C. *J. Chem. Phys.* **1999**, *110*, 168.
(152) Groenenboom, G. C.; Mas, E. M.; Bukowski, R.; Szalewicz, K.; Wormer, P. E. S.; van der Avoird, A. *Phys. Rev. Lett.* **2000**, *84*, 4072.
(153) Morokuma, K. *J. Chem. Phys.* **1968**, *48*, 3275.
(154) Kollman, P. A.; Allen, L. C. *J. Chem. Phys.* **1969**, *51*, 3286.
(155) Bene, J. D.; Pople, J. A. *J. Chem. Phys.* **1970**, *52*, 1301.
(156) Hankins, D.; Moskowitz, J. W.; Stillinger, F. H. *J. Chem. Phys.* **1970**, *53*, 4544.
(157) Matsuoka, O.; Clementi, E.; Yoshimine, M. *J. Chem. Phys.* **1976**, *64*, 1351.
(158) Scheiner, S. *Annu. Rev. Phys. Chem.* **1994**, *45*, 23.
(159) Dyke, T. R. *J. Chem. Phys.* **1977**, *66*, 492.
(160) Coudert, L. H.; Hougen, J. T. *J. Mol. Spectrosc.* **1988**, *130*, 86.
(161) Coudert, L. H.; Hougen, J. T. *J. Mol. Spectrosc.* **1990**, *139*, 259.
(162) Coker, D. F.; Watts, R. O. *J. Phys. Chem.* **1987**, *91*, 2513.
(163) Hougen, J. T. *J. Mol. Spectrosc.* **1985**, *114*, 395.
(164) Althorpe, S. C.; Clary, D. C. *J. Chem. Phys.* **1994**, *101*, 3603.
(165) Althorpe, S. C.; Clary, D. C. *J. Chem. Phys.* **1995**, *102*, 4390.
(166) Gregory, J. K.; Clary, D. C. *J. Chem. Phys.* **1995**, *102*, 7817.
(167) Leforestier, C.; Braly, L. B.; Liu, K.; Elrod, M. J.; Saykally, R. J. *J. Chem. Phys.* **1997**, *106*, 8527.
(168) Leforestier, C. *J. Chem. Phys.* **1994**, *101*, 7357.
(169) Groenenboom, G. C.; Wormer, P. E. S.; van der Avoird, A.; Mas, E. M.; Bukowski, R.; Szalewicz, K. *J. Chem. Phys.* **2000**, in press.
(170) Echave, J.; Clary, D. C. *Chem. Phys. Lett.* **1992**, *190*, 225.
(171) Harris, D. O.; Engerholm, G. G.; Gwinn, W. D. *J. Chem. Phys.* **1965**, *43*, 1515.
(172) Colbert, D. T.; Miller, W. H. *J. Chem. Phys.* **1992**, *96*, 1982.
(173) Groenenboom, G. C.; Colbert, D. T. *J. Chem. Phys.* **1993**, *99*, 9681.
(174) Millot, C.; Stone, A. *J. Mol. Phys.* **1992**, *77*, 439.
(175) Mas, E. M.; Szalewicz, K.; Bukowski, R.; Jeziorski, B. *J. Chem. Phys.* **1997**, *107*, 4207.
(176) Jeziorski, B.; Szalewicz, K. Intermolecular interactions by perturbation theory. In *Encyclopedia of Computational Chemistry*; von Ragué Schleyer, P., Allinger, N. L., Clark, T., Gasteiger, J., Kollman, P. A., Schaefer, H. F., Schreiner, P. R., Eds.; Wiley: New York, 1998; Vol. 2.
(177) Braly, L. B.; Cruzan, J. D.; Liu, K.; Fellers, R. S.; Saykally, R. J. *J. Chem. Phys.* **2000**, *112*, 10293.
(178) Braly, L. B.; Liu, K.; Brown, M. G.; Keutsch, F. N.; Fellers, R. S.; Saykally, R. J. *J. Chem. Phys.* **2000**, *112*, 10314.
(179) Xantheas, S.; Dunning, T. H. *J. Chem. Phys.* **1993**, *99*, 8774.
(180) Klopper, W.; Lüthi, H. P. *Mol. Phys.* **1999**, *96*, 559.
(181) Curtiss, L. A.; Frurip, D. J.; Blander, M. *J. Chem. Phys.* **1979**, *71*, 2703.
(182) Åstrand, P. O.; Linse, P.; Karlström, G. *Chem. Phys.* **1995**, *191*, 195.
(183) Reimers, J. R.; Watts, R. O.; Klein, M. L. *Chem. Phys.* **1982**, *64*, 95.

(184) Xantheas, S.; Dunning, T. H. *J. Chem. Phys.* **1993**, *98*, 8037.
(185) Fowler, J. E.; Schaefer, H. F. *J. Am. Chem. Soc.* **1995**, *117*, 446.
(186) Wales, D. J. *J. Am. Chem. Soc.* **1993**, *115*, 11180.
(187) Bürgi, T.; Graf, S.; Leutwyler, S.; Klopper, W. *J. Chem. Phys.* **1995**, *103*, 1077.
(188) Sabo, D.; Bačić, Z.; Graf, S.; Leutwyler, S. *J. Chem. Phys.* **1999**, *110*, 5745.
(189) Schütz, M.; Bürgi, T.; Leutwyler, S.; Bürgi, H. B. *J. Chem. Phys.* **1993**, *99*, 5228.
(190) Schütz, M.; Bürgi, T.; Leutwyler, S.; Bürgi, H. B. *J. Chem. Phys.* **1994**, *100*, 1780.
(191) Klopper, W.; Schütz, M. *Chem. Phys. Lett.* **1995**, *237*, 536.
(192) Sabo, D.; Bačić, Z.; Bürgi, T.; Leutwyler, S. *Chem. Phys. Lett.* **1995**, *244*, 283.
(193) Olthof, E. H. T.; van der Avoird, A.; Wormer, P. E. S.; Liu, K.; Saykally, R. J. *J. Chem. Phys.* **1996**, *105*, 8051.
(194) Sabo, D.; Bačić, Z.; Graf, S.; Leutwyler, S. *Chem. Phys. Lett.* **1996**, *261*, 318.
(195) Walsh, T. R.; Wales, D. J. *J. Chem. Soc., Faraday Trans.* **1996**, *92*, 2505.
(196) Geleijns, M.; van der Avoird, A. *J. Chem. Phys.* **1999**, *110*, 823.
(197) Sabo, D.; Bačić, Z.; Graf, S.; Leutwyler, S. *J. Chem. Phys.* **1999**, *111*, 5331.
(198) Sabo, D.; Bačić, Z.; Graf, S.; Leutwyler, S. *J. Chem. Phys.* **1999**, *111*, 10727.
(199) Gregory, J. K.; Clary, D. C. *J. Chem. Phys.* **1995**, *103*, 8924.
(200) Sorenson, J. M.; Gregory, J. K.; Clary, D. C. *Chem. Phys. Lett.* **1996**, *263*, 680.
(201) Wales, D. J. Rearrangements and Tunneling in Water Clusters. In *Advances in Molecular Vibrations and Collision Dynamics*; Bowman, J. M., Bačić, Z., Eds.; JAI press: Stamford, 1998.
(202) Owicki, J. C.; Shipman, L. L.; Scheraga, H. A. *J. Phys. Chem.* **1975**, *79*, 1794.
(203) Liu, K.; Brown, M. G.; Viant, M. R.; Cruzan, J. D.; Saykally, R. J. *Mol. Phys.* **1996**, *89*, 1373.
(204) Kemble, E. C. *The Fundamental Principles of Quantum Mechanics*; McGraw-Hill: New York, 1937.
(205) Biedenharn, L. C.; Louck, J. D. Angular Momentum in Quantum Physics. *Encyclopedia of Mathematics*; Addison-Wesley: Reading, 1981; Vol. 8.
(206) Zare, R. N. *Angular Momentum*; Wiley: New York, 1988.
(207) Hershbach, D. R. *J. Chem. Phys.* **1959**, *31*, 91.
(208) Riedle, E.; van der Avoird, A. *J. Chem. Phys.* **1996**, *104*, 882.
(209) Herzberg, G. Molecular Spectra and Molecular Structure. *Infrared and Raman Spectra of Polyatomic Molecules*; Van Nostrand: New York, 1945; Vol. 2.
(210) Moszynski, R.; Wormer, P. E. S.; Jeziorski, B.; van der Avoird, A. *J. Chem. Phys.* **1995**, *103*, 8058.
(211) Moszynski, R.; Wormer, P. E. S.; Jeziorski, B.; van der Avoird, A. *J. Chem. Phys.* **1997**, *107*, E672.
(212) Lotrich, V. F.; Szalewicz, K. *J. Chem. Phys.* **1997**, *106*, 9668.
(213) Lotrich, V. F.; Szalewicz, K. *J. Chem. Phys.* **2000**, *112*, 112.
(214) Wormer, P. E. S.; Moszynski, R.; van der Avoird, A. *J. Chem. Phys.* **2000**, *112*, 3159.
(215) Jorgensen, W. L.; Chandrasekhar, J.; Madura, J. D.; Impey, R. W.; Klein, M. L. *J. Chem. Phys.* **1983**, *79*, 926.
(216) Dham, A. K.; McCourt, F. R. W.; Meath, W. J. *J. Chem. Phys.* **1995**, *103*, 8477.
(217) Wang, F.; McCourt, F. R. W.; LeRoy, R. J. *Mol. Phys.* **1996**, *88*, 821.
(218) Naumkin, F. Y. *Mol. Phys.* **1997**, *90*, 875.
(219) Fernández, B.; Koch, H.; Makarewicz, J. *J. Chem. Phys.* **1999**, *110*, 8525.
(220) Roche, C. F.; Dickinson, A. S.; Ernesti, A.; Hutson, J. M. *J. Chem. Phys.* **1997**, *107*, 1824.
(221) Hutson, J. M.; Ernesti, A.; Law, M. M.; Roche, C. F.; Wheatly, R. J. *J. Chem. Phys.* **1996**, *105*, 9130.
(222) Misquitta, A. J.; Bukowski, R.; Szalewicz, K. *J. Chem. Phys.* **2000**, *112*, 5308.
(223) Heijmen, T. G. A.; Moszynski, R.; Wormer, P. E. S.; van der Avoird, A. *J. Chem. Phys.* **1997**, *107*, 9921.
(224) Moszynski, R.; Korona, T.; Wormer, P. E. S.; van der Avoird, A. *J. Phys. Chem. A* **1997**, *101*, 4690.
(225) Moszynski, R.; Wormer, P. E. S.; van der Avoird, A. *J. Chem. Phys.* **1995**, *102*, 8385.
(226) Bemish, R. J.; Oudejans, L.; Miller, R. E.; Moszynski, R.; Heijmen, T. G. A.; Korona, T.; Wormer, P. E. S.; van der Avoird, A. *J. Chem. Phys.* **1998**, *109*, 8968.
(227) Reid, J. P.; Simpson, C. J. S. M.; M.Quiney, H. *J. Chem. Phys.* **1997**, *107*, 9929.
(228) Antonova, S.; Lin, A.; Tsakotellis, A. P.; McBane, G. C. *J. Chem. Phys.* **1999**, *110*, 2384.
(229) Heck, E. L.; Dickinson, A. S. *Mol. Phys.* **1997**, *91*, 31.
(230) Randall, R. W.; Cliffe, A. J.; Howard, B. J.; McKellar, A. R. W. *Mol. Phys.* **1993**, *79*, 1113.
(231) McKellar, A. R. W.; Chan, M. C. *Mol. Phys.* **1998**, *93*, 253.
(232) McBane, G. C.; Cybulski, S. M. *J. Chem. Phys.* **1999**, *110*, 11734.
(233) Jansen, G. *Chem. Phys. Lett.* **1994**, *223*, 377.
(234) Jansen, G. *J. Chem. Phys.* **1996**, *105*, 89.
(235) Shin, S.; Shin, S. K.; Tao, F. M. *J. Chem. Phys.* **1996**, *104*, 183.
(236) Castells, V.; Halberstadt, N.; Shin, S. K.; Beaudet, R. A.; Wittig, C. *J. Chem. Phys.* **1994**, *101*, 1006.
(237) Jäger, W.; Gerry, M. C. L. *J. Chem. Phys.* **1995**, *102*, 3587.
(238) McKellar, A. R. W. *Mol. Phys.* **2000**, *98*, 111.
(239) Brookes, M. D.; McKellar, A. R. W. *Mol. Phys.* **1999**, *97*, 127.
(240) Heijmen, T. G. A.; Moszynski, R.; Wormer, P. E. S.; van der Avoird, A.; Buck, U.; Ettischer, I.; Krohne, R. *J. Chem. Phys.* **1997**, *107*, 7260.
(241) Buck, U.; Ettischer, I.; Schlemmer, S.; Yang, M.; Vohralik, P.; Watts, R. O. *J. Chem. Phys.* **1993**, *99*, 3494.
(242) Heijmen, T. G. A.; Moszynski, R.; Wormer, P. E. S.; van der Avoird, A.; Rudert, A. D.; Halpern, J. B.; Martin, J.; Gao, W. B.; Zacharias, H. *J. Chem. Phys.* **1999**, *111*, 2519.
(243) Brupbacher, T.; Bauder, A. *Chem. Phys. Lett.* **1990**, *173*, 435.
(244) Brupbacher, T.; Makarewicz, J.; Bauder, A. *J. Chem. Phys.* **1994**, *101*, 9736.
(245) Riedle, E.; Sussmann, R.; Weber, T.; Neusser, H. J. *J. Chem. Phys.* **1996**, *104*, 865.
(246) Kim, W.; Felker, P. M. *J. Chem. Phys.* **1997**, *107*, 2193.
(247) Neuhauser, R.; Braun, J.; Neusser, H. J.; van der Avoird, A. *J. Chem. Phys.* **1998**, *108*, 8408.
(248) Satink, R. G.; Piest, H.; von Helden, G.; Meijer, G. *J. Chem. Phys.* **1999**, *111*, 10750.
(249) Koch, H.; Fernández, B.; Christiansen, O. *J. Chem. Phys.* **1998**, *108*, 2784.
(250) Koch, H.; Fernández, B.; Makarewicz, J. *J. Chem. Phys.* **1999**, *111*, 198.
(251) Fernández, B.; Koch, H.; Makarewicz, J. *J. Chem. Phys.* **1999**, *111*, 5922.
(252) Piest, H.; von Helden, G.; Meijer, G. *J. Chem. Phys.* **1999**, *110*, 2010.
(253) Becucci, M.; Lakin, N. M.; Pietraperzia, G.; Castellucci, E.; Brechignac, P.; Coutant, B.; Hermine, P. *J. Chem. Phys.* **1999**, *110*, 9961.
(254) Lakin, N. M.; Pietraperzia, G.; Becucci, M.; Castellucci, E.; Coreno, M.; Giardini-Guidoni, A.; van der Avoird, A. *J. Chem. Phys.* **1999**, *108*, 1836.
(255) Sussmann, R.; Neusser, H. J. *J. Chem. Phys.* **1995**, *102*, 3055.
(256) Champagne, B. B.; Pfanstiel, J. F.; Pratt, D. W.; Ulsh, R. C. *J. Chem. Phys.* **1995**, *102*, 6432.
(257) Korter, T. M.; Küpper, J.; Pratt, D. W. *J. Chem. Phys.* **1999**, *111*, 3946.
(258) Droz, T.; Leutwyler, S.; Mandziuk, M.; Bačić, Z. *J. Chem. Phys.* **1994**, *101*, 6412.
(259) Droz, T.; Leutwyler, S.; Mandziuk, M.; Bačić, Z. *J. Chem. Phys.* **1995**, *102*, 4715.
(260) Droz, T.; Leutwyler, S.; Mandziuk, M.; Bačić, Z. *J. Chem. Phys.* **1995**, *103*, 4855.
(261) Parneix, P.; Halberstadt, N.; Brechignac, P.; Amar, F. G.; van der Avoird, A. *J. Chem. Phys.* **1993**, *98*, 2709.
(262) Elrod, M. J.; Saykally, R. J. *Chem. Rev.* **1994**, *94*, 1975.
(263) Lotrich, V. F.; Szalewicz, K. *J. Chem. Phys.* **1997**, *106*, 9688.
(264) Lotrich, V. F.; Jankowski, P.; Szalewicz, K. *J. Chem. Phys.* **1998**, *108*, 4725.
(265) Ernesti, A.; Hutson, J. M. *Phys. Rev. A* **1995**, *51*, 239.
(266) Ernesti, A.; Hutson, J. M. *J. Chem. Phys.* **1997**, *106*, 6288.
(267) Chalasiński, G.; Szczęśniak, M. M.; Cybulski, S. M. *J. Chem. Phys.* **1990**, *92*, 2481.
(268) Chalasiński, G.; Szczęśniak, M.; Kendall, R. *J. Chem. Phys.* **1994**, *101*, 8860.
(269) Szczęśniak, M. M.; Chalasiński, G.; Piecuch, P. *J. Chem. Phys.* **1993**, *99*, 6732.
(270) Cybulski, S. M.; Szczęśniak, M. M.; Chalasiński, G. *J. Chem. Phys.* **1994**, *101*, 10708.
(271) Moszynski, R.; Wormer, P. E. S.; Heijmen, T. G. A.; van der Avoird, A. *J. Chem. Phys.* **1998**, *108*, 579.
(272) González-Lezana, T.; Rubayo-Soneira, J.; Miret-Artés, S.; Gianturco, F. A.; Delgado-Barrio, G.; Villarreal, P. *Phys. Rev. Lett.* **1999**, *82*, 1648.
(273) González-Lezana, T.; Rubayo-Soneira, J.; Miret-Artés, S.; Gianturco, F. A.; Delgado-Barrio, G.; Villarreal, P. *J. Chem. Phys.* **1999**, *110*, 9000.
(274) Wright, N. J.; Hutson, J. M. *J. Chem. Phys.* **1999**, *110*, 902.
(275) Ernesti, A.; Hutson, J. M. *J. Chem. Phys.* **1995**, *103*, 3386.
(276) Cooper, A. R.; Jain, S.; Hutson, J. M. *J. Chem. Phys.* **1993**, *98*, 2160.
(277) Xu, Y.; Jäger, W.; Gerry, M. C. L. *J. Chem. Phys.* **1994**, *100*, 4171.
(278) Schöllkopf, W.; Toennies, J. P. *J. Chem. Phys.* **1996**, *104*, 1155.
(279) Farrell, J. T.; Nesbitt, D. J. *J. Chem. Phys.* **1996**, *105*, 9421.
(280) Chuang, C.-C.; Tsang, S. N.; Hanson, J. G.; Klemperer, W.; Chang, H.-C. *J. Chem. Phys.* **1997**, *107*, 7041.
(281) Xu, Y. J.; Armstrong, G. S.; Jäger, W. *J. Chem. Phys.* **1999**, *110*, 4354.
(282) Liu, S.; Bačić, Z.; Moskowitz, J. W.; Schmidt, K. E. *J. Chem. Phys.* **1994**, *101*, 6359.
(283) Liu, S.; Bačić, Z.; Moskowitz, J. W.; Schmidt, K. E. *J. Chem. Phys.* **1994**, *100*, 7166.

(284) Lewerenz, M. *J. Chem. Phys.* **1996**, *104*, 1028.
(285) Niyaz, P.; Bačić, Z.; Moskowitz, J. W.; Schmidt, K. E. *Chem. Phys. Lett.* **1996**, *252*, 23.
(286) Dykstra, C. E. *J. Chem. Phys.* **1998**, *108*, 6619.
(287) Hutson, J. M.; Liu, S.; Moskowitz, J. W.; Bačić, Z. *J. Chem. Phys.* **1999**, *111*, 8378.
(288) Grigorenko, B. L.; Nemukhin, A. V.; Apkarian, V. A. *J. Chem. Phys.* **1996**, *104*, 5510.
(289) McIlroy, A.; Lascola, R.; Lovejoy, C. M.; Nesbitt, D. J. *J. Chem. Phys.* **1991**, *95*, 2636.
(290) Farrell, J. T.; Davis, S.; Nesbitt, D. J. *J. Chem. Phys.* **1995**, *103*, 2395.
(291) Quack, M.; Suhm, M. A. *Theor. Chim. Acta* **1996**, *93*, 61.
(292) Bačić, Z.; Miller, R. E. *J. Phys. Chem.* **1996**, *100*, 12945.
(293) Dyke, T. R.; Howard, B. J.; Klemperer, W. *J. Chem. Phys.* **1972**, *56*, 2442.
(294) Lafferty, W. J.; Suenram, R. D.; Lovas, F. J. *J. Mol. Spectrosc.* **1987**, *123*, 434.
(295) Peterson, K. A.; Dunning, T. H. *J. Chem. Phys.* **1995**, *102*, 2032.
(296) Collins, C. L.; Morihashi, K.; Yamaguchi, Y.; Schaefer, H. F. *J. Chem. Phys.* **1995**, *103*, 6051.
(297) Tschumper, G. S.; Kelty, M. D.; Schaefer, H. F. *Mol. Phys.* **1999**, *96*, 493.
(298) Klopper, W.; Quack, M.; Suhm, M. A. *Mol. Phys.* **1998**, *94*, 105.
(299) Quack, M.; Suhm, M. A. *J. Chem. Phys.* **1991**, *95*, 28.
(300) Hodges, M. P.; Stone, A. J.; Lago, E. C. *J. Phys. Chem. A* **1998**, *102*, 2455.
(301) Klopper, W.; Quack, M.; Suhm, M. A. *J. Chem. Phys.* **1998**, *108*, 10096.
(302) Zhang, D. H.; Wu, Q.; Zhang, J. Z. H.; von Dirke, M.; Bačić, Z. *J. Chem. Phys.* **1995**, *102*, 2315.
(303) Necoechea, W. C.; Truhlar, D. G. *Chem. Phys. Lett.* **1994**, *224*, 297.
(304) Necoechea, W. C.; Truhlar, D. G. *Chem. Phys. Lett.* **1995**, *231*, 125(E).
(305) von Dirke, M.; Bačić, Z.; Zhang, D. H.; Wu, Q.; Zhang, J. Z. H. *J. Chem. Phys.* **1995**, *102*, 4382.
(306) Volobuev, Y.; Necoechea, W. C.; Truhlar, D. G. *J. Chem. Phys.* **1997**, *101*, 3045.
(307) Wu, X. T.; McCoy, A. B.; Hayes, E. F. *J. Chem. Phys.* **1999**, *110*, 2354.
(308) Wu, X. T.; Hayes, E. F.; McCoy, A. B. *J. Chem. Phys.* **1999**, *110*, 2365.
(309) Vissers, G. W. M.; Groenenboom, G. C.; van der Avoird, A. Manuscript in preparation.
(310) Chang, H.-C.; Klemperer, W. *J. Chem. Phys.* **1994**, *100*, 1.
(311) Chang, H.-C.; Klemperer, W. *J. Chem. Phys.* **1996**, *104*, 7830.
(312) Anderson, D. T.; Davis, S.; Nesbitt, D. J. *J. Chem. Phys.* **1996**, *104*, 6225.
(313) Anderson, D. T.; Davis, S.; Nesbitt, D. J. *J. Chem. Phys.* **1996**, *105*, 4488.
(314) Davis, S.; Anderson, D. T.; Farrell, J. T.; Nesbitt, D. J. *J. Chem. Phys.* **1996**, *104*, 8197.
(315) Davis, S.; Anderson, D. T.; Nesbitt, D. J. *J. Chem. Phys.* **1996**, *105*, 6645.
(316) Pine, A. S.; Howard, B. J. *J. Chem. Phys.* **1986**, *84*, 590.
(317) Bohac, E. J.; Marshall, M. D.; Miller, R. E. *J. Chem. Phys.* **1992**, *96*, 6681.
(318) Schuder, M. D.; Nelson, D. D.; Nesbitt, D. J. *J. Chem. Phys.* **1989**, *91*, 4418.
(319) Blake, G. A.; Bumgarner, R. E. *J. Chem. Phys.* **1989**, *91*, 7300.
(320) Elrod, M. J.; Saykally, R. J. *J. Chem. Phys.* **1995**, *103*, 921.
(321) Elrod, M. J.; Saykally, R. J. *J. Chem. Phys.* **1995**, *103*, 933.
(322) Karpfen, A.; Bunker, P. R.; Jensen, P. *Chem. Phys.* **1991**, *149*, 299.
(323) Bunker, P. R.; Epa, V. C.; Jensen, P.; Karpfen, A. *J. Mol. Spectrosc.* **1991**, *146*, 200.
(324) Qiu, Y.; Bačić, Z. *J. Chem. Phys.* **1997**, *106*, 2158.
(325) Hermida-Ramon, J. M.; Engkvist, O.; Karlström, G. *J. Comput. Chem.* **1998**, *19*, 1816.
(326) Imura, K.; Kasai, T.; Ohoyama, H.; Naaman, R. *J. Chem. Phys.* **1999**, *110*, 355.
(327) Liu, K.; Dulligan, M.; Bezel, I.; Kolessov, A.; Wittig, C. *J. Chem. Phys.* **1998**, *108*, 9614.
(328) Quack, M.; Schmitt, U.; Suhm, M. A. *Chem. Phys. Lett.* **1997**, *269*, 29.
(329) Wales, D. J.; Walsh, T. R. *J. Chem. Phys.* **1997**, *106*, 7193.
(330) Graf, S.; Leutwyler, S. *J. Chem. Phys.* **1998**, *109*, 5393.
(331) Sabo, D.; Bačić, Z.; Graf, S.; Leutwyler, S. *J. Chem. Phys.* **1998**, *109*, 5404.
(332) Graf, S.; Mohr, W.; Leutwyler, S. *J. Chem. Phys.* **1999**, *110*, 7893.
(333) Wales, D. J.; Walsh, T. R. *J. Chem. Phys.* **1996**, *105*, 6957.
(334) Pedulla, J. M.; Vila, F.; Jordan, K. D. *J. Chem. Phys.* **1996**, *105*, 11091.
(335) Pedulla, J. M.; Kim, K.; Jordan, K. D. *Chem. Phys. Lett.* **1998**, *291*, 78.
(336) Kim, J.; Kim, K. S. *J. Chem. Phys.* **1998**, *109*, 5886.
(337) Gregory, J. K.; Clary, D. C. *J. Chem. Phys.* **1996**, *105*, 6626.
(338) Severson, M. W.; Buch, V. *J. Chem. Phys.* **1999**, *111*, 10866.
(339) Blume, D.; Whaley, K. B. *J. Chem. Phys.* **2000**, *112*, 2218.
(340) Tsai, C. J.; Jordan, K. D. *J. Chem. Phys.* **1991**, *95*, 3850.
(341) Knochenmuss, R.; Leutwyler, S. *J. Chem. Phys.* **1992**, *96*, 5233.
(342) Lee, C.; Chen, H.; Fitzgerald, G. *J. Chem. Phys.* **1995**, *102*, 1266.
(343) Estrin, D. A.; Paglieri, L.; Corongiu, G.; Clementi, E. *J. Phys. Chem.* **1996**, *100*, 8701.
(344) Fredericks, S. Y.; Pedulla, J. M.; Jordan, K. D.; Zwier, T. S. *Theor. Chem. Acc.* **1997**, *96*, 51.
(345) Blanton, W. B.; Gordonwylie, S. W.; Clark, G. R.; Jordan, K. D.; Wood, J. T.; Geiser, U.; Collins, T. J. *J. Am. Chem. Soc.* **1999**, *121*, 3551.
(346) Kim, J.; Majumdar, D.; Lee, H. M.; Kim, K. S. *J. Chem. Phys.* **1999**, *110*, 9128.
(347) Pedulla, J. M.; Jordan, K. D. *Chem. Phys.* **1998**, *239*, 593.
(348) Rodriguez, J.; Laria, D.; Marceca, E. J.; Estrin, D. A. *J. Chem. Phys.* **1999**, *110*, 9039.
(349) Dang, L. X. *J. Chem. Phys.* **1999**, *110*, 1526.
(350) Huisken, F.; Kaloudis, M.; Kulcke, A. *J. Chem. Phys.* **1996**, *104*, 17.
(351) Buck, U.; Ettischer, I.; Melzer, M.; Buch, V.; Sadlej, J. *Phys. Rev. Lett.* **1998**, *80*, 2578.
(352) Brudermann, J.; Melzer, M.; Buck, U.; Kazimirski, J.; Sadlej, J.; Buch, V. *J. Chem. Phys.* **1999**, *110*, 10649.
(353) Kim, K.; Jordan, K. D.; Zwier, T. S. *J. Am. Chem. Soc.* **1994**, *116*, 11568.
(354) Rowland, B.; Kadagathur, S.; Devlin, J. P.; Buch, V.; Feldmann, T.; Wojcik, M. *J. Chem. Phys.* **1995**, *102*, 8328.
(355) Gruenloh, C. J.; Carney, J. R.; Arrington, C. A. *J. Chem. Phys.* **1993**, *99*, 9681.
(356) Gruenloh, C. J.; Carney, J. R.; Hagemeister, F. C.; Zwier, C. A. A. T.; Fredericks, S. Y.; Wood, J. T.; Jordan, K. D. *J. Chem. Phys.* **1998**, *109*, 6601.
(357) Stockman, P. A.; Blake, G. A.; Lovas, F. J.; Suenram, R. D. *J. Chem. Phys.* **1997**, *107*, 3782.
(358) Masella, M.; Flament, J.-P. *J. Chem. Phys.* **1998**, *108*, 7141.
(359) Iosue, J. L.; Benoit, D. M.; Clary, D. C. *Chem. Phys. Lett.* **1999**, *301*, 275.
(360) Carney, J. R.; Hagemeister, F. C.; Zwier, T. S. *J. Chem. Phys.* **1998**, *108*, 3379.
(361) Helm, R. M.; Clara, M.; Grebner, T. L.; Neusser, H. J. *J. Phys. Chem. A* **1998**, *102*, 3268.
(362) Braun, J. E.; Grebner, T. L.; Neusser, H. J. *J. Phys. Chem. A* **1998**, *102*, 3273.
(363) Korter, T. M.; Pratt, D. W.; Küpper, J. *J. Phys. Chem. A* **1998**, *102*, 7211.
(364) Guchhait, N.; Ebata, T.; Mikami, N. *J. Chem. Phys.* **1999**, *111*, 8438.
(365) Berden, G.; Meerts, W. L.; Schmitt, M.; Kleinermanns, K. *J. Chem. Phys.* **1996**, *104*, 972.
(366) Helm, R. M.; Vogel, H.-P.; Neusser, H. J. *J. Chem. Phys.* **1998**, *108*, 4496.
(367) Schmitt, M.; Jacoby, C.; Kleinermanns, K. *J. Chem. Phys.* **1998**, *108*, 4486.
(368) Watanabe, T.; Ebata, T.; Tanabe, S.; Mikami, N. *J. Chem. Phys.* **1996**, *105*, 408.
(369) Gerhards, M.; Schmitt, M.; Kleinermanns, K.; Stahl, W. *J. Chem. Phys.* **1996**, *104*, 967.
(370) Schütz, M.; Bürgi, T.; Leutwyler, S.; Fischer, T. *J. Chem. Phys.* **1993**, *98*, 3763.
(371) Courty, A.; Mons, M.; Dimicoli, N.; Piuzzi, F.; Gaigeot, M. P.; Brenner, V.; Depujo, P.; Millie, P. *J. Phys. Chem. A* **1998**, *102*, 6590.
(372) Suzuki, S.; Green, P. G.; Bumgarner, R. E.; Dasgupta, S.; Goddard, W. A.; Blake, G. A. *Science* **1992**, *257*, 942.
(373) Gutowsky, H. S.; Emilsson, T.; Arunan, E. *J. Chem. Phys.* **1993**, *99*, 4883.
(374) Gotch, A. J.; Zwier, T. S. *J. Chem. Phys.* **1992**, *96*, 3388.
(375) Pribble, R. N.; Garrett, A. W.; Haber, K.; Zwier, T. S. *J. Chem. Phys.* **1995**, *103*, 531.
(376) Gregory, J. K.; Clary, D. C. *Mol. Phys.* **1996**, *88*, 33.
(377) Karlström, G.; Linse, P.; Wallqvist, A.; Jönsson, B. *J. Am. Chem. Soc.* **1983**, *104*, 3777.
(378) Kim, W.; Neuhauser, D.; Wall, M. R.; Felker, P. M. *J. Chem. Phys.* **1999**, *110*, 8461.
(379) Maxton, P. M.; Schaeffer, M. W.; Felker, P. M. *Chem. Phys. Lett.* **1995**, *241*, 603.
(380) Sorenson, J. M.; Clary, D. C. *J. Chem. Phys.* **1997**, *106*, 849.
(381) Rode, M.; Sadlej, J.; Moszynski, R.; Wormer, P. E. S.; van der Avoird, A. *Chem. Phys. Lett.* **1999**, *314*, 326.
(382) Jung, J. O.; Gerber, R. B. *J. Chem. Phys.* **1996**, *105*, 10332.
(383) Milot, R.; Jansen, A. P. J. *J. Chem. Phys.* **1998**, *109*, 1996.
(384) Raab, A.; Burghardt, I.; Meyer, H. D. *J. Chem. Phys.* **1999**, *111*, 8759.

CR990046E